10. SCIAMACHY's View of the Changing Earth's Environment

H. Bovensmann[1], I. Aben[2], M. Van Roozendael[3], S. Kühl[4], M. Gottwald[5], C. von Savigny[1], M. Buchwitz[1], A. Richter[1], C. Frankenberg[6], P. Stammes[7], M. de Graaf[7], F. Wittrock[1], M. Sinnhuber[1], B.-M. Sinnhuber[1], A. Schönhardt[1], S. Beirle[4], A. Gloudemans[2], H. Schrijver[2], A. Bracher[8,1], A.V. Rozanov[1], M. Weber[1], J.P. Burrows[1]

[1] Institute of Environmental Physics / Institute of Remote Sensing (IUP-IFE), University of Bremen, Otto-Hahn-Allee 1, 28359 Bremen, Germany
[2] SRON, Netherlands Institute for Space Research, Sorbonnelaan 2, 3584 CA Utrecht, The Netherlands
[3] Belgian Institute for Space Aeronomie (BIRA-IASB), 3 Avenue Circulaire, 1180 Brussels, Belgium
[4] Max Planck Institute for Chemistry, Johann-Joachim-Becher-Weg 27, 55128 Mainz, Germany
[5] Remote Sensing Technology Institute, German Aerospace Center (DLR-IMF), Oberpfaffenhofen, 82234 Wessling, Germany
[6] Jet Propulsion Laboratory, California Institute of Technology, 4800 Oak Grove Drive, 91109 Pasadena, CA, USA
[7] Royal Netherlands Meteorological Institute (KNMI), Wilhelminalaan 10, 3732 GK De Bilt, The Netherlands
[8] Alfred Wegener Institute for Polar and Marine Research, Bussestraße 24, 27570 Bremerhaven, Germany

Abstract: Since August 2002, SCIAMACHY has been delivering a wealth of high-quality data permitting the study of the status of the Earth's atmosphere. Enhanced concentrations of greenhouse gases are identified as the major source of global warming and their atmospheric concentrations are increasing. SCIAMACHY monitors the most prominent species such as CO_2, CH_4 and water vapour, the latter including isotope variants. Further anthropogenic impacts on the troposphere occur by emission of reactive trace gases contributing to pollution and affecting air quality. With SCIAMACHY their global, regional and even local signatures can be detected. Long-term analyses document how the emissions of NO_2, SO_2, HCHO, CHOCHO and CO evolve with time. In addition, the halogen cycle of polar BrO and IO, both of natural origin, is studied. The stratosphere is the layer where public interest in the Earth's atmosphere has begun to grow since the detection of the ozone hole in the mid-1980's. Until the mid-1990s, a steady decrease has been observed in the ozone abundance. The most striking feature is the massive loss of stratospheric ozone over Antarctica during each southern spring. In order to detect possible signs of recovery, SCIAMACHY contributes to the continuous monitoring of the ozone layer, the ozone hole, Polar Stratospheric Clouds (PSC) and species impacting the ozone chemistry such as NO_2, OClO and BrO. A much more poorly explored region is the mesosphere and lower thermosphere, which forms the transition between interplanetary space and the terrestrial atmosphere. This region is dominated by extraterrestrial impacts as well as couplings to the lower atmosphere. With SCIAMACHY's limb viewing capabilities, Noctilucent Clouds (NLC) are studied providing insight into generation and depletion mechanisms. At times of strong solar activity, SCIAMACHY measurements reveal how the chemistry of the upper atmosphere is disturbed. By analysis of emission lines in SCIAMACHY spectra, the composition of the thermosphere above 100 km can be studied. SCIAMACHY is the first instrument to globally observe the metal layers in the upper mesosphere / lower thermosphere (MLT) region. Meanwhile, it is now possible to derive vegetation information over land and phytoplankton characteristics in the oceans from SCIAMACHY data when applying appropriate retrieval techniques. Finally, SCIAMACHY has even proven to be useful in planetary science by measuring spectra of our solar system neighbour Venus.

Keywords: Earth's atmosphere – Greenhouse gases – Air quality – Reactive gases – Ozone layer – Solar-terrestrial interactions – Troposphere – Stratosphere – Mesosphere – Lower thermosphere

Expectations were high when SCIAMACHY was launched in March 2002. Since August 2002, a continuous stream of high quality data has been acquired at the ground stations and disseminated for further processing, scientifically and operationally. With more than 8 years in orbit, SCIAMACHY's data 'harvest' considerably exceeded the original objective – and even more can be expected for the next years, provided that the ENVISAT mission extension operates as planned. During the past years, numerous scientific results from the SCIAMACHY mission have been derived, clearly demonstrating the high 'return on investment' of this enterprise. New and exciting insights into the Earth-atmosphere system are obtained. They contribute significantly to atmospheric physics and chemistry, as well as to global climate change research. Many scientific groups at various institutes in Europe and abroad were and are actively involved in the analysis of the data. Their efforts made these excellent results possible. In the following tour through the atmosphere, we will highlight some of the most spectacular findings. This summary is by no means complete but gives a good impression how SCIAMACHY explores our changing environment.

10.1 Tropospheric Composition – Greenhouse Gases

SCIAMACHY measurements provide information on tropospheric constituents as solar radiation penetrates the atmosphere down to the surface. Our civilisation imposes a significant stress upon the troposphere. Concentrations of greenhouse gases are increasing and have been identified as the source of global warming. SCIAMACHY permits not only the monitoring of the global status of the major greenhouse gases but also the retrieval of knowledge about the distribution of their sources such as e.g. densely populated regions or wetlands.

Carbon Dioxide – CO_2

CO_2, the most important anthropogenic greenhouse gas, is regulated by the Kyoto Protocol and can be considered as a synonym for the impact of industrialisation on our environment. In pre-industrial times, CO_2 mixing ratios dating back several thousands of years were about 300 ppm at maximum. Present values are around 390 ppm, i.e., 30% higher, with the increase mainly attributed to the past 50 years – a clear indication of an anthropogenic effect. Carbon dumped into natural sinks over millions of years is now being released into the atmosphere by fossil fuel burning (oil, coal, gas). In addition, other anthropogenic activities such as deforestation destroy important CO_2 sinks and reduce nature's ability to recycle atmospheric CO_2 efficiently. A thorough study of carbon dioxide is therefore necessary to understand the global carbon cycle and to predict how greenhouse gas concentrations evolve with time. Currently, about 50% of the emitted CO_2 remains in the atmosphere, the other half is taken up by the oceans and in the biosphere. Photosynthesis extracts carbon dioxide from the troposphere over land. Thus, large forest areas act as a CO_2 sink. The North American and Siberian boreal forests in summer are examples for such extended CO_2 sinks. These sink regions can be observed by SCIAMACHY, as illustrated in Fig. 10-1 displaying atmospheric CO_2 levels from April to June compared to July to September, where CO_2 concentrations are lower due to uptake by the terrestrial biosphere. This seasonal 'CO_2 breathing' is superimposed on the steady increase of atmospheric CO_2 with much higher concentrations in 2009 than in 2003. Both phenomena can be clearly observed by SCIAMACHY. It is even possible to detect localised elevated CO_2 over anthropogenic source regions such as Central Europe's highly populated and industrialised Rhine-Main area (Fig. 10.2). SCIAMACHY nadir observations in the SWIR spectral region formed the basis for the retrieved CO_2 information (Buchwitz et al. 2005a, 2007a, Bösch et al. 2006, Barkley et al. 2007, Reuter et al. 2010, Schneising et al. 2008). The CO_2 mixing ratio is obtained by normalising the CO_2 column with the simultaneously retrieved airmass from oxygen measurements (Schneising et al. 2008) or by using meteorological surface pressure (Barkley et al. 2007).

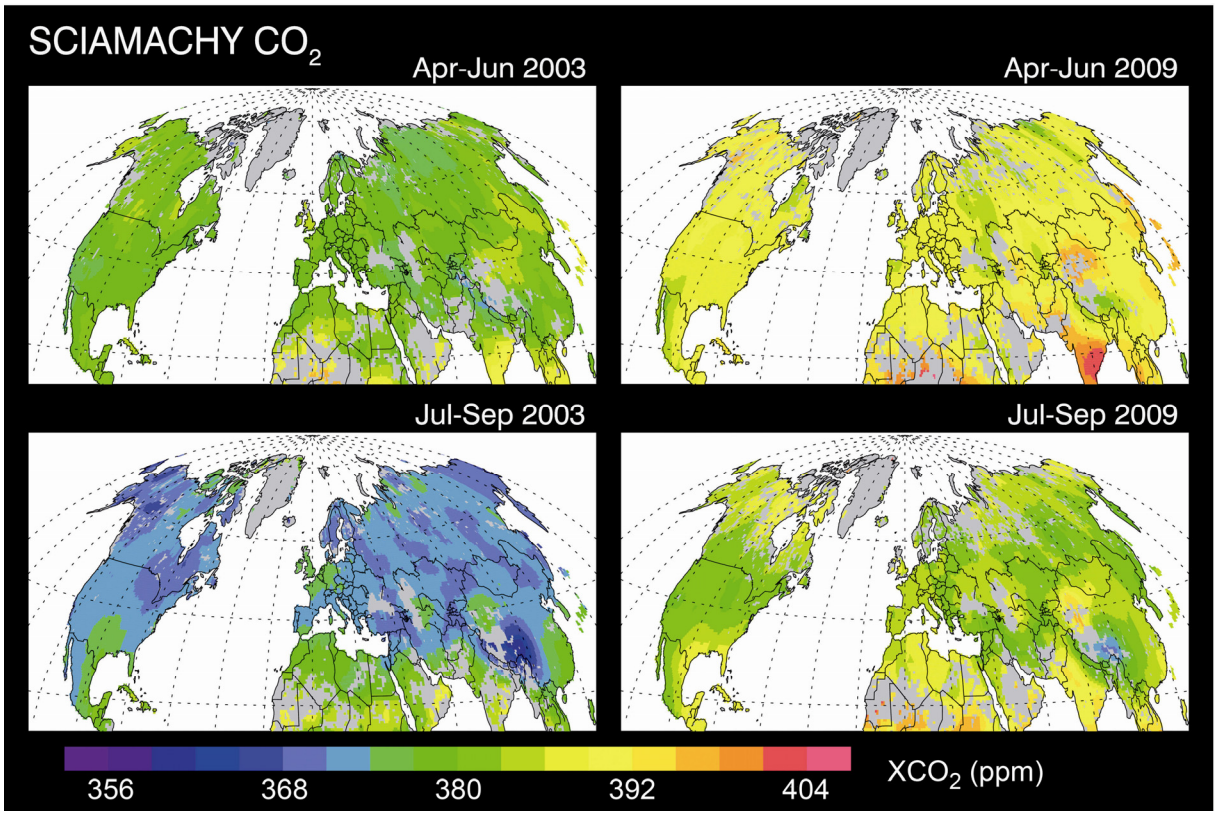

Fig. 10-1: Northern hemispheric CO_2 distribution as observed by SCIAMACHY. The differences between spring and summer are due to the CO_2 'breathing' of the vegetation. (Courtesy: M. Buchwitz, IUP-IFE, University of Bremen)

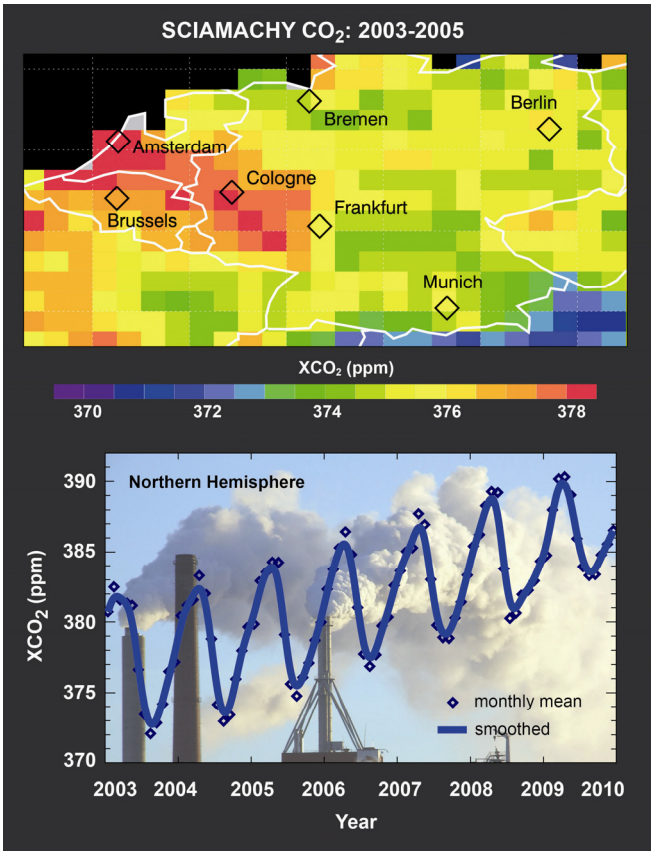

Fig. 10-2: Top: Elevated CO_2 (shown in red) as observed by SCIAMACHY over Central Europe's most populated Rhine-Main area. Bottom: Increase of Northern hemispheric CO_2 derived from SCIAMACHY measurements. (Courtesy: M. Buchwitz, IUP-IFE, University of Bremen)

Methane – CH_4

CH_4 is the second most important anthropogenic greenhouse gas next to CO_2. It is regulated by the Kyoto Protocol, as well. Compared to pre-industrial times, CH_4 concentrations have more than doubled due to anthropogenic activities. Although the total sum of all CH_4 sources, about 550 Tg/year, is relatively well known, the distribution among different source categories is highly uncertain and impedes our capability to reliably predict CH_4 source strengths in a warming climate.

First results from SCIAMACHY showed substantially higher tropical CH_4 abundances than previously estimated (Frankenberg et al. 2005). Even though these results were recently partially revised (Frankenberg et al. 2008), the fact that tropical emissions are very high, constituting about a third of all CH_4 emissions, remains true. In general, SCIAMACHY CH_4 retrievals have substantially matured and results from several independent studies (see also Buchwitz et al. 2005b, Schneising et al. 2009) draw a consistent picture of the global distribution of this greenhouse gas.

For CH_4, already improved emission estimates have been obtained on the basis of SCIAMACHY data. An atmospheric general circulation model, in which the current knowledge of global sources is implemented, is used to model the worldwide CH_4 distribution. The source terms in this model can be adjusted in magnitude, region and timing until the modelled distribution provides the best match with SCIAMACHY observations, thus obtaining *inverted* source estimates using satellite data (Meirink et al. 2008). Recent inversion studies (Bergamaschi et al. 2009) result in significant changes in the spatial patterns of emissions and their seasonality compared to the bottom-up inventories. Large CH_4 emissions are attributed to various wetland regions in tropical South America and Africa, seasonally varying and opposite in phase with CH_4 emissions from biomass burning. As obvious in Fig. 10-3, India, China and South East Asia are characterised by pronounced emissions from rice paddies peaking in the third quarter of the year, in addition to further anthropogenic emissions throughout the year.

Water Vapour – H_2O

Water is the key to the Earth's climate system. As vapour, it is the strongest greenhouse gas and as precipitation, it is the essential ingredient for making our planet habitable. Water vapour is a highly variable component of the atmosphere with direct anthropogenic impact on its amount being usually negligible. Its contribution may reach up to 4% of the atmospheric volume in the tropics and amounts to less than 1% in dry air conditions. Due to the relation between temperature and humidity, water vapour acts as a positive feedback to anthropogenic radiative forcing and is thereby indirectly affected by human activity.

In contrast to microwave instruments, SCIAMACHY water vapour data is available over both land and ocean down to the surface for at least partly cloud-free scenes. Because of their independence from other *in situ* or remote sensing measurements, SCIAMACHY water vapour columns provide a new important global dataset (Noël et al. 2004, Schrijver et al. 2009). A combination of SCIAMACHY water vapour with corresponding data derived from GOME and follow-on instruments allows the study of water vapour long-term trends now already spanning more than 15 years, with the potential of extension until 2020 when GOME-2 data on METOP is considered. Using linear and non-linear methods from time series analysis and standard statistics, the trends of H_2O columns and their errors have been derived from GOME and SCIAMACHY for the years 1996 to 2007 (Mieruch et al. 2008). The trends clearly show elevated water vapour levels in years of strong El-Niño activity. How these trends are distributed on a global scale is further demonstrated in Fig. 10-4. Increasing long-term trends in water vapour have been observed for Greenland, Eastern Europe, Siberia and Oceania, whereas decreasing trends occur for the northwest US, Central America, Amazonia, Central Africa and the Arabian Peninsula.

Heavy Water – HDO

When water evaporates from the Earth's oceans and surface, moves through the atmosphere and falls back as rain, evaporation and condensation processes change the content of heavy water (HDO). Therefore, the isotopic composition contains information about the history of water. SCIAMACHY's measurements permit obtaining a global view on the water vapour isotopic composition in the

atmosphere (Frankenberg et al. 2009). These are the first global isotope measurements with high sensitivity towards the lowest layers of the atmosphere down to the surface, where most of the water vapour resides. By exploiting the capability of SCIAMACHY to retrieve H_2O and its heavier isotopologue HDO, new insights into the hydrological cycle are provided. Fig. 10-5 presents the global distribution of the water isotope HDO shown as relative abundance of water vapour. High fractions of HDO are found in the tropics and sub-tropics where water evaporates from the oceans and is then transported towards the poles. The relative amount of heavy water in the remaining water vapour will be reduced as the heavy isotope rains out preferentially resulting in lower abundances at higher latitudes. The same occurs when moist air from the oceans travels over the continents as e.g. clearly seen in North America. The satellite data bear the potential to rigorously test and subsequently improve the description of such cycles in climate models. This will eventually even result in better predictions of the changes in the hydrological processes, e.g. drought and precipitation in a future climate.

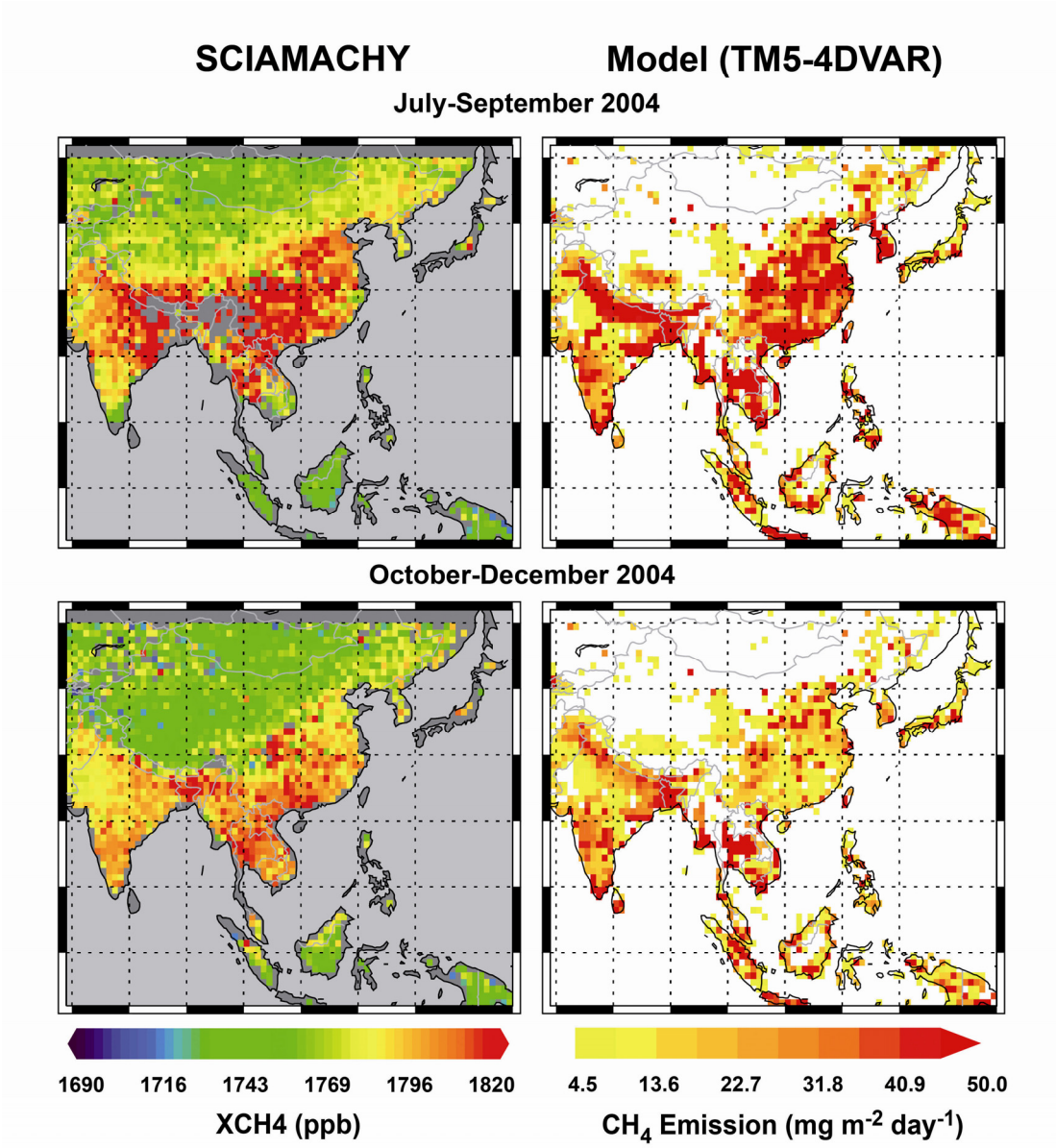

Fig. 10-3: Methane emission derived from SCIAMACHY data. Left column: Column-averaged CH_4 mixing ratios (XCH_4) over South-East Asia from SCIAMACHY for summer and autumn 2004. Right column: Modelled emissions per 1° × 1° grid cell. (Courtesy: adapted from Bergamaschi et al. 2009, reproduced by permission of American Geophysical Union)

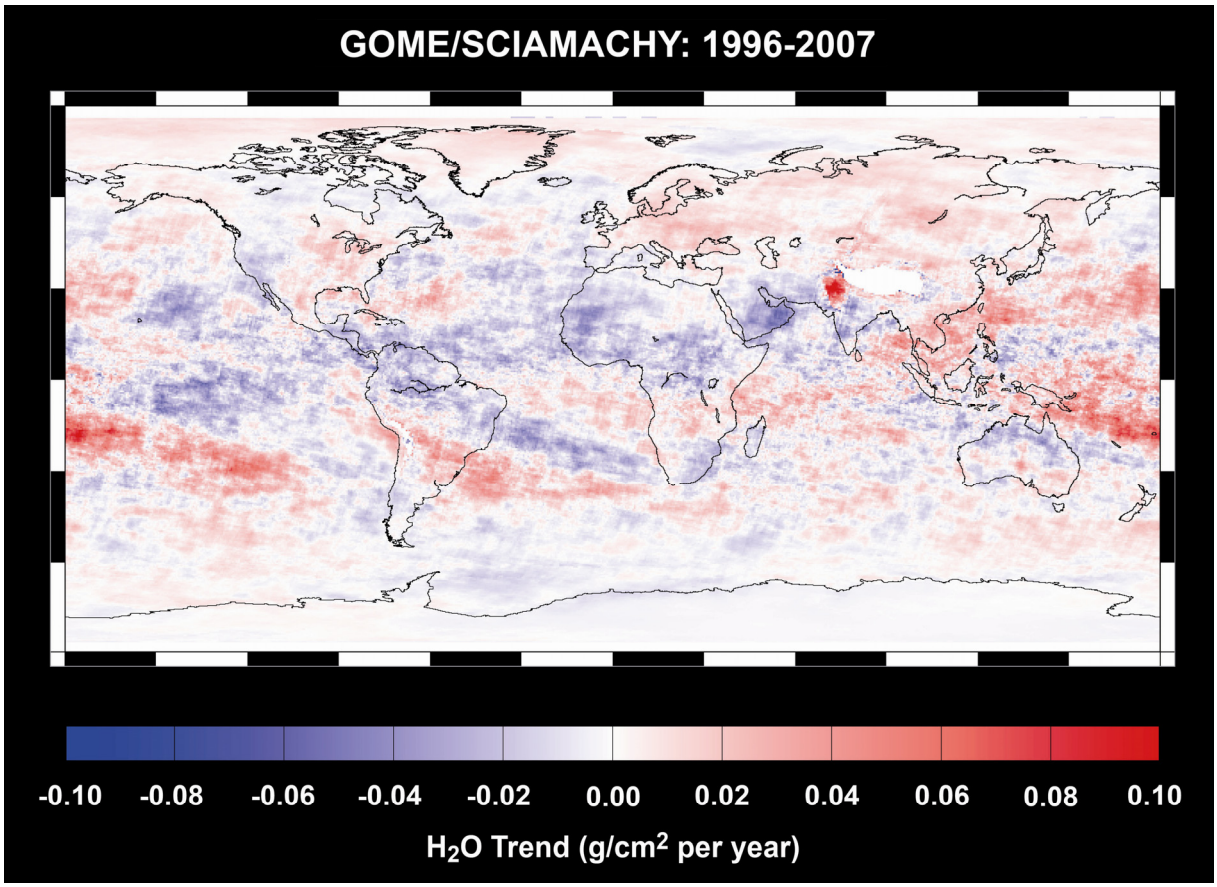

Fig. 10-4: Water vapour trends for 1996 to 2007 as derived from GOME and SCIAMACHY. (Courtesy: S. Mieruch, IUP-IFE, University of Bremen)

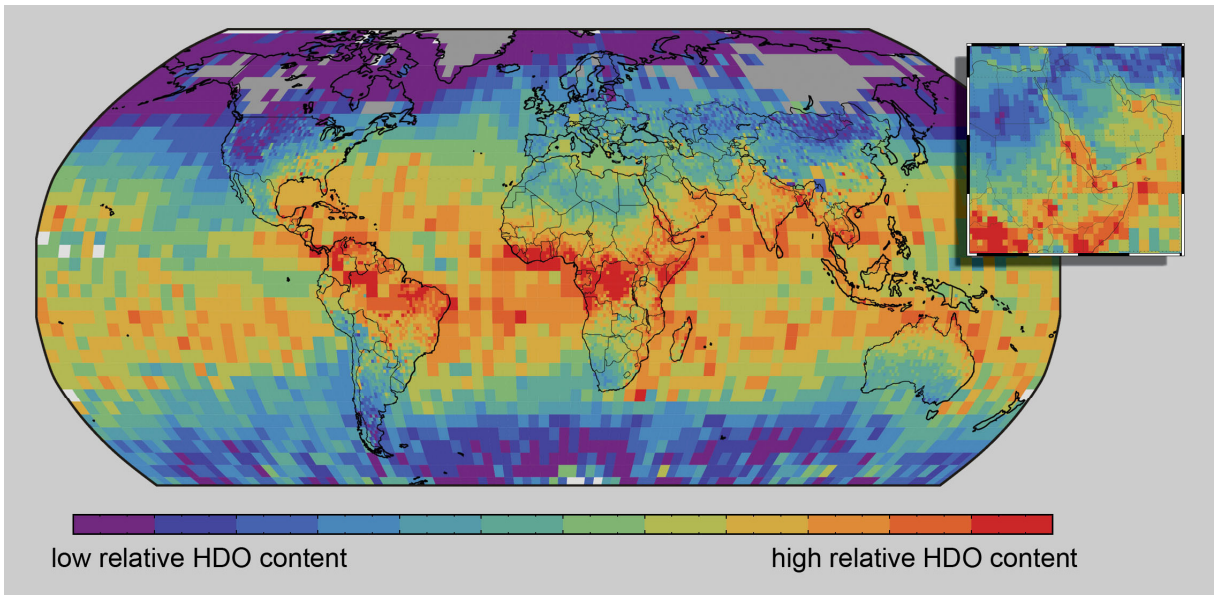

Fig. 10-5: Global distribution of the water isotope HDO shown as relative abundance of water vapour averaged between 2003 and 2005. The inset displays enhanced HDO fractions due to strong evaporation over the Red Sea (Courtesy: C. Frankenberg, SRON – now JPL)

Absorbing Aerosol Index and Precipitation

Water in the form of precipitation plays a dominant role in local climate and weather. This is particularly the case in Africa where the monsoon is the driving mechanism for the climate and therefore, also for the social and economical development. The northern part of Africa hosts large dry areas such as the Sahara and the Sahel. Dust storms arise frequently from the dry areas and have a profound impact on the weather conditions and lives of the local people. A linkage between the African monsoon systems and aerosol loading in Africa is suggested by the analysis of GOME and SCIAMACHY measurements. De Graaf et al. (2010) investigated multi-year satellite observations of UV-absorbing aerosols and compared these with precipitation data. The main UV-absorbing aerosol types occurring over Africa are desert dust and biomass burning aerosols. Their abundances can be characterised by using Absorbing Aerosol Index (AAI) data from GOME and SCIAMACHY. Time series of regionally averaged AAI from 1995 to 2008 show the seasonal variations of aerosols in Africa. When relating the zonally averaged daily AAI to monthly mean precipitation data, they indicate monsoon-controlled atmospheric aerosol loadings, which are different for the West African and East African monsoons owing to their different dynamics caused by the asymmetric distribution of land masses around the equator. Fig. 10-6 clearly shows that the seasonal variation of the aerosol distribution is linked to the seasonal cycle of the monsoonal wet and dry periods in both areas. During dry periods, the AAI varies freely, driven by emissions from deserts and biomass burning events. During wet periods the AAI depends linearly on the amount of precipitation due to scavenging of aerosols and the prevention of aerosol emissions from wet surfaces.

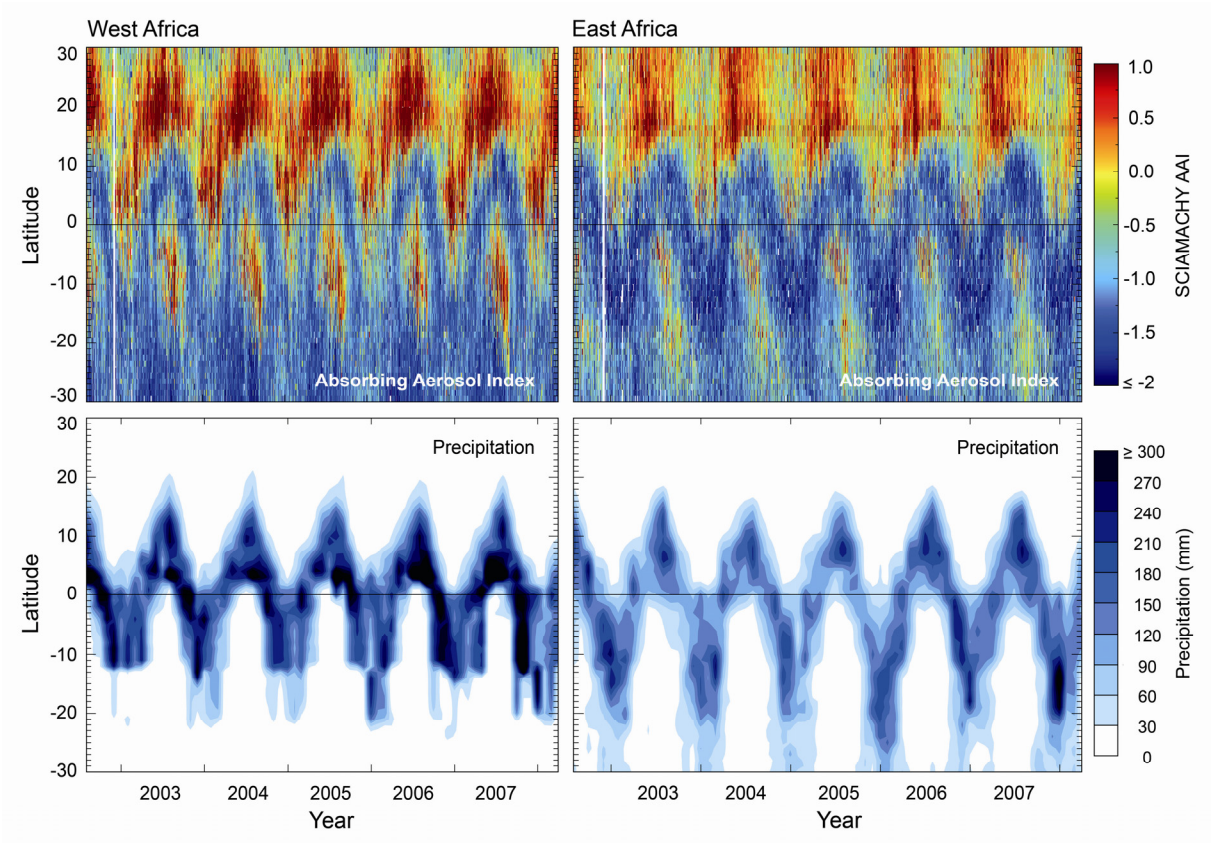

Fig. 10-6: Zonally averaged AAI from SCIAMACHY for each day between August 2002 and April 2008 as a function of latitude in Western and Eastern Africa (upper panels). The bottom panels display the monthly and zonally averaged precipitation for the same areas and the same period. (Courtesy: M. de Graaf, KNMI)

10.2 Tropospheric Composition – Reactive Gases

Emissions of greenhouse gases are not the only anthropogenic impact onto the lowest layer of the Earth's atmosphere. Pollution and air quality have become a major concern in an ever increasing industrialised world. SCIAMACHY is able to detect and monitor the global, regional and local signatures of trace gases contributing to air pollution and to follow how emissions evolve with time.

Nitrogen Dioxide – NO_2

NO_2 is an important indicator of air pollution and a cause of summer smog. NO_2 catalyses ozone production, contributes to acidification and also adds to radiative forcing. The main sources of NO_2 are anthropogenic in origin, e.g. power plants, vehicular traffic, forced biomass burning and both heavy and agricultural industry. Other but slightly less important sources comprise natural biomass burning, lightning and microbiological soil activity. NO_2 emissions have increased by more than a factor of 6 since pre-industrial times, with concentrations being highest in large urban areas.

Global monitoring of tropospheric NO_2 emissions is a crucial task. SCIAMACHY's predecessor GOME has already demonstrated the unique ability to monitor tropospheric air pollution. Fig. 10-7 shows a global survey of tropospheric NO_2 as seen by SCIAMACHY. The inset in Fig. 10-7 presents a time series of these concentrations over China. The periodic trend in NO_2 columns each year can mainly be explained by seasonal variations in energy consumption while the overall increase in tropospheric NO_2 over China is a result of the increase in industrial activity (Richter et al. 2005a). The inset also demonstrates how well SCIAMACHY matches with GOME and GOME-2. NO_2 vertical columns of both instruments perfectly overlap around the turn of the year 2002 and from 2007 onwards.

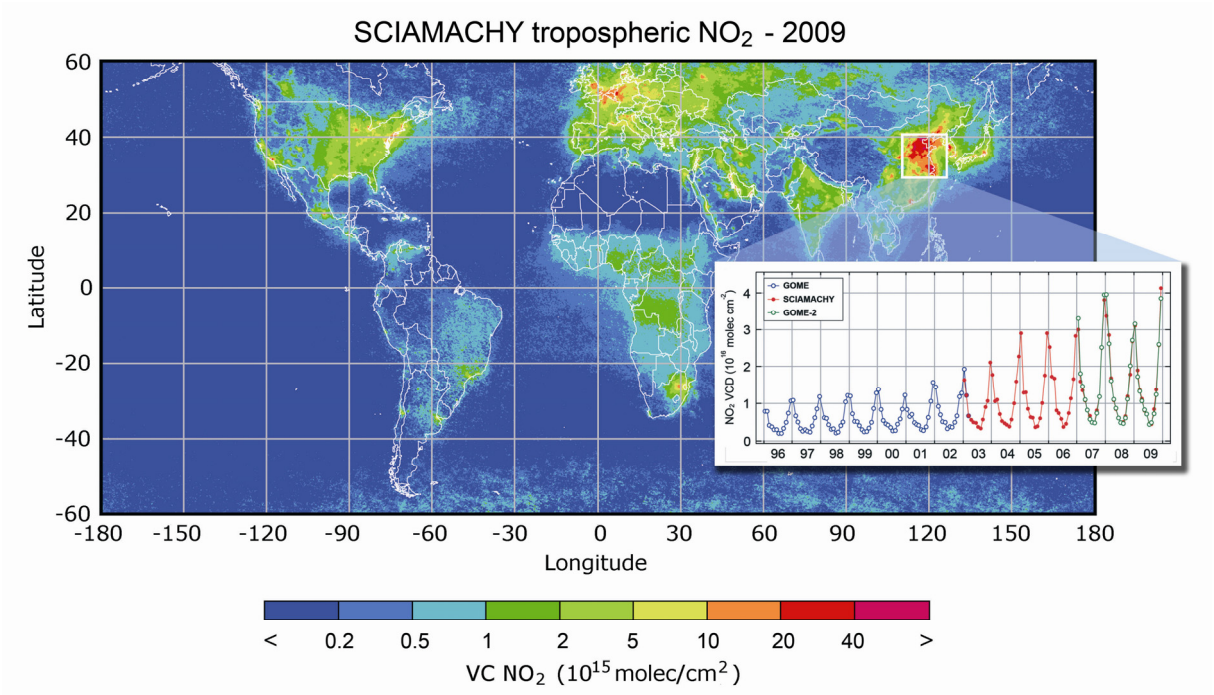

Fig. 10-7: Global survey of tropospheric vertical column (VC) NO_2 for 2009. Clearly visible are the industrialised regions in the northern hemisphere and the regions of biomass burning in the southern hemisphere. The inset illustrates how NO_2 concentrations have risen in China from 1996-2009. The trend analysis uses data from GOME (1996-2002) and SCIAMACHY (2003-2009). While 'old' industrialised countries were able to stop the increase of NO_2 emissions, the economical growth in China turns out to be a strong motor for pollution. (Courtesy: A. Richter, IUP-IFE, University of Bremen)

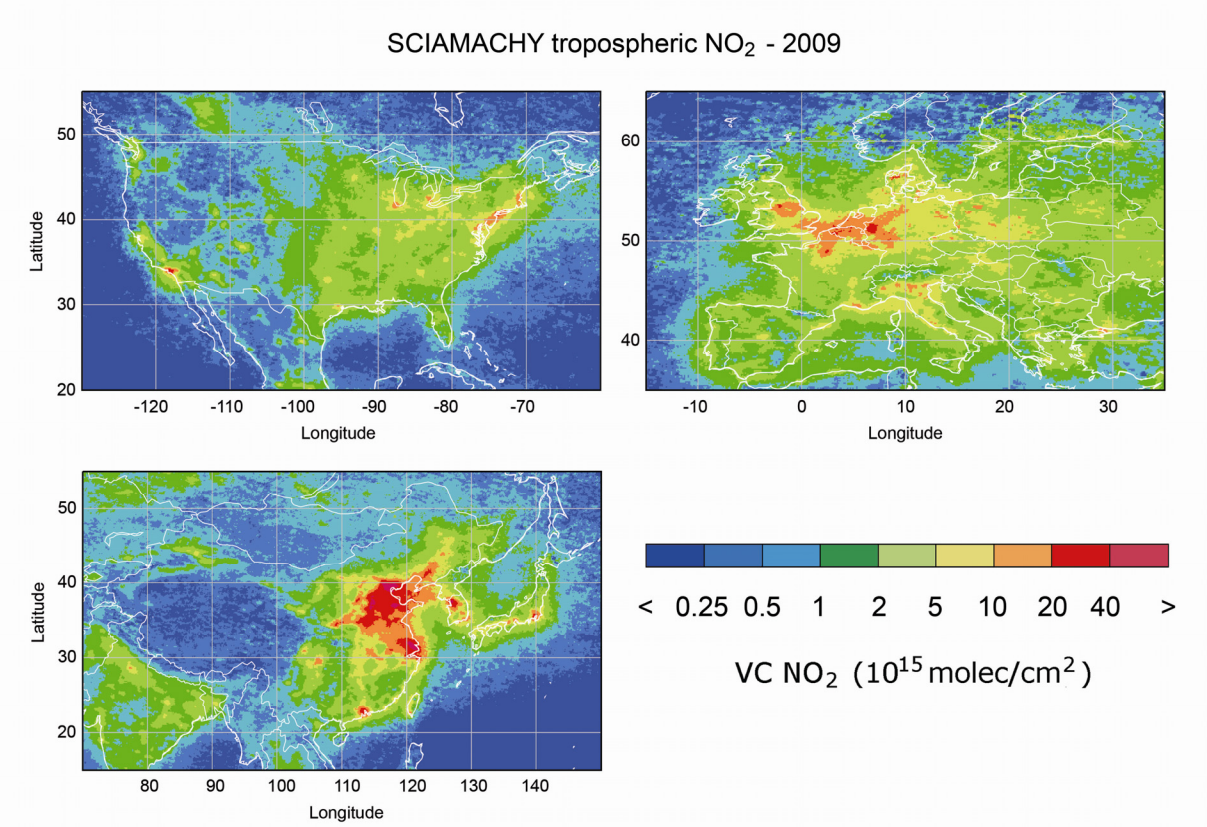

Fig. 10-8: Mean tropospheric vertical column (VC) NO_2 densities over Europe, the United States and China in 2009. (Courtesy: A. Richter, IUP-IFE, University of Bremen)

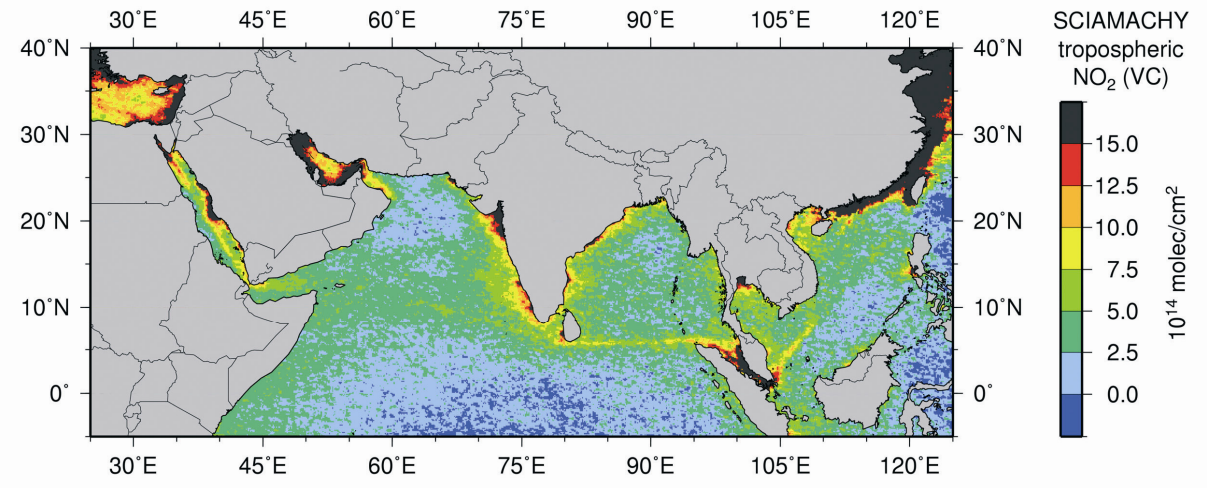

Fig. 10-9: NO_2 densities over the Indian Ocean and the Red Sea as derived from measurements between August 2002 and April 2004. Ship routes from Eastern Asia to the Suez Canal can be clearly seen. Along the industrialised coast lines, strong NO_2 concentrations are related to urban areas. (Courtesy: A. Richter, IUP-IFE, University of Bremen)

Due to its higher spatial resolution (60 km × 30 km as compared to 320 km × 40 km for GOME), SCIAMACHY enables very detailed observations of polluted regions. This is obvious in Fig. 10-8 where industrialised regions of North America, Europe and China are displayed. As a result of these new datasets, individual cities (Beirle et al. 2004) and even large power plants (Kim et al. 2009) can be identified. Similar small scale structure in NO_2 emissions can also be detected over the oceans. The high sensitivity and spatial resolution of the SCIAMACHY measurements permits localising

frequently used ship routes (Richter et al. 2004), as illustrated in Fig. 10-9. Using data from GOME, SCIAMACHY and GOME-2, Franke et al. (2009) could even derive temporal changes in these 'tiny' signatures of anthropogenic activity.

Particularly interesting are studies concerning the global trend in NO_2 concentrations (Richter et al. 2005a, Stavrakou et al. 2008, van der A et al. 2008). By combining SCIAMACHY results with those of previous missions, e.g. GOME, it is possible to investigate how the tropospheric NO_2 load has changed over the past decade. A strong increase in nitrogen dioxide is observed by SCIAMACHY in countries and areas with a booming economy, particularly in China (see inset Fig. 10-7), while in Europe, SCIAMACHY has observed a stabilisation of NO_2 levels which is attributed partly to slightly increased traffic emissions after a period of reducing nitrogen dioxide levels in the 1990's as a result of EU regulations. For the US, SCIAMACHY results indicate a decrease in NO_2 emissions related to the recent implementation of pollution controls for power plants (Kim et al. 2006).

The spatial and temporal characteristics of a multi-year dataset provides much improved constraints for attempts to identify main emission sources and to quantify emission strengths by inverse modelling. It also facilitates the derivation of independent top-down estimates of emissions not only on a country-by-country basis but even on regional scales. Konovalov et al. (2008, 2010) investigated such trends within Europe for a 10 year time period showing that while emissions are decreasing in many countries, emissions have increased especially in the Mediterranean area, along the coastlines, as well as in Eastern Europe. Van der A et al. (2008) analysed the spatial and temporal patterns in a multi-year dataset of GOME and SCIAMACHY tropospheric NO_2 and identified the most dominating emission sources (Fig. 10-10) from this data. Whereas in the northern hemisphere, the NO_2 mainly stems from anthropogenic sources and from soils, biomass burning is the dominating origin of tropospheric NO_2 in the southern hemisphere.

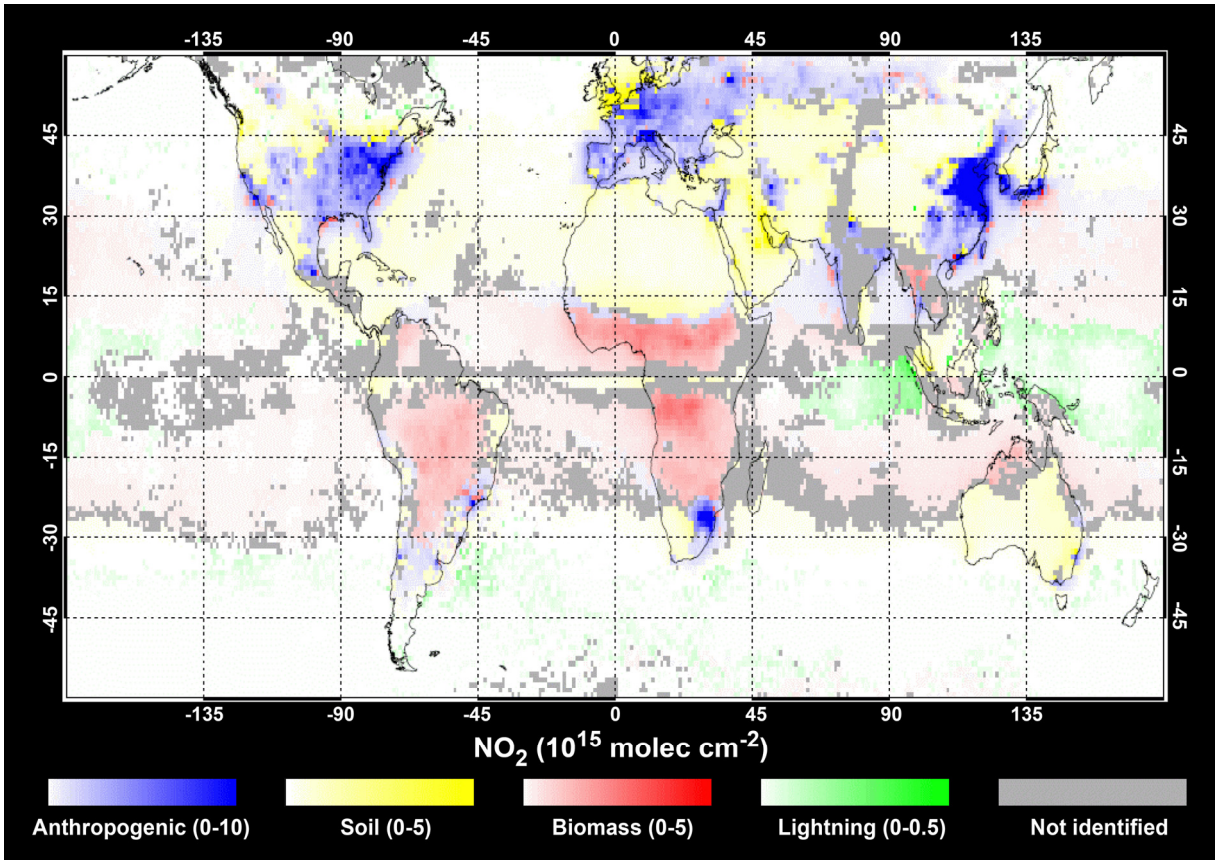

Fig. 10-10: Dominant NO_x source identification based on analyses of the time series of measured tropospheric NO_2 from GOME and SCIAMACHY satellite observations (1996-2006). (Courtesy: van der A et al. 2008, reproduced by permission of the American Geophysical Union)

By combining SCIAMACHY NO_2 observations at 10:00 local time with NO_2 observations from OMI at 13:30 local time, it even becomes possible to get a first glimpse on the diurnal variations of tropospheric chemistry and emissions from space. These measurements suggest a decrease in tropospheric NO_2 between 10:00 and 13:30 over fossil fuel source regions due to photochemical loss. Over tropical biomass burning regions, the opposite effect – an increase due to a midday peak in emissions - is obvious (Boersma et al. 2008).

Sulphur Dioxide – SO_2

SO_2 is another pollutant leaving a clear absorption signature in SCIAMACHY spectra. Sources of SO_2 are combustion of sulphur rich coal and other fossil fuels or volcanic eruptions including degassing. Although SO_2 emissions have been reduced significantly over the last decades, clear signals can be detected over the Eastern US and, in particular, the polluted areas of China (Fig. 10-11). As in the case of NO_2, the high spatial resolution facilitates source identification and makes the dataset an interesting new data source for air pollution research. By combining GOME and SCIAMACHY results, the long-term trend of SO_2 emissions in heavily polluted areas can be inferred and compared with similar analyses for NO_2 (see inset of Fig. 10-11).

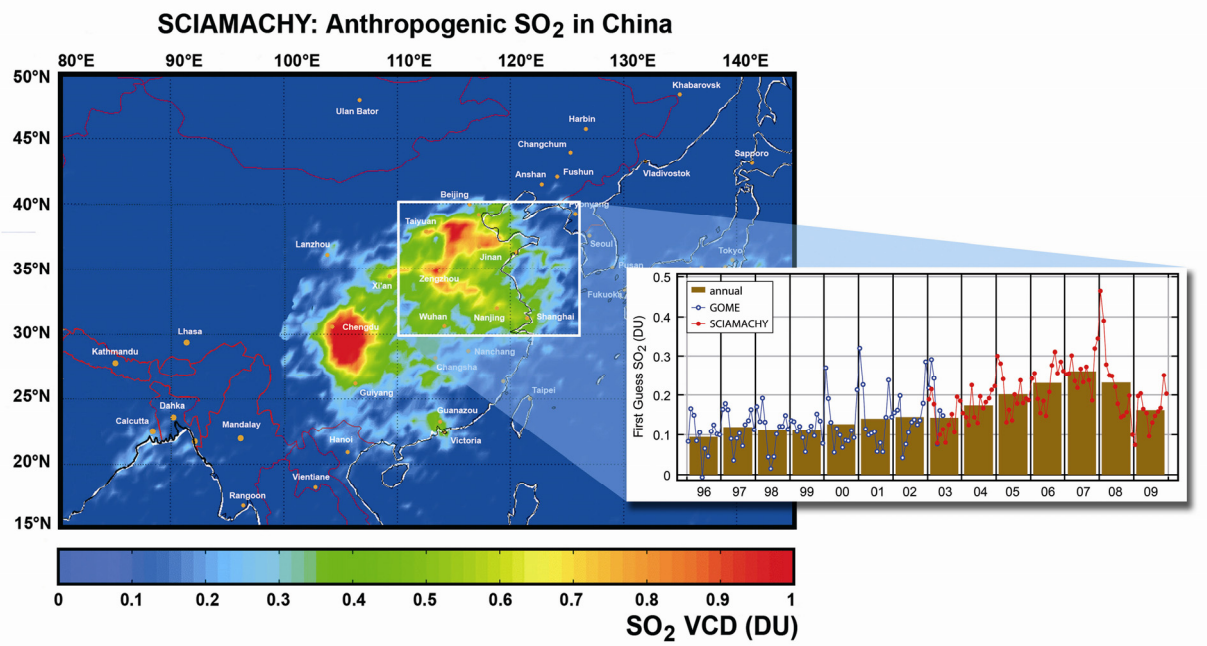

Fig. 10-11: Average SO_2 vertical column densities (VCD) over eastern China during the year 2003. SCIAMACHY's improved spatial resolution permits to identify localised emissions due to anthropogenic activities. The trend analysis uses data from GOME (1996-2002) and SCIAMACHY (2003-2009). (Courtesy: map – M. Van Roozendael, BIRA-IASB; trend – A. Richter, IUP-IFE, University of Bremen)

Volcanoes are a natural source of SO_2. Since the start of SCIAMACHY's routine observations, a few of the several hundred existing active volcanoes have been erupting and were overpassed by ENVISAT. In October 2002, Mt. Etna on the island of Sicily entered an explosive phase. The rectangular overlay in Fig. 10-12 represents a SCIAMACHY nadir measurement displaying SO_2 emissions which match well with the ash plume visible on an image simultaneously obtained by MERIS on ENVISAT. The SO_2 emissions of volcanic eruptions are usually associated with such volcanic ash plumes. These could be a major threat for air traffic. Therefore, SCIAMACHY SO_2 retrievals are used in early warning services in support of aviation control. Whenever elevated SO_2 densities are obtained in regions with known volcanoes, an alert is issued indicating a potential volcanic ash cloud.

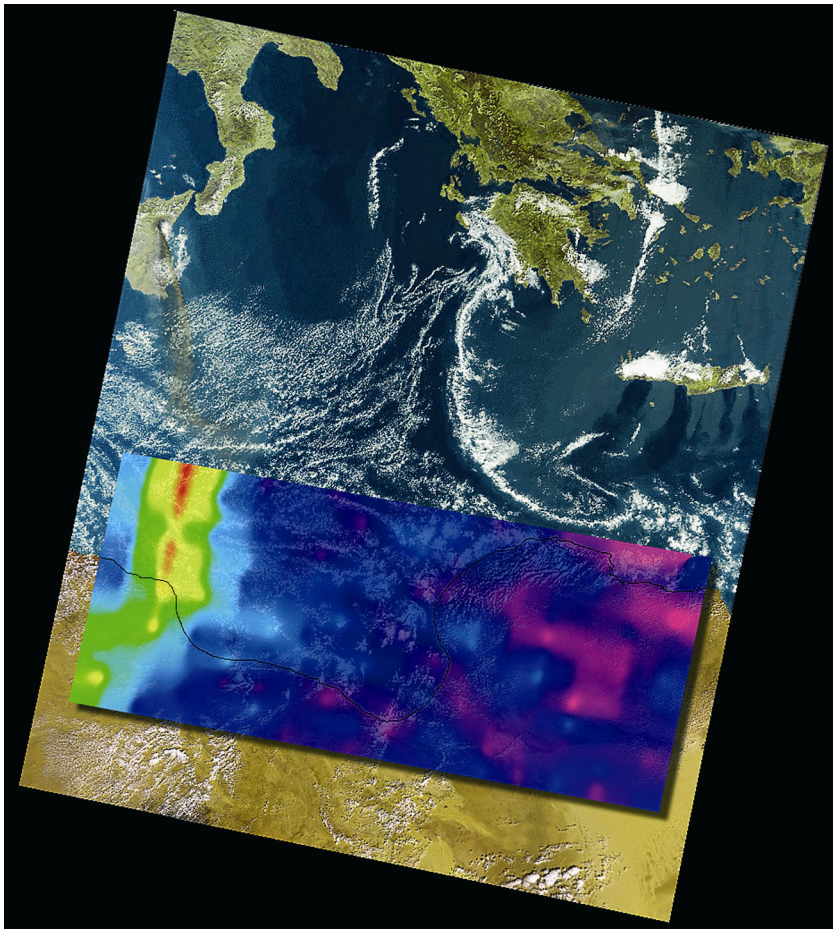

Fig. 10-12: The Mt. Etna volcanic eruption in 2002 with obvious SO_2 emissions (reddish plume). The SCIAMACHY nadir measurement is overlayed on a MERIS image showing that the plume of SO_2 and the visible ash cloud match well. (Courtesy: ESA and Brockmann Consult)

Formaldehyde (HCHO) and Glyoxal (CHOCHO)

In the presence of nitrogen oxides, the photochemical degradation of volatile organic compounds (VOC) leads to secondary gaseous and particulate products, such as ozone and secondary organic aerosols (SOA). Both are important contributors to air pollution with severe impacts on human health, ecosystems, and regional climate. Two important intermediate products in the oxidation of volatile organic compounds are HCHO and CHOCHO. Since both trace gases have short lifetimes, their distribution mainly resembles the source areas and can be used as indicators of tropospheric VOC emissions. SCIAMACHY's capability to measure HCHO and CHOCHO from space on a global scale was demonstrated by Wittrock et al. (2006). Since then, several studies have been carried out using these data to compare directly with the output from chemical transport models (CTM) and thereby substantially improving the models' accuracy and reliability. In addition, VOC emission strengths have been derived for biospheric, pyrogenic and anthropogenic sources, respectively.

A consistent dataset of global tropospheric HCHO (Fig. 10-13) has been created by De Smedt et al. (2008) using GOME and SCIAMACHY data covering more than a decade. This dataset has been utilised by Stavrakou et al. (2009) to evaluate the performance of pyrogenic and biogenic emission inventories and to investigate trends in HCHO overAsia and large cities worldwide (De Smedt et al. 2010). More regional aspects on the different emissions strengths of VOC based on HCHO data were investigated for Europe (Dufour et al. 2009) and Amazonia (Barkley et al. 2009). In general, for regions with high biogenic emissions like tropical rainforests, a reasonable agreement was found between modelled and measured HCHO columns. Other areas having more variable or less emissions of VOC reveal higher discrepancies. Recently, Marbach et al. (2009) even succeeded in determining HCHO emissions from ships in the Indian Ocean.

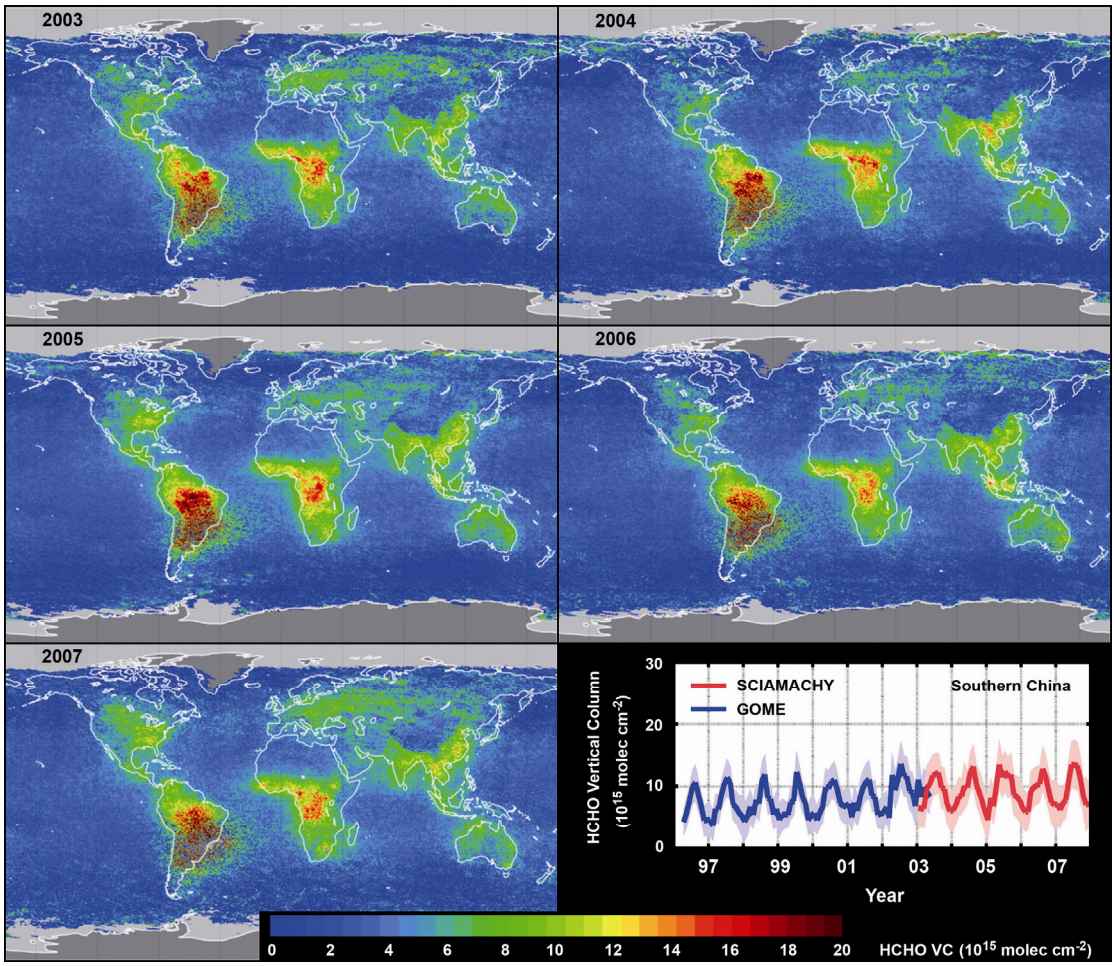

Fig. 10-13: Yearly averaged SCIAMACHY HCHO vertical columns from 2003-2007. The HCHO trend over China is indicated in the bottom right panel,. (Courtesy: adapted from De Smedt et al. 2008)

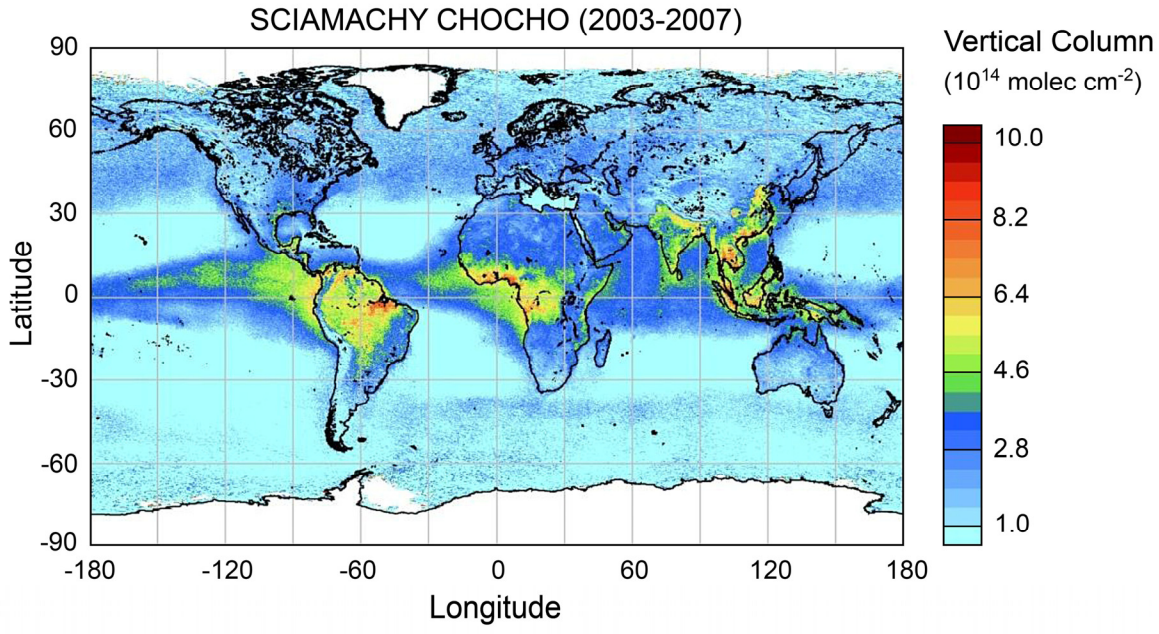

Fig. 10-14: Multiannual (2003-2007) SCIAMACHY CHOCHO vertical columns. The largest amounts are found over the tropics and sub-tropics where vegetation and biomass burning is abundant. (Courtesy: Vrekoussis et al. 2009)

Myriokefalitakis et al. (2008) adapted a global chemistry-transport model to simulate the temporal and spatial distribution of CHOCHO columns in the global troposphere focussing on the anthropogenic contribution. They found indication for a missing CHOCHO source of about 20 Tg/ year or an overestimate of its sinks by the model. In addition, Fu et al. (2008) examined the potential of CHOCHO as a source of secondary organic aerosol. Apparently, irreversible uptake of CHOCHO by aqueous aerosols and clouds could make a significant contribution to the global SOA production. The long SCIAMACHY time series also revealed seasonal and year-to-year variability above several photo-chemical hot spots. This has been studied by Vrekoussis et al. (2009) for CHOCHO (Fig. 10-14). For the period 2002-2007, a significant annual increase in CHOCHO in addition to a seasonal cycle was reported over northeastern Asia. In general, the regions influenced by anthropogenic pollution encounter enhanced amounts of CHOCHO.

Carbon Monoxide – CO

CO plays a central role in tropospheric chemistry because it is the leading sink of the hydroxyl radical, which itself determines the oxidising capacity of the troposphere to a large extent. Therefore, CO is of prime importance for the troposphere's self-cleansing efficiency and for the concentration of greenhouse gases such as CH_4. CO also has a large impact on air quality because it is toxic and is a precursor of tropospheric ozone, a secondary pollutant which is associated with respiratory problems and decreased crop yields.

CO detection with SCIAMACHY is an ambitious task. Carbon monoxide vertical columns can be retrieved from a number of CO absorption lines located around 2.3 μm in the SWIR range. The retrieval is not straightforward because these lines are relatively weak, much weaker than the absorption structures of the overlapping absorbers water vapour and CH_4. In addition, CO retrieval is hampered by a number of calibration issues that are mainly related to large variable dark signals and changing instrument characteristics as a result of the growth of an ice layer on the channel 8 detector (e.g. Gloudemans et al. 2005). Nevertheless, a first survey of global CO over land had been performed which shows elevated CO in the case of fires due to biomass burning. These results are consistent with MOPITT and model predictions to a large degree (de Laat et al. 2006, Buchwitz et al. 2007b). Gloudemans et al. (2009) also succeeded in deriving CO over the ocean, when using scenes with low maritime clouds. This yielded a five-year CO dataset over both land and clouded ocean scenes between 2003 and 2007 (Fig. 10-15). The CO measurements over clouded ocean scenes have been compared with co-located modelled CO columns over the same clouds and agree well. Using clouded ocean scenes quadruples the number of useful CO measurements compared to land-only measurements. The five-year dataset shows significant inter-annual variability over land and over clouded ocean areas, like Asian outflow of pollution over the northern Pacific, biomass-burning outflow over the Indian Ocean originating from Indonesia, and biomass burning in Brazil. In general, there is good agreement between observed and modelled seasonal cycles and inter-annual variability.

Besides the global CO view, SCIAMACHY also allows to investigate CO over urban areas (Buchwitz et al. 2007b), as illustrated in Fig. 10-16. This information helps to constrain local to regional emission estimates and air quality studies. Assimilation of SCIAMACHY CO data was also used to improve CO emission estimates in the Middle East (Tangborn et al. 2009). One remarkable result is the finding that CO emissions over Dubai have more than doubled in 2004 compared to those in the available emissions inventory based on data from 1998.

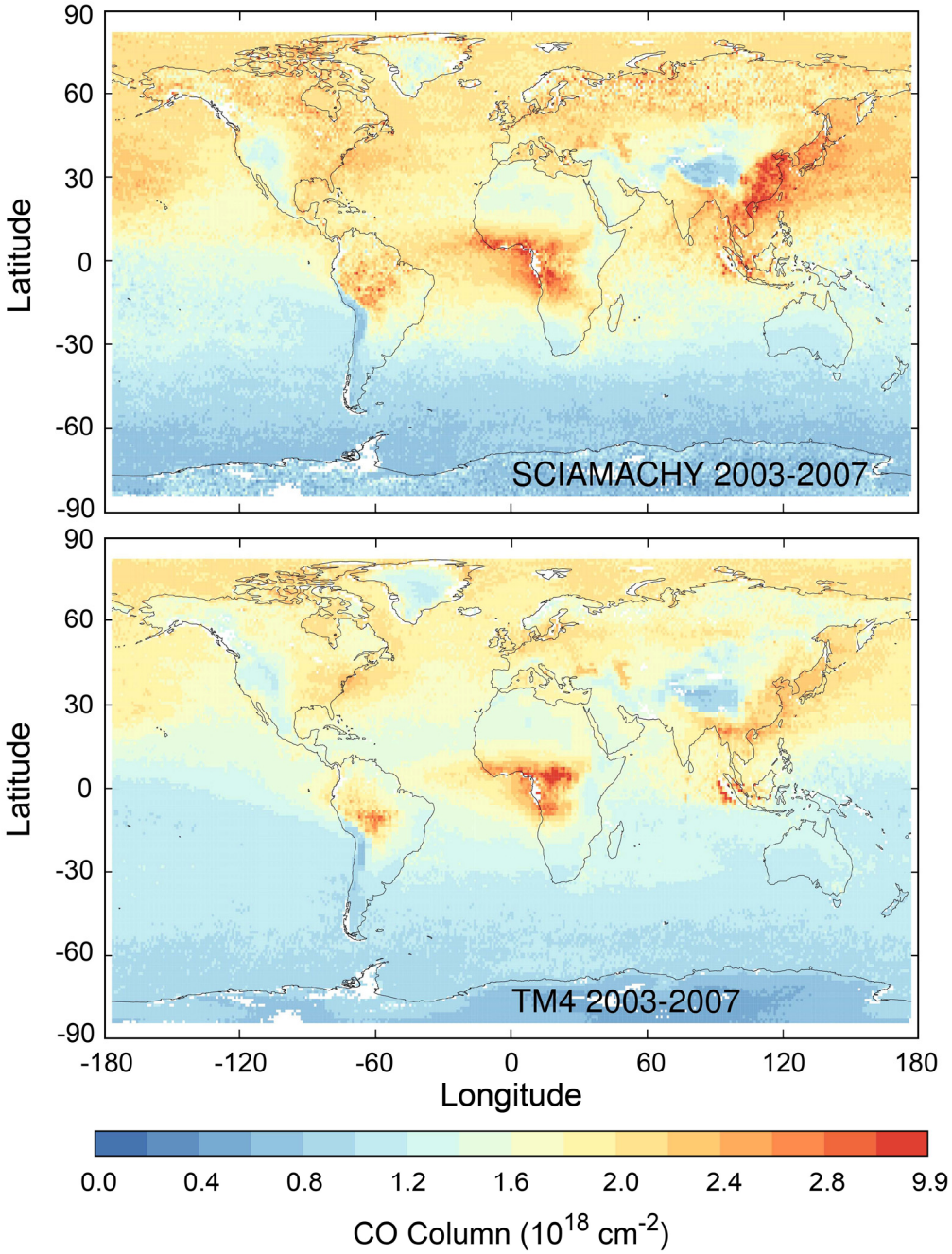

Fig. 10-15: Five year (2003-2007) average CO total columns on a 1° × 1° grid as retrieved by SCIAMACHY (top) and the TM4 chemistry-transport model (bottom). The SCIAMACHY CO columns above low clouds over sea are filled up with TM4 CO densities below the cloud to obtain total columns (Courtesy: Gloudemans et al. 2009)

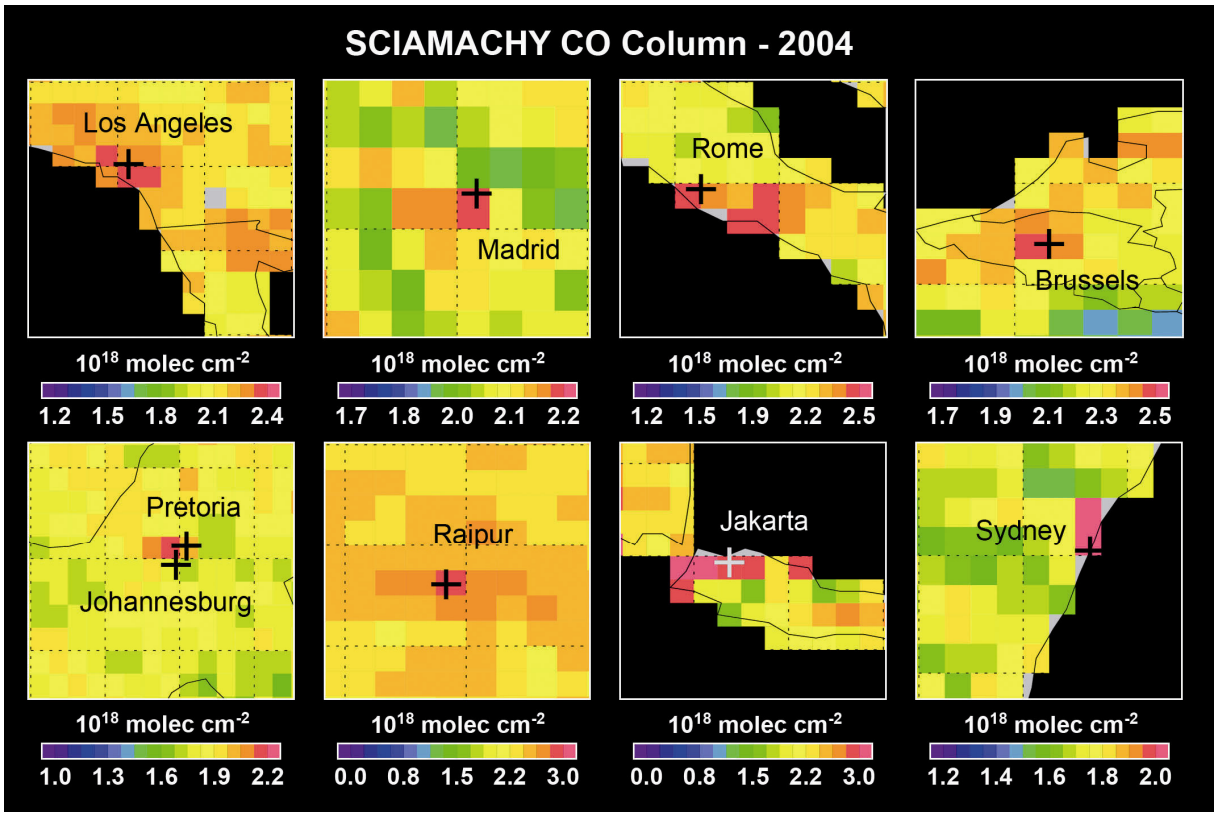

Fig. 10-16: A variety of urban areas as detected in SCIAMACHY CO data in 2004. (Courtesy: M. Buchwitz, IUP-IFE, University of Bremen)

Tropospheric Halogen Oxides – BrO and IO

BrO and IO are reactive halogen radicals which have gained growing interest in recent years (Simpson et al. 2007). Both compounds impact on tropospheric chemistry. They react with ozone and change the oxidation pathways of several atmospheric species. Bromine compounds have been identified as initiator of strong boundary layer ozone depletion events in polar spring (Barrie et al. 1988). The IO molecule constitutes the starting point for iodine nucleation and the formation of fine aerosol particles, which affect the atmospheric radiation balance and which may potentially grow to cloud condensation nuclei (O'Dowd et al. 2002). Widespread plumes of enhanced BrO are regularly observed in the Arctic, as well as in the Antarctic, shortly after polar sunrise where they persist for several months. The spatial distributions and locations of these plumes move rapidly on a daily basis (Begoin et al. 2010), with the BrO probably not only being situated in the boundary layer but also at higher altitudes. A strong link exists between the BrO patterns and sea ice cover. Sources of BrO are most likely of inorganic nature. Current discussions consider young sea ice, frost flowers, aerosols and brine (Kaleschke et al. 2004; Piot and von Glasow, 2008).
Recent analyses of SCIAMACHY nadir observations using spectral data around 420 nm have enabled the detection of tropospheric IO columns (Saiz-Lopez et al. 2007, Schönhardt et al. 2008). IO amounts are small and close to the instrument's detection limit, but through efficient reaction cycles, even these small amounts still have a considerable impact on the polar tropospheric chemistry. A variety of details in the temporal and spatial distribution of both IO and BrO over the Antarctic polar region is revealed in Fig. 10-17. Monthly means from October through austral summer until March are shown, in each case data is averaged over four subsequent years. As for BrO, largest amounts of IO appear in Antarctic spring time. Besides this general similarity, spatial distributions are quite different. BrO is observed predominantly above sea ice regions during spring, and furthermore along coast lines and on shelf ice regions in summer. Abundances vanish towards autumn. IO, however, shows larger variability throughout the time series. Regions with enhanced IO include the sea ice, ice shelves, coast lines, but also the continent (in October). Enhanced IO above the sea ice in the characteristic ring-like

pattern only occurs much later in spring (November) in contrast to BrO, where enhancements can already be observed in August well before the time period illustrated in Fig. 10-17. When southern autumn approaches, IO concentrations begin to increase again. While BrO behaves similarly on both hemispheres, no widespread enhanced IO abundances are observed in the Arctic spring time.

The details of the spatial and temporal patterns of IO in comparison to BrO are not well understood yet. However, the observed differences in the distributions suggest that the two halogen oxides are released by different processes. While the BrO is produced by inorganic emissions and the bromine explosion cycle, it is an open question whether the majority of IO is of biological origin. The cold Antarctic waters show high biological activity, and cold water diatoms may produce organic iodine species. Considerable differences between the South and North Polar regions might be linked to the fact that the biospheres are distinct and are emitting iodine compounds in different amounts and speciation.

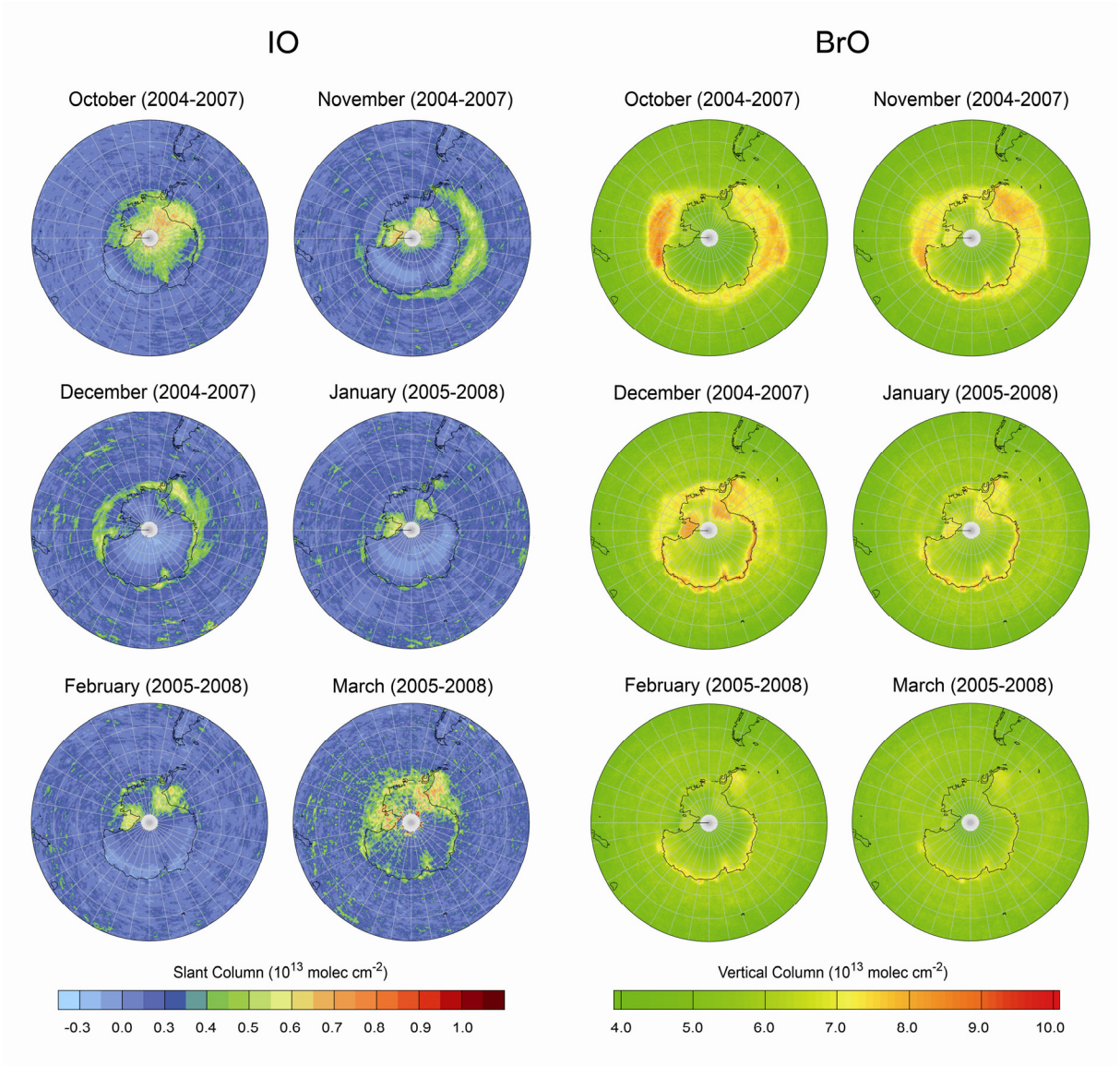

Fig. 10-17: Monthly maps of SCIAMACHY observations of IO (left) and BrO (right), averaged over four subsequent years from 2004-2008. A stratospheric air mass factor (AMF) is applied to the BrO columns only, leaving the patterns of IO and BrO still comparable. (Courtesy: A. Schönhardt, IUP-IFE, University of Bremen)

10.3 The Stratospheric Ozone Layer

As early as the second half of the 20th century, the stratosphere was seen as fragile to human perturbation. Public interest grew even more with the detection of the Antarctic ozone hole in the mid-1980's. Until the mid 1990s, a steady decrease of up to 3-6% per decade in the ozone abundance has been observed over the South Pole, North Pole and the mid latitudes. The most striking feature is the massive loss of stratospheric ozone over Antarctica every southern spring. This ozone loss is so large because very low stratospheric temperatures over Antarctica in wintertime foster the underlying depletion processes. The polar vortex isolates the air during the polar night and allows the cold conditions to remain stable and Polar Stratospheric Clouds (PSC) to grow (Fig. 10-18). In this environment the chemistry of ozone depletion begins with the conversion of reservoir species to chemically active molecules on the surface of the PSC. These react with ozone in catalytical reaction cycles resulting in the effective destruction of the O_3 molecules. In addition, ozone loss was also observed in the tropics and mid-latitudes. Today, there is broad agreement that a continuous monitoring of stratospheric ozone, the ozone hole and of those species impacting the ozone chemistry is necessary in order to detect possible signs of recovery, and to find out how far the cooling of the stratosphere and the strengthening of the Brewer-Dobson circulation as a consequence of climate change will delay or accelerate the recovery of the ozone layer (Rex et al. 2006, Newman et al. 2007).

Fig. 10-18: Polar Stratospheric Clouds over Southern Norway in January 2003, taken from the NASA DC-8 aircraft at an altitude of 11 km. The PSC hover well above the tropospheric cloud cover. (Photo: P. Newman, NASA/GSFC)

SCIAMACHY allows exploitation of new opportunities using the limb backscatter, as well as solar or lunar occultation measurement modes, to determine PSC and vertically resolved concentration profiles of trace gases in the stratosphere, in addition to the established column measurements from the nadir mode.

Ozone – O_3

The important role of ozone in the Earth's atmosphere is attributed to the fact that it absorbs solar UV radiation which would otherwise reach the surface where it can cause damage to the biosphere. In the wavelength range below 290 nm, UV photons are almost completely blocked. Radiation from 290 nm to 320 nm is strongly attenuated so that dose levels on ground become harmless. Ozone does not only impact conditions at the bottom of the troposphere but also in the upper atmosphere through the effects of absorption of UV to IR radiation and subsequent heating. The heating produces a temperature profile which makes the stratosphere vertically stable. Even transport mechanisms in the layers above – the mesosphere and thermosphere – were found to be influenced by the energy content of the stratosphere.

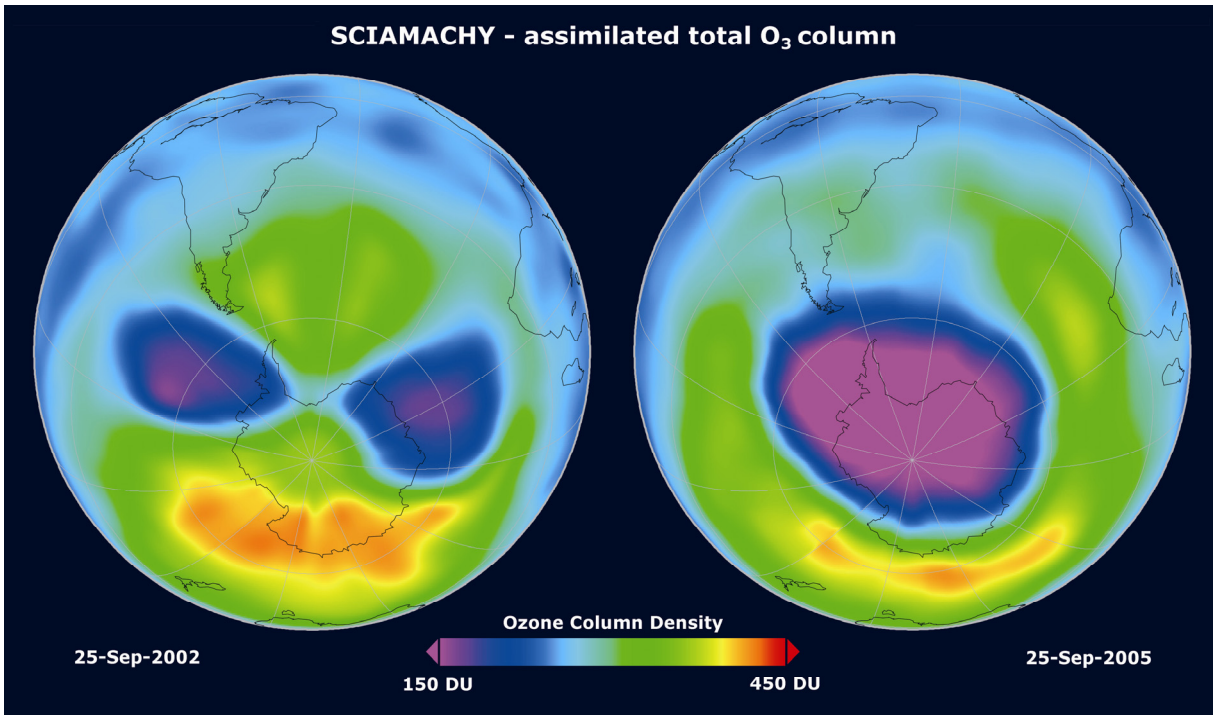

Fig. 10-19: The Antarctic ozone hole in 2002 (left) and 2005 (right). SCIAMACHY total column ozone measurements from 25 September have been analysed with the ROSE assimilation model to generate this view. Due to meteorological conditions, the hole was split and reduced in size in 2002 but appeared 'as normal' in 2005. (Courtesy: T. Erbertseder, DLR-DFD)

In the year of ENVISAT's launch, the ozone hole over Antarctica differed significantly from what had been observed before and after. Its extent was reduced in 2002 by 40% as compared to previous years (Fig. 10-19). However, this did not indicate a recovery of the ozone layer but was actually caused by peculiar meteorological conditions where an unprecedented major stratospheric warming led to a split-up of the polar vortex, thereby interrupting the heterogeneous processes that usually lead to massive ozone destruction. A more detailed view of this September 2002 event was obtained by retrieving stratospheric profiles over Antarctica (von Savigny et al. 2005a). The vertically resolved SCIAMACHY limb measurements showed that the ozone hole split did not occur throughout the entire stratosphere but only above about 24 km. At 20 km there was still a single elongated area with low O_3 values (Fig. 10-20). In normal cold Antarctic winters, however, the O_3 profiles display a more regularly shaped ozone hole throughout the altitude range, as depicted for 2005 in Fig. 10-20. The anomalous ozone hole in 2002 also developed quickly in time. Ozone losses computed from assimilated concentrations indicate that the situation changed drastically within a few days (Fig. 10-21). This ozone hole split-up was already predicted in the 9-day ozone forecast at KNMI (see Eskes et al. 2005). The following years displayed again an ozone hole similar in size to those observed by SCIAMACHY's predecessor GOME (see Fig. 10-22).

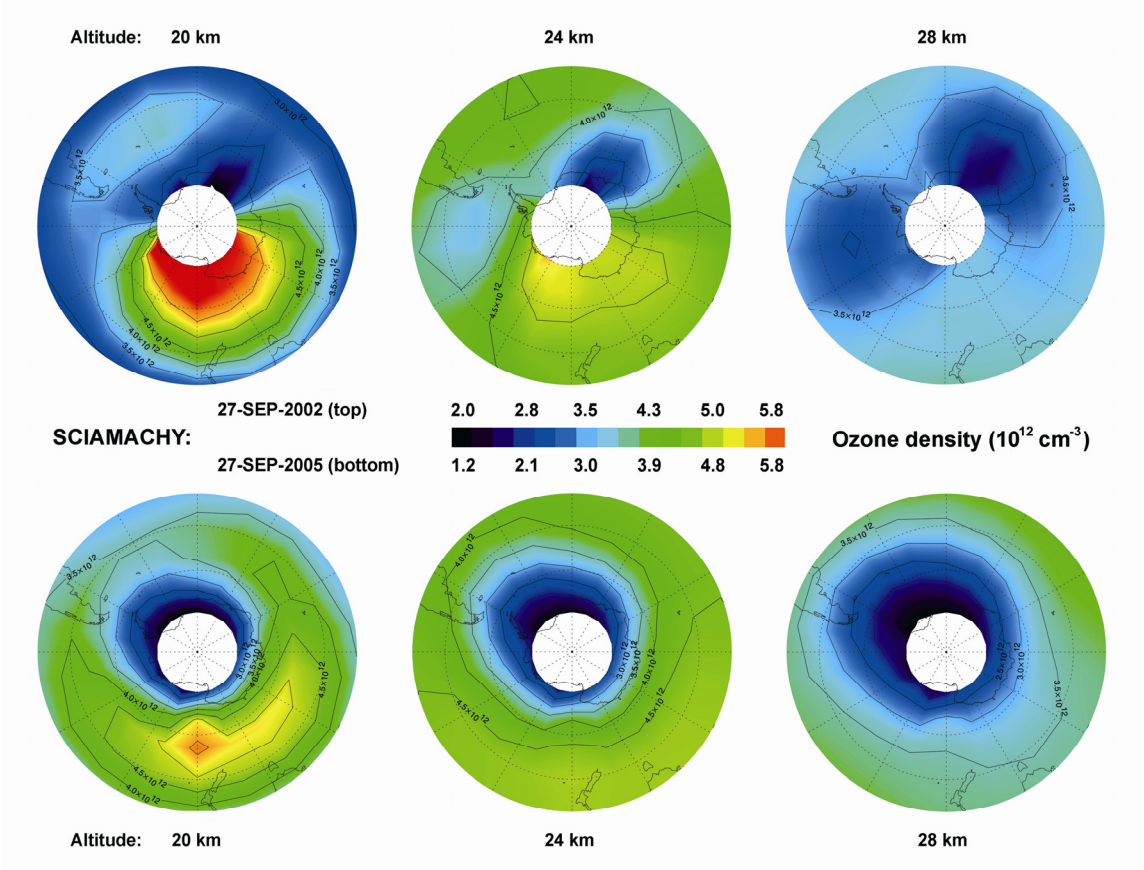

Fig. 10-20: Slices of the polar southern hemisphere ozone field at altitudes of approximately 20, 24 and 28 km on 27 September 2002 and 27 September 2005 as measured by SCIAMACHY. The observed split of the ozone hole in 2002 is not so obvious in the lower stratosphere around 20 km, but clearly visible at 24 and 28 km. In 2005, an ozone hole of 'normal shape' existed at all altitudes. (Courtesy: C. von Savigny, IUP-IFE, University of Bremen)

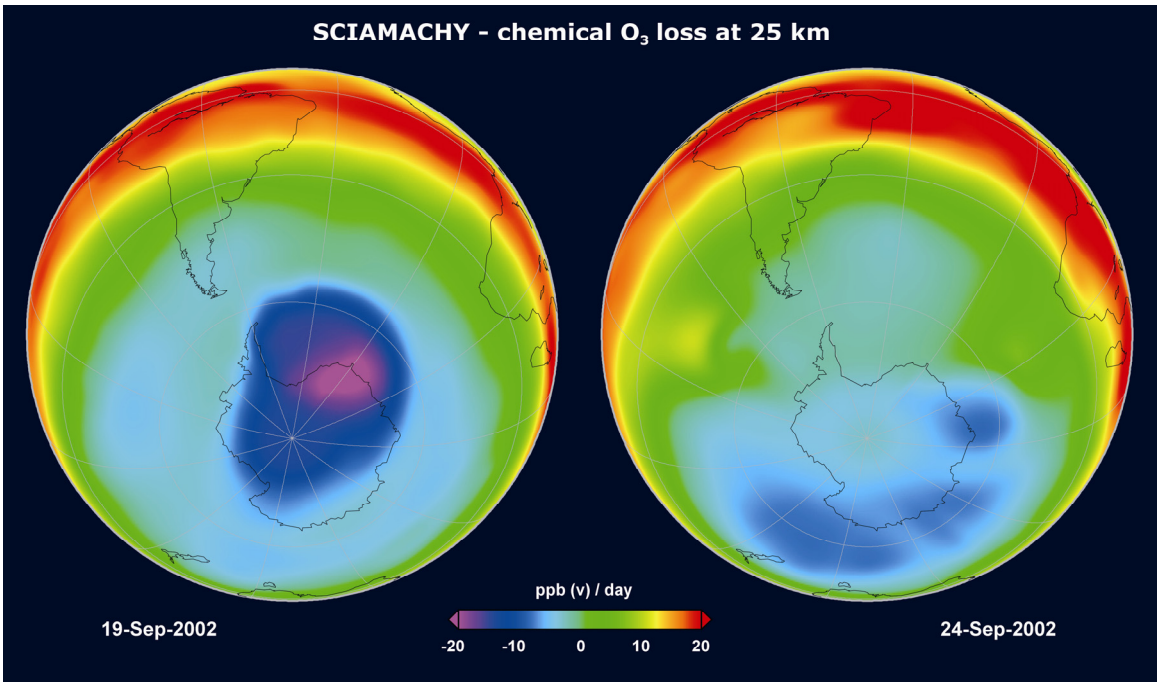

Fig. 10-21: Chemical ozone loss rates on two days in September 2002 in the mid-stratosphere at about 25 km, relative to the previous day. While on 19 September the ozone hole was still developing its usual shape, 5 days later the split-up of the vortex has reduced ozone loss rates. (Courtesy: T. Erbertseder, DLR-DFD)

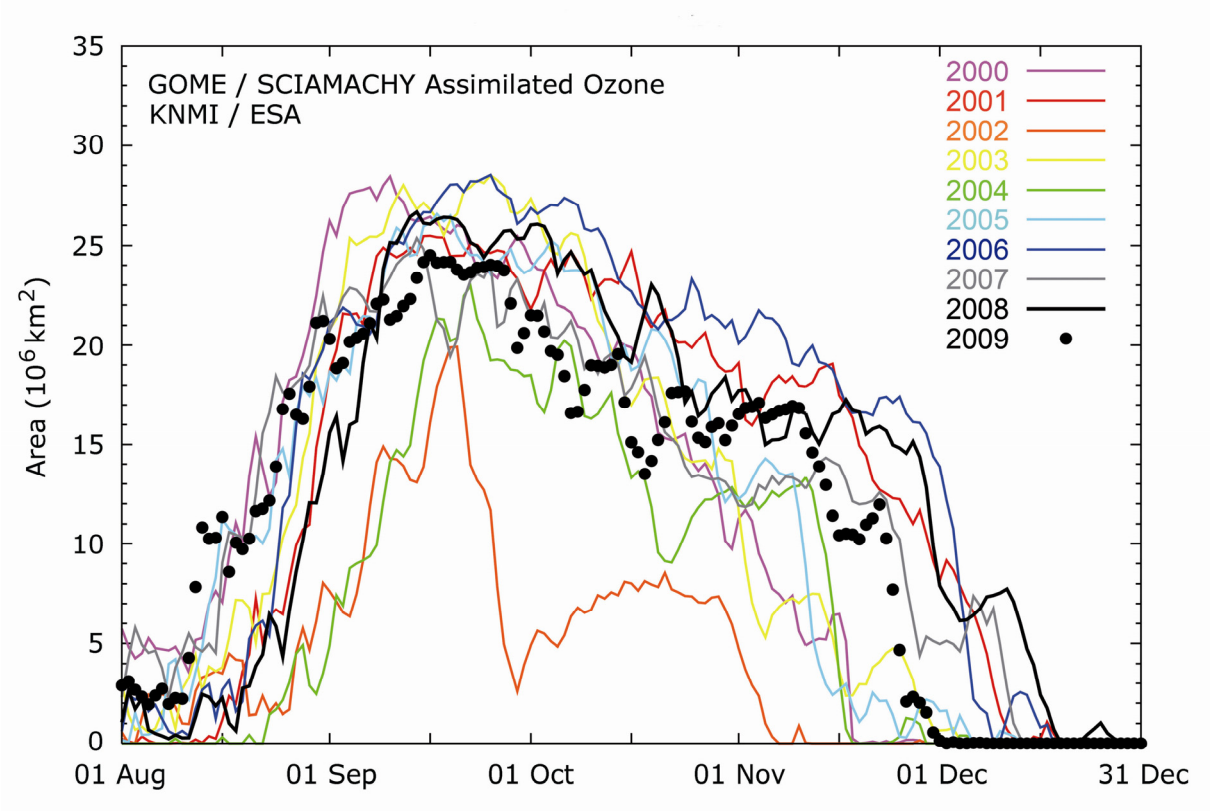

Fig. 10-22: Time series of the size of the Antarctic ozone hole from 2000-2009 based on observations of GOME and SCIAMACHY. The area includes ozone column values below 30°S lower than 220 Dobson Units. (Courtesy: TEMIS KNMI/ESA)

Over the Arctic, stratospheric temperatures are usually higher than over Antarctica, i.e. the polar vortex is less stable and PSC are a rare phenomenon. Thus, ozone depletion is not observed as regularly as in high southern latitudes at the end of the winter. However, unexpected cold northern winters change the situation, as was the case in 2005 (e.g. Bracher et al. 2005). Measurements obtained with SCIAMACHY from January to March 2005 were compared with observations of 2004 (see Fig. 10-23). A significant loss of ozone occurred over parts of Europe in February as a result of chlorine activation on PSC when the Sun rose after the long polar night. In March, conditions had recovered and the O_3 levels approached their normal values (Fig. 10-23).

While most studies of the chemical ozone loss inside the polar vortices focused mainly on the northern hemisphere because of the strong inter-annual variability in the stability of the vortex and the following ozone loss, Sonkaew et al. (2010) also analysed ozone depletion inside the Antarctic polar vortex by using limb ozone profiles. They determined the chemical ozone loss via the difference between the observed vortex-average ozone abundance and the abundance modelled without considering chemical processes, but with including dynamically induced ozone changes. Fig. 10-24 depicts the relative chemical ozone losses at the 475 K isentropic level – corresponding to an altitude of about 18 km – for the period 2002-2009 in the Arctic and Antarctic polar vortices. Several obvious differences exist between the two hemispheres. The chemical ozone losses in the Antarctic polar vortex do not vary much from year to year. Even in the anomalous year 2002 (see above), the relative ozone loss inside the vortex is similar to all other years. In the northern hemisphere, however, significant inter-annual variability exists, with some years, e.g. 2005 and 2007, exhibiting relatively strong chemical ozone losses and other years (2004, 2006) showing little or no ozone loss.

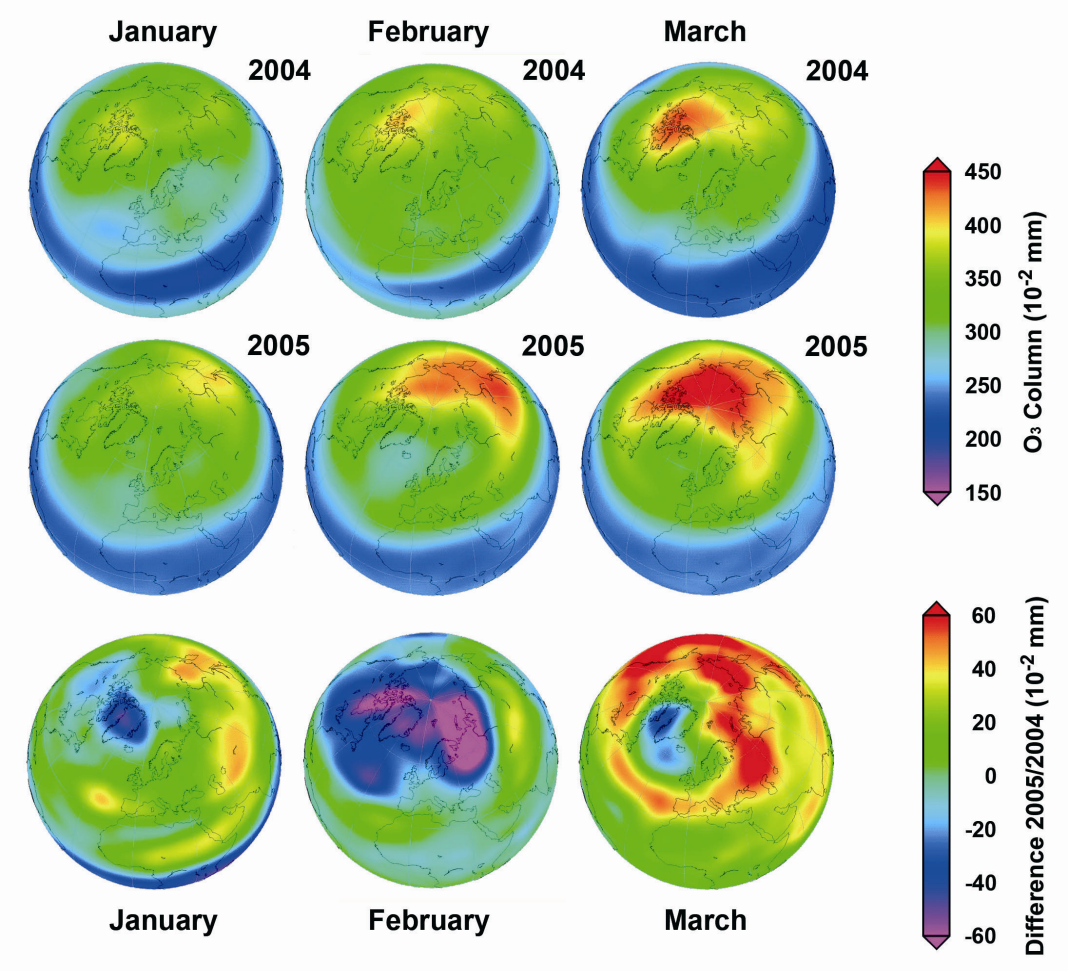

Fig. 10-23: Ozone columns over the northern hemisphere for late winter/early spring 2004 (top row), 2005 (mid row) and the difference between both years (bottom row). Owing to unusual low temperatures in the stratosphere over the Arctic, significant ozone loss occurred in February 2005 with a recovery of the ozone layer in March. (Courtesy: J. Meyer-Arnek, DLR-DFD)

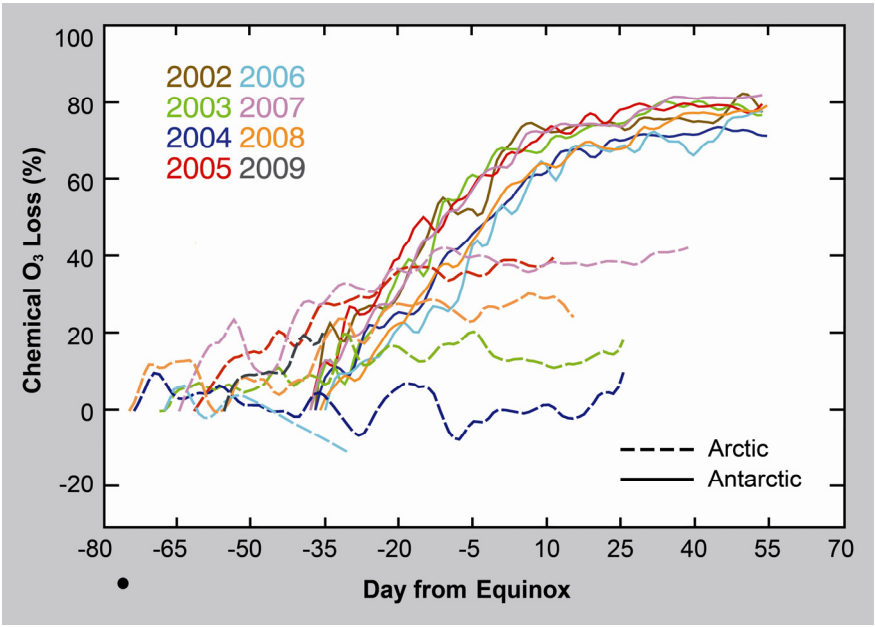

Fig. 10-24: Relative chemical ozone losses at the 475 K isentropic level (around 18 km) for the period 2002-2009 in the Arctic (dotted lines) and Antarctic (solid lines) polar vortices. (Courtesy: IUP-IFE, University of Bremen)

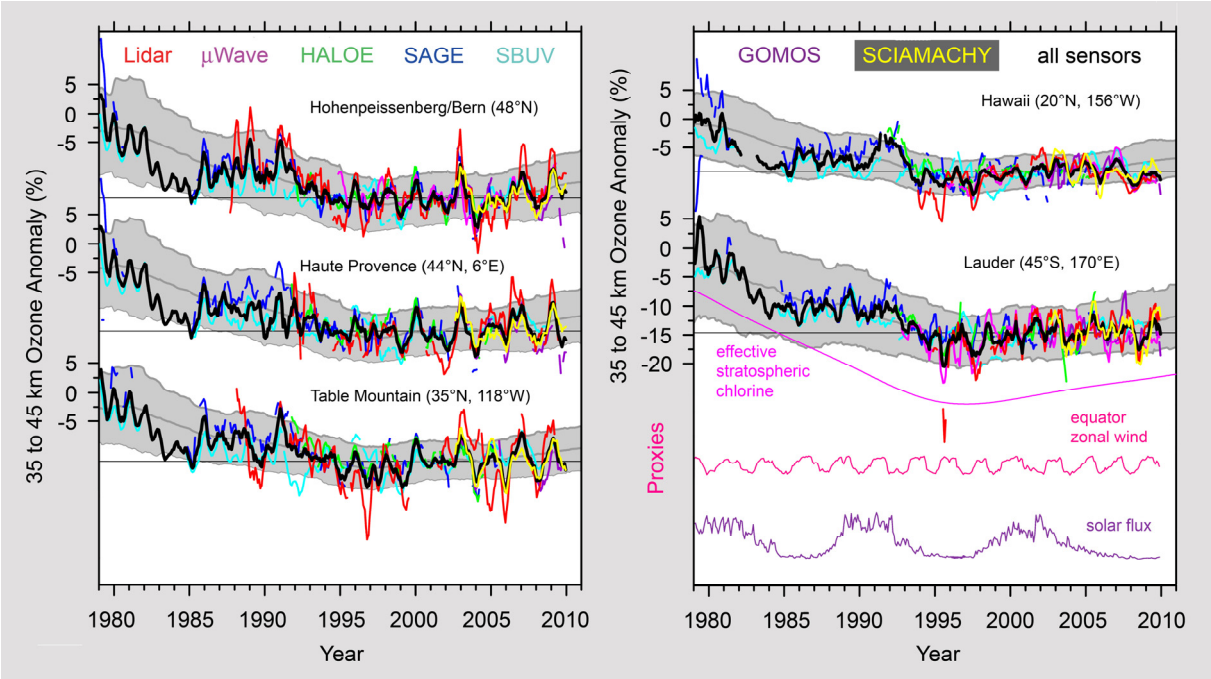

Fig. 10-25: Ozone anomalies from 1979 to 2009 derived from different datasets at five NDACC stations. The anomalies are averaged over the 35-45 km range. The all-instrument average is shown in black. All time series were smoothed by a 5-month running mean. At the bottom of the right hand panel 3 proxies are given: The negative 10 hPa zonal wind at the equator for the QBO, the 10.7 cm solar flux for the 11-year solar cycle and the inverted effective stratospheric chlorine for ozone destruction by chlorine. The grey line and the grey shaded area show model simulations and their 2-sigma standard deviation. (Courtesy: adapted from Steinbrecht et al. 2009, reproduced/modified by permission of American Geophysical Union)

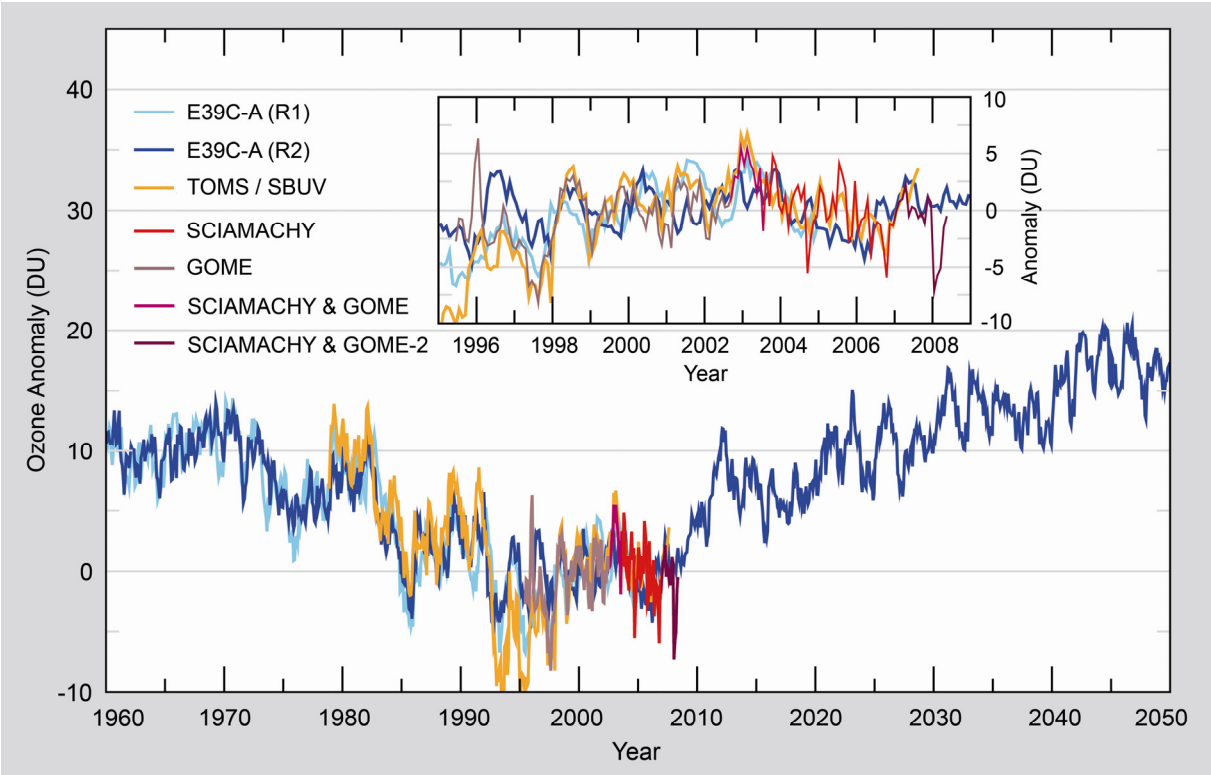

Fig. 10-26: Total ozone anomaly from 60°N to 60°S from the merged GOME/SCIAMACHY/GOME-2 dataset. For comparison, the results from the merged TOMS/SBUV/OMI are given, together with predictions from climate-chemistry model runs. (Courtesy: Loyola et al. 2009, reproduced/modified by permission of American Geophysical Union)

Ozone depletion occurring during winter and spring in each hemisphere inside the polar vortices is a more localised phenomenon when compared to the global and continuous effects of anthropogenic halogen emissions on the stratospheric ozone layer. Again, O_3 limb profiles have proven a valuable tool for investigating long-term trends in stratospheric ozone. Steinbrecht et al. (2009) determined upper stratospheric ozone trends for several latitude bands from 1979 to 2008 using ground-based LIDAR and microwave as well as satellite observations with SAGE II, HALOE, SBUV, GOMOS and SCIAMACHY. Fig. 10-25 shows ozone anomalies, i.e. monthly averaged ozone measurements minus average seasonal component, at five different latitudes. SCIAMACHY observations are indicated in yellow. The time series at all 5 locations display a decline until about the mid-1990's, followed by a stagnation of the negative trend or even a slight positive trend, in very good qualitative agreement with the time dependence of the effective stratospheric chlorine load. Since the quasi-biennial oscillation (QBO) variation has not been removed, it is clearly visible in most time series.

As demonstrated by Steinbrecht et al. (2009), 'witnessing' the recovery of stratospheric ozone requires long-term datasets. These are usually not provided by a single instrument but by a series of preferably similar sensors. Since SCIAMACHY is GOME heritage, combining GOME, GOME-2 and SCIAMACHY total columns from nadir measurements generates a unique repository. Loyola et al. (2009) formed a homogeneous dataset by merging O_3 columns from June 1995 to August 2009. Measurements from over 70 globally distributed Dobson and Brewer ground stations served as validation reference. Since the GOME data record is very stable, it was used as a transfer standard and SCIAMACHY and GOME-2 data in periods of instrument overlap were adjusted accordingly. Global ozone trends were then derived by applying statistical methods, including the entire 60°N-60°S average serving as a near global mean. Fig. 10-26 illustrates how well the merged GOME/GOME-2/SCIAMACHY dataset of total ozone columns compares with results from the chemistry-climate model (CCM) E39C-A. This figure again displays the so-called 'O_3 anomaly' which is the residual when subtracting the mean annual cycle from the satellite measurements. Apparently, the phase of minimum stratospheric ozone is just occurring and a recovery can be expected in the next decades. The current good match between the CCM and the observations in Fig. 10-26 is a hint that the models' predications are trustworthy.

Chlorine Dioxide – OClO

One key question related to the expected recovery of stratospheric ozone is the degree of chlorine activation observed in polar winter and spring in both hemispheres. This effect depends not only on the total available inorganic chlorine amount but also on the presence of PSC for the activation of the chlorine reservoirs. The latter is a function of temperature and polar vortex stability and therefore is impacted by changes of the stratospheric dynamics and temperatures in response to increased concentrations of greenhouse gases. One good indicator for chlorine activation is the presence of OClO which is formed by reaction of BrO and ClO.

While SCIAMACHY observations in nadir (Kühl et al. 2006) continue the global measurements of total columns of OClO started with GOME (Wagner et al. 2001, Kühl et al. 2004, Richter et al. 2005b), vertical profiles of OClO can also be derived from the limb observations (Kühl et al. 2008). By applying a tomographic 2D approach (Puķīte et al. 2008), the retrieval can take into account horizontal gradients in the distribution of OClO, which is particularly important at the edge of the polar vortex. Fig. 10-27 shows the OClO number density at 19 km altitude above the northern hemisphere derived from the SCIAMACHY limb observations (top), and the corresponding total column derived from nadir view (bottom) for mid of February in the Arctic winters 2002/03 to 2008/09. The data displays strong stratospheric chlorine activation only inside the polar vortex for cold winters, reflecting the strong dependence of the degree of chlorine activation on the meteorological conditions of the respective winter, such as temperature and potential vorticity. While almost no OClO is found for the warm winters 2003, 2004, 2006 and 2009, much stronger activation of chlorine is observed for the cold winters 2005, 2007 and 2008. These findings are in good agreement with observations of the main active ozone depleting chlorine species ClO, the determining meteorological parameters, results from atmospheric chemistry models, and the related chemical ozone loss (compare Figs. 10.23 and 10.24 in the section on ozone). The strong inter-annual variability in the degree of chlorine activation reveals that despite the decrease of the stratospheric inorganic chlorine loading, large enhancements of OClO are still observed in the Arctic stratosphere during cold

winters. Therefore, monitoring of stratospheric chlorine activation and detailed investigation of the relation to meteorological parameters is necessary to broaden the understanding of the related processes.

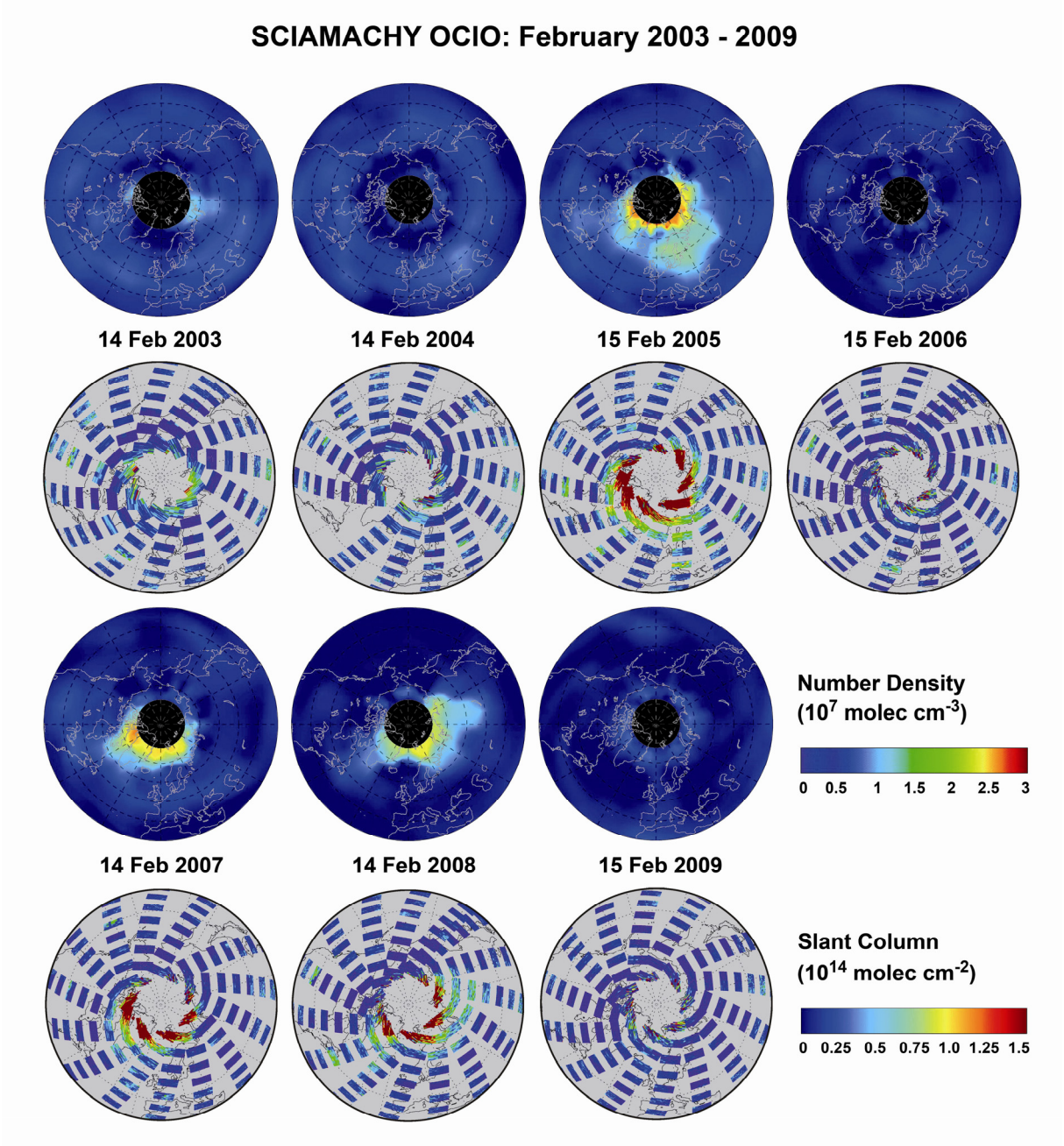

Fig. 10-27: OClO number density at 19 km altitude above the northern hemisphere derived from SCIAMACHY limb observations (rows 1 and 3), and the corresponding total OClO slant column derived from nadir views (rows 2 and 4) for mid of February in the Arctic winters 2002/03 to 2008/09. (Courtesy: S. Kühl; MPI for Chemistry, Mainz)

Bromine Oxide – BrO

Bromine compounds play an important role in the catalytic destruction of stratospheric ozone. Despite their importance, however, there are only few measurements of bromine compounds in the stratosphere. For the first time, SCIAMACHY provided global observations of stratospheric BrO profiles down to the lower stratosphere (Rozanov et al. 2005, Sioris et al. 2006, Kühl et al. 2008). The long-term changes of BrO as observed from SCIAMACHY agree well with ground-based

observations at mid-latitudes (Hendrick et al. 2009). A comparison with ground-based UV-VIS zenith-sky observations by BIRA-IASB at Harestua, Norway (60°N) has already been presented in Fig. 9-18. The seasonal cycle, including the activation during winter and long-term changes, are consistently seen by both instruments. When comparing zonal mean BrO at selected stratospheric altitudes obtained from limb observations and from model simulations, an additional source of stratospheric bromine from very short-lived substances (VSLS) is required (Fig. 10-28) to explain the difference. This component amounts to about 3 to 6 parts per trillion by volume (pptv), or about 20% (WMO 2007, Sinnhuber et al. 2005). In an opposite analysis approach, Theys et al. (2009) used the SCIAMACHY limb stratospheric BrO observations to demonstrate the validity of a new stratospheric BrO profile climatology.

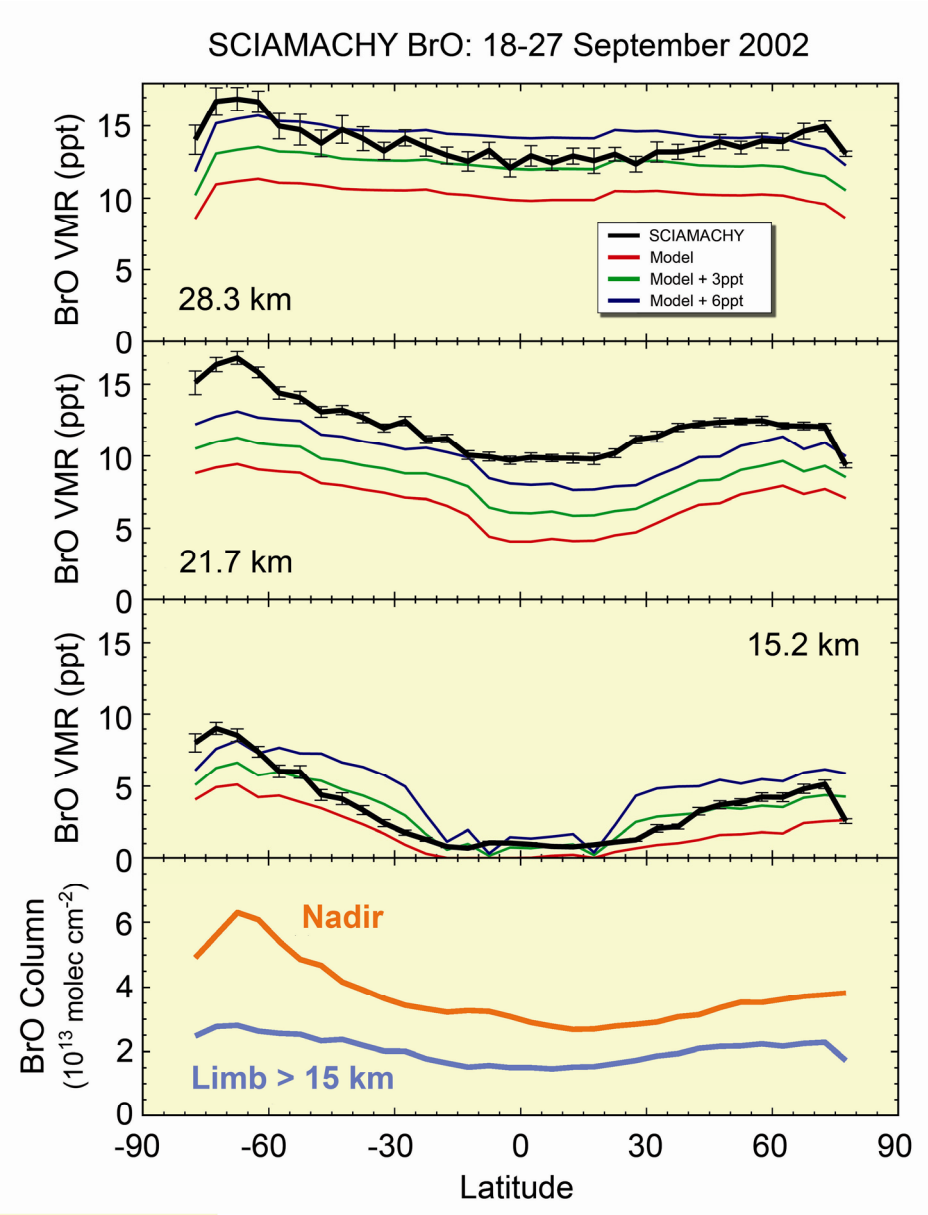

Fig. 10-28: Zonal mean BrO at selected altitudes obtained from SCIAMACHY limb observations and from model calculations. Additional bromine of 0, 3, and 6 pptv, respectively, has been added to the model calculations to account for the contribution from very short-lived substances (VSLS). (Courtesy: adapted from WMO 2007 – based on Sinnhuber et al. 2005)

Polar Stratospheric Clouds – PSC

Polar Stratospheric Clouds play a key role in the chemical processes which lead to severe ozone depletion in the polar stratosphere. These clouds are necessary for transferring inactive chlorine compound reservoirs such as HCl and $ClONO_2$ to active Cl that participates in different catalytic O_3 destruction cycles. PSC form at altitudes of about 15-25 km and exist as different types. Type Ia consists of crystalline NAT (nitric acid tri-hydrate) particles, the liquid type Ib PSC consist of ternary solutions of nitric acid, sulphuric acid and water. Type II PSC are made of water ice. A common feature of all types is that they only form at very low temperatures of less than about -78°C (195 K). PSC scatter solar radiation and thus affect the measured limb radiance spectra. Since PSC are rather Mie-scatterers than Rayleigh-scatterers in the UV-SWIR spectral range, the spectral dependence – although highly variable – of their scattering cross section differs from the λ^{-4} spectral dependence of the molecular Rayleigh scatterering. This spectral difference can be exploited in a colour-index approach to detect PSC (von Savigny et al. 2005b).

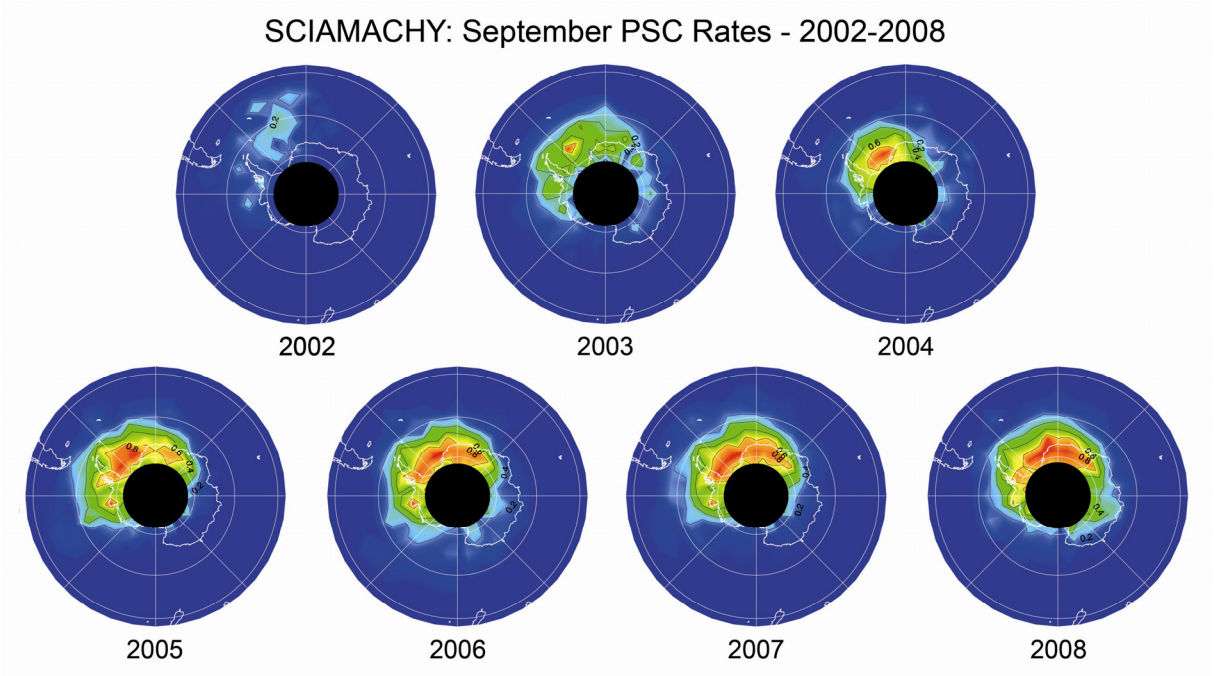

Fig. 10-29: Maps of PSC occurrence rates for September of the years 2002-2008. Contours levels correspond to 0.2, 0.4, 0.6, and 0.8. Red areas indicate occurrence rates exceeding 0.8. (Courtesy: C. von Savigny, IUP-IFE, University of Bremen)

Fig. 10-29 shows the occurrence rate of PSC in the southern hemisphere for September in the years 2002 to 2008. With the exception of 2002, the PSC occurrence rate at high southern latitudes is typically quite large. It is obvious that PSC are not symmetrically distributed around the South Pole, but the distribution is characterised by a wave-1 structure with a maximum in the South Atlantic sector and a minimum in the Australian sector. The low PSC occurrence rates in September 2002 are due to the anomalous mid-winter major stratospheric warming after 22 September, which caused PSC to disappear. In most cases there is a good correspondence between the detected PSC and their formation threshold of -78° C.

10.4 The Upper Atmosphere and Solar Activity

The upper atmosphere, i.e. the mesosphere and lower part of the thermosphere (MLT region), is still a relatively poorly explored region. The MLT region forms a transition between interplanetary space and the terrestrial atmosphere, both influenced by extraterrestrial impacts – e.g. solar radiation, solar wind, meteors or cosmic dust – as well as by impacts from the lower atmosphere. Thus, there are indications that effects of global climate change in the upper atmosphere can be detected rather early.

Solar-terrestrial interactions can be studied, and at the same time, the impact of anthropogenic emissions on our atmosphere at remote altitudes can be investigated.

Noctilucent Clouds – NLC

Noctilucent Clouds, also referred to as *Polar Mesospheric Clouds*, are a high latitude summertime mesospheric phenomenon, even observable from ground. They occur at altitudes of about 83-85 km near the polar summer mesopause and consist of H_2O ice particles with radii ranging from a few nm up to about 80-100 nm. NLC received a significant amount of scientific interest in recent years, since they may be early indicators of global change. This is because they react very sensitively to small changes in ambient conditions, particularly to changes in temperature and H_2O abundance. The scattering properties of the NLC particles allow mapping of these high altitude clouds. Since they scatter solar radiation efficiently, they affect the measured limb radiance profiles significantly, especially in the northern hemisphere where scattering angles at polar latitudes are particularly small for SCIAMACHY limb observations. The NLC component of the measured limb signal, the blue curve in Fig. 10-30, can be 2 orders of magnitude larger than the Rayleigh signal (red curve in Fig. 10-30) at the NLC altitude, allowing for a simple detection of NLC.

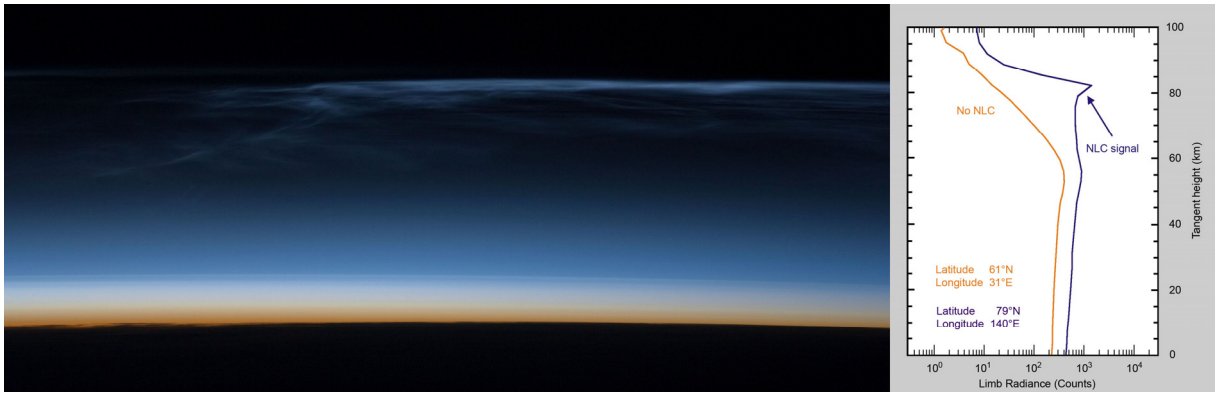

Fig. 10-30: NLC as seen from the International Space Station on 22 July 2008 (left panel), together with the NLC signature in a SCIAMACHY UV limb radiance profile from 3 July 2002 (right panel). The scattering by ice particles in the NLC leads to a significant increase of the observed limb radiance profile peaking at the characteristic NLC altitude of about 83-85 km (blue line). For comparison, a limb radiance measurement in the absence of NLC is shown in red. (Courtesy: C. von Savigny, IUP-IFE, University of Bremen; ISS photo: NASA)

SCIAMACHY observations of NLC have contributed in different ways to the current research on the polar summer mesopause. The main focus of these investigations was to improve the scientific understanding of the natural variability in NLC in order to better understand the role of NLC as indicators of global change. The natural variability is partially driven by the solar input and by dynamical processes such as planetary waves.

SCIAMACHY NLC observations were used to observe a depletion of NLC for the first time during a solar proton event (SPE, von Savigny et al. 2007a). Associated with such an event in January 2005, highly energetic solar protons precipitated into the Earth's polar cap areas. The January 2005 SPE is included in the period covered by Fig. 10-31. This graph shows SCIAMACHY NLC occurrence rates at different latitudes in the southern hemisphere during the 2004/2005 NLC season, together with the ionisation caused by the precipitating solar protons. At the time of the SPE, the NLC occurrence rate in both southern latitude bands decreased rapidly. A mechanism for SPE-induced NLC depletion is proposed by Becker and von Savigny (2010) using model simulations with a General Circulation Model (GCM). It suggests that a polar mesopause warming is caused by the SPE-driven catalytic ozone loss in the middle mesosphere, followed by different stages of dynamic processes, and finally leading to a reduced upwelling above the pole, i.e. reduced adiabatic cooling. The January 2005 event is not the only event where NLC depletion has been detected. Rahpoe et al. (2010) demonstrated that a depletion of NLC also occured during some of the other strong SPE in the last three decades.

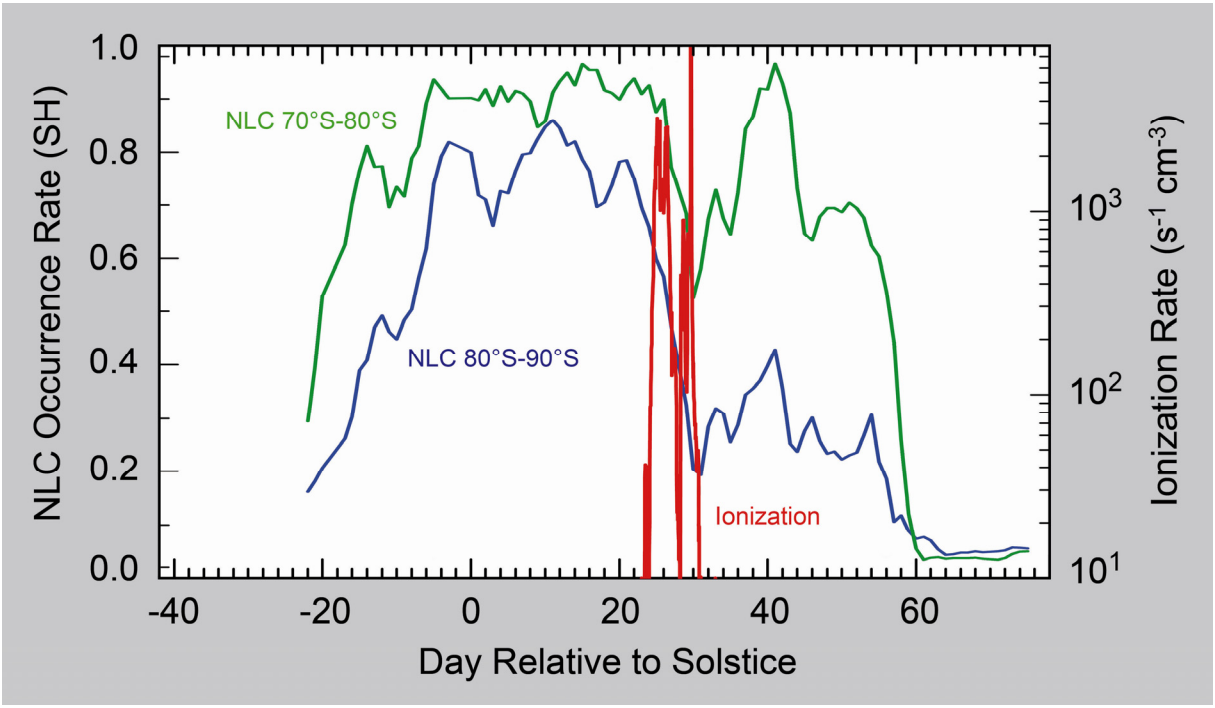

Fig. 10-31: Smoothed zonally averaged NLC occurrence rates in the southern hemisphere NLC season 2004/2005 (left abscissa) and ionisation rates at 82 km (right abscissa). At the time of the solar proton event, the ionisation rate increases and causes a drop in the NLC rate. (Courtesy: C. von Savigny, IUP-IFE, University of Bremen)

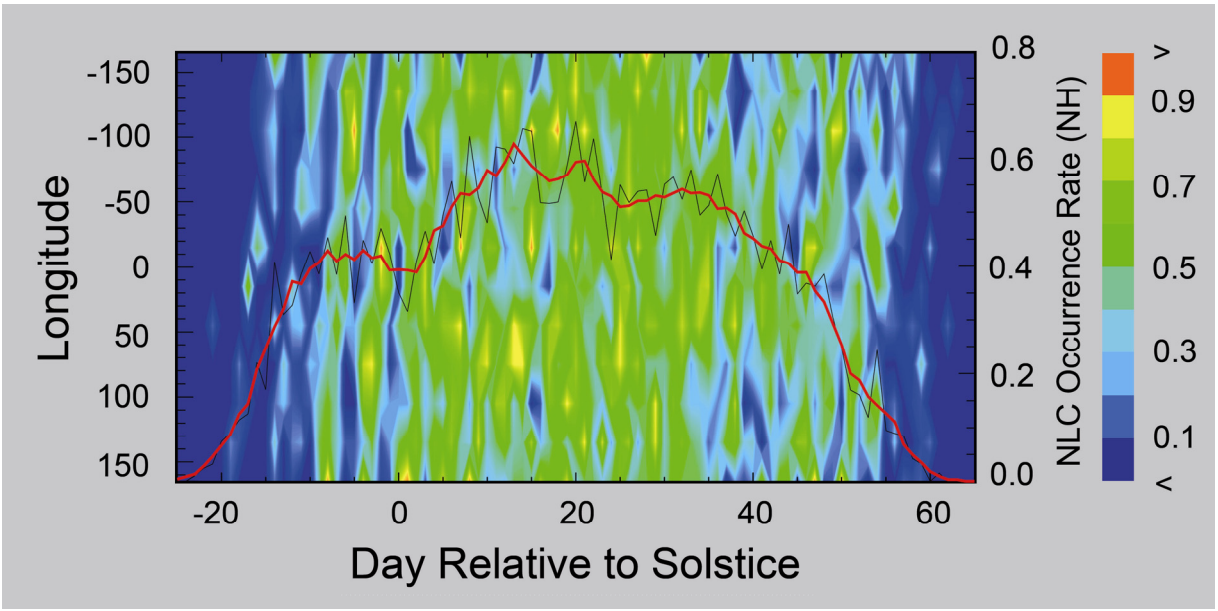

Fig. 10-32: Contour plot of the longitude and time dependence of the NLC occurrence rate for 2005 in the northern hemisphere with the zonally averaged NLC occurrence rate overlaid (red curve, right abscissa). The 5-day wave pattern is clearly visible at the beginning of the NLC season as a westward propagating signature with wavenumber 1 and a period of 5 days. (Courtesy: C. von Savigny, IUP-IFE, University of Bremen)

Solar proton events are rather intermittent and irregular events mainly occurring during solar maximum. They are not the only cause for NLC variability linked to solar impacts seen in SCIAMACHY observations. A 27-day solar cycle signature in NLC was identified for the first by Robert et al. (2010). Maxima in solar activity associated with the 27-day solar cycle – quantified for example using the MgII index described below (Skupin et al. 2004) – coincide with minima in the

NLC occurrence frequency. Using MLS (Microwave Limb Sounder) observations of middle atmospheric temperatures, a 27-day solar cycle signature in the polar mesopause temperature was identified as the immediate cause of the apparent 27-day signature in NLC.

Another important driver for variability in NLC are planetary wave signatures. The most important of these signatures are the quasi-2-day-wave and the quasi-5-day-wave. Both of them are caused by instabilities of the summer mesosphere jet and occur intermittently during the NLC seasons in both hemispheres. SCIAMACHY NLC observations, again in combination with MLS temperature observations, showed for the first time, that the quasi 5-day-wave signatures in NLC are caused by similar wave signatures in mesopause temperatures (von Savigny et al. 2007b). The 5-day-wave signatures appear as fairly regular westward propagating perturbations on the NLC field (Fig. 10-32) with a period of 5-days, and are most pronounced at the beginning and at the end of the NLC seasons for the case shown.

Apart from the detection and mapping of NLC, SCIAMACHY observations also permit the estimation of the NLC particle size. For wavelengths below about 310 nm, the multiple scattering and surface reflection components to the limb signal are negligible. In single scattering approximation, the spectral exponent of the NLC scattering spectrum can be related to the NLC particle size assuming for example Mie theory and the refractive index of H_2O ice (von Savigny et al. 2004a). NLC particle sizes of 40-50 nm were determined from a distance of about 3300 km. The SCIAMACHY NLC size dataset currently presents the most comprehensive satellite dataset of NLC particle sizes. The derived particle sizes are in good agreement with independent observations (von Savigny and Burrows 2007, von Savigny et al. 2009).

Mesospheric Ozone and the October/November 2003 Solar Storm

Highly energetic protons ejected from the Sun during phases of high coronal activity, such as solar flares or solar coronal mass ejections, reach the Earth with the solar wind, ionise the atmosphere and lead to the formation of HO_x and NO_x in the mesosphere and upper stratosphere. Both families participate in catalytic O_3 destruction cycles, with HO_x being more efficient above about 50 km and NO_x below about 50 km. Consequently, enhanced O_3 destruction is expected after strong solar proton events. A good opportunity to study the impact of solar activity on mesospheric ozone fields was a period in October/November 2003 – also known as the ‘Halloween Storm’ – when the Sun exhibited extremely large coronal SPE. Fig. 10-33 presents an analysis of the impact of the solar proton event at the end of October 2003 on the upper atmospheric O_3 (Rohen et al. 2005). A strong ozone depletion of more than 50% even deep in the stratosphere is observed at high geomagnetic latitudes in the northern hemisphere, whereas the observed ozone depletion in the more sunlit southern hemisphere is much weaker. SCIAMACHY measurements of the O_3 loss due to SPE agree well with model simulations, indicating that the main processes leading to the O_3 loss are fairly well understood.

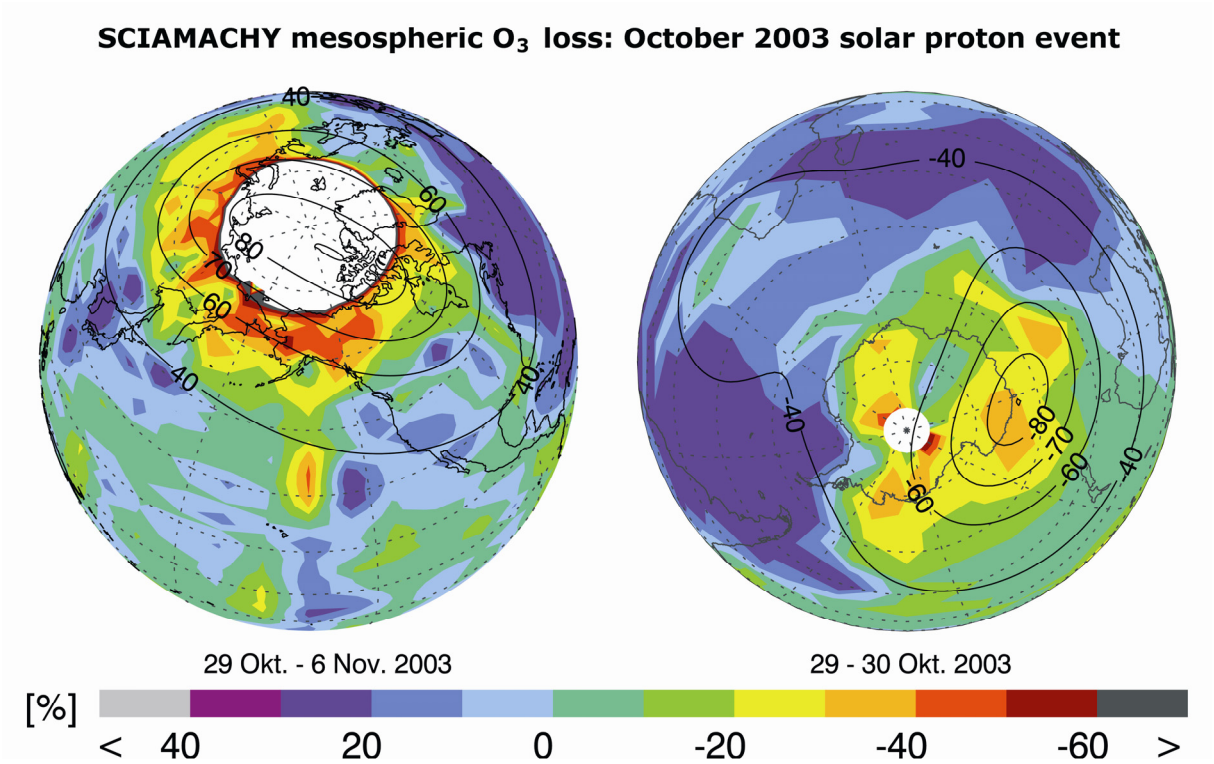

Fig. 10-33: Measured change of ozone concentration at 49 km altitude due to the strong solar proton events end of October 2003 in the northern and southern hemisphere relative to the reference period of 20-24 October 2003. White areas depict regions with no observations. The black solid lines are the Earth's magnetic latitudes at 60 km altitude for 2003. (Courtesy: Rohen et al. 2005)

Mesopause Temperatures, Thermospheric NO and Metal Layers

A number of atomic and molecular emission signals from the mesosphere and lower thermosphere (MLT) can be detected throughout the SCIAMACHY spectral range, e.g. neutral and ionised magnesium (Mg) lines as well as NO gamma bands in the UV, OH Meinel band emissions in the SWIR, several transitions from excited-state O_2 or sodium lines and atomic oxygen in the VIS range. These emission signals can be used to characterise the distribution of the atoms, ions and molecules in the upper atmosphere.

SCIAMACHY measurements of molecular emissions in the upper atmosphere provided for the first time the retrieval of OH^* rotational temperatures at the mesopause from satellite measurements during night. OH^* is vibrationally excited at the mesopause through the reaction of H and O_3. This produces an OH^* emission layer centred at about 87 km with a width of 8-10 km. Several of the OH^* Meinel emission bands are observable in the SCIAMACHY spectral range, e.g. the OH^* (3-1) band at around 1500 nm. This emission band is used for the retrieval of OH^* rotational temperatures because it is one of the most intense emission bands. From the relative intensity of two or more rotational lines, the effective temperature of the emitting layer can be retrieved from SCIAMACHY data. For several decades, this method has been applied to retrieve mesopause OH^* rotational temperatures from ground measurements (e.g. Bittner et al. 2002). Therefore, coincident ground-based OH^* rotational temperature measurements over Germany in Wuppertal and Hohenpeissenberg, as well as over Hawaii, had originally been used to validate the novel SCIAMACHY space-based approach (von Savigny et al. 2004b). A comparison of both methods yielded very good agreement. Fig. 10-34 shows the monthly averaged mesopause temperatures retrieved from SCIAMACHY OH^* (3-1) emission measurements for January, April, July and October 2009 as an example. As the observations used for the retrievals are made on the Earth's nightside, the OH rotational temperatures are only available at higher latitudes during wintertime.

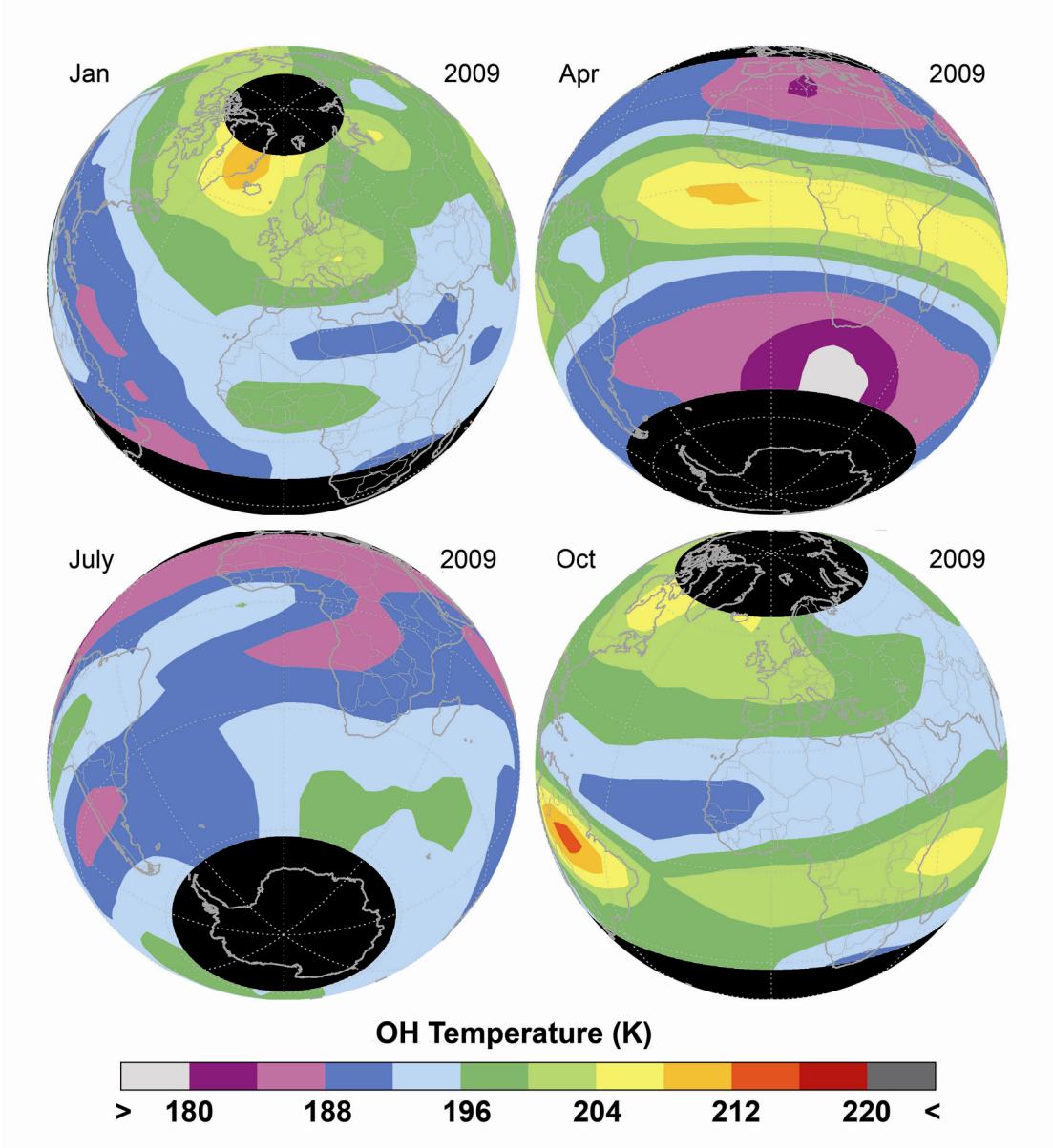

Fig. 10-34: Monthly averaged SCIAMACHY retrievals of OH rotational temperatures at about 87 km for January, April, July and October 2009. (Courtesy: K.-U. Eichmann, IUP-IFE, University of Bremen)

Retrieval of OH^* rotational temperatures is not the only scientific application of SCIAMACHY's OH Meinel-band emission observations. The data can also be used to study atmospheric wave signatures (Ern et al. 2009) or to determine chemical heating rates associated with the exothermic chemical reaction $H + O_3 \rightarrow OH^* + O_2$, which forms the vibrationally excited OH molecules as mentioned above (Kaufmann et al. 2007).

Also notably interesting are UV wavelengths. Here, emissions from the NO gamma-bands and atomic oxygen are observed, as well as a number of metallic species and their ions, e.g. MgI/MgII and FeI/FeII (Fig. 10-35) which have the bulk of their abundances in the lower thermosphere around 100-200 km. In order to fully exploit SCIAMACHY's capabilities in this exotic atmospheric region, limb measurements are specifically adjusted since summer 2008 for about 60 orbits per month to scan the region between 60 km up to 160 km.

From the NO gamma-band emissions, slant column densities of NO along the line-of-sight can be derived. NO is produced in the thermosphere and upper mesosphere by ionisation processes related to auroral electron precipitation in polar regions and to photoionisation in low latitudes. As the lifetime of NO in the MLT region is restricted by photolysis, NO abundances are largest in high-latitude winter. However, short increases at high latitudes can occur due to energetic particle precipitation

events related to geomagnetic disturbances, leading to the well-known correlation between thermospheric NO and the geomagnetic activity index (Fig. 10-36).

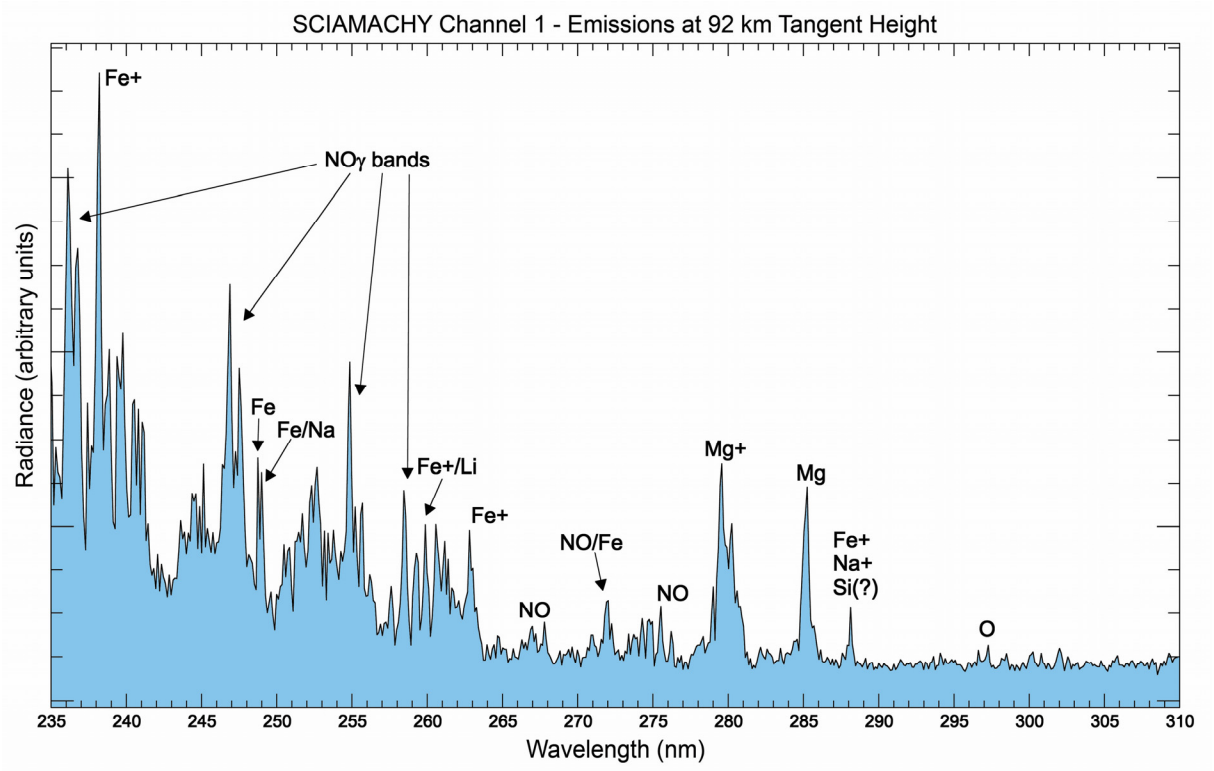

Fig. 10-35: Emission lines in SCIAMACHY limb radiance in channel 1 at the highest limb tangent altitude, normalised to the solar irradiance, in arbitrary units. A number of emission signals are detected. The most dominant features are the NO gamma-bands and MgII, but signals from neutral Mg, atomic oxygen, Si, Fe and Fe+ are observed, as well. (Courtesy: M. Sinnhuber, IUP-IFE, University of Bremen)

Neutral and singly ionised magnesium can be derived from their emissions at 280 and 285 nm, respectively (see Fig. 10-35). Vertical profiles of number density of atmospheric Mg species were derived from a satellite sensor for the first time using SCIAMACHY measurements (Scharringhausen et al. 2008). While atmospheric abundances of many species – including NO and most metals and metal ions – are largest in the lower thermosphere, the topmost tangent altitude of SCIAMACHY in the nominal limb mode remains below this region. To overcome that limitation, a 'tomographic' two-dimensional retrieval was developed using simultaneous information from all limb- and nadir measurements of one orbit to derive number densities up to altitudes of 400 km, albeit with a limited vertical resolution above 93 km (Scharringhausen 2007). The vertical structure of MgII derived from this tomographic retrieval is very comparable to that obtained from the mesosphere-thermosphere mode (Fig. 10-37), with a pronounced maximum around ~100-110 km, but generally showing lower peak values due to the strong smoothing of the profile above 90 km for the nominal limb mode. In the tropics, MgII is rather stable, with a sharp increase above 90 km and no distinguishable annual cycle. In mid-latitudes, the MgII maximum shows a seasonal cycle with maxima closely following solar illumination, as shown e.g. for total column values using GOME data by Correira et al. (2008). This seasonal cycle apparently extends down to altitudes of ~85 km, where enhanced values are observed around mid-summer. At high latitudes, the maximum is shifted to autumn/winter. Around the winter solstice, values in the upper mesosphere are again increased (Fig. 10-38). No correlation of MgII or Mg with meteor activity is observed, emphasising the dependency of the ionised metal on local chemistry rather than on meteoric influx.

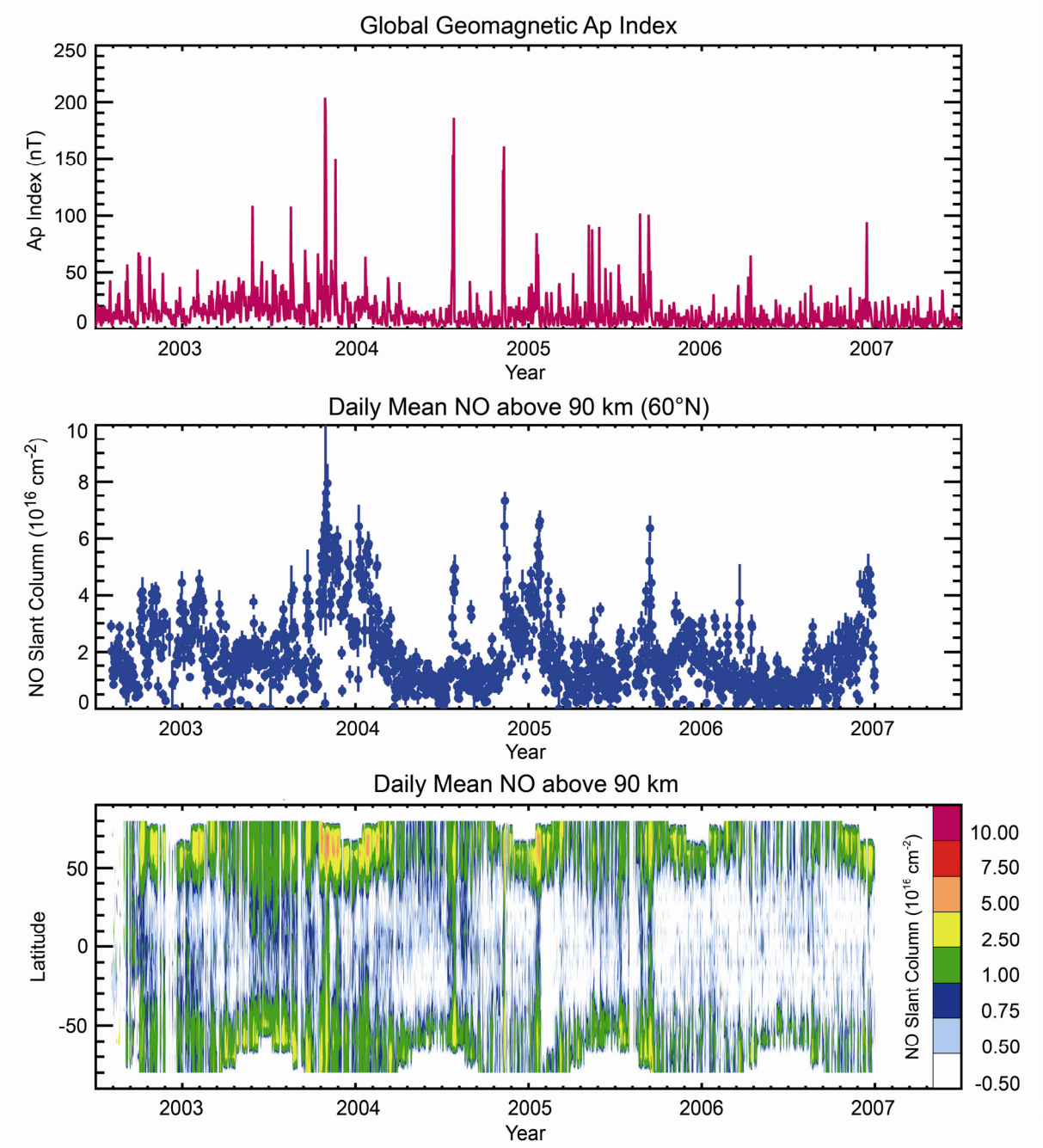

Fig. 10-36: SCIAMACHY NO slant column densities, averaged daily into 10° latitude bins. Top panel: Global Ap index, a proxy for disturbances of the geomagnetic field. Mid panel: Temporal evolution of NO at 60°N. Lower panel: Global temporal evolution. (Courtesy: M. Sinnhuber, IUP-IFE, University of Bremen; data courtesy Ap index: NOAA NGDC)

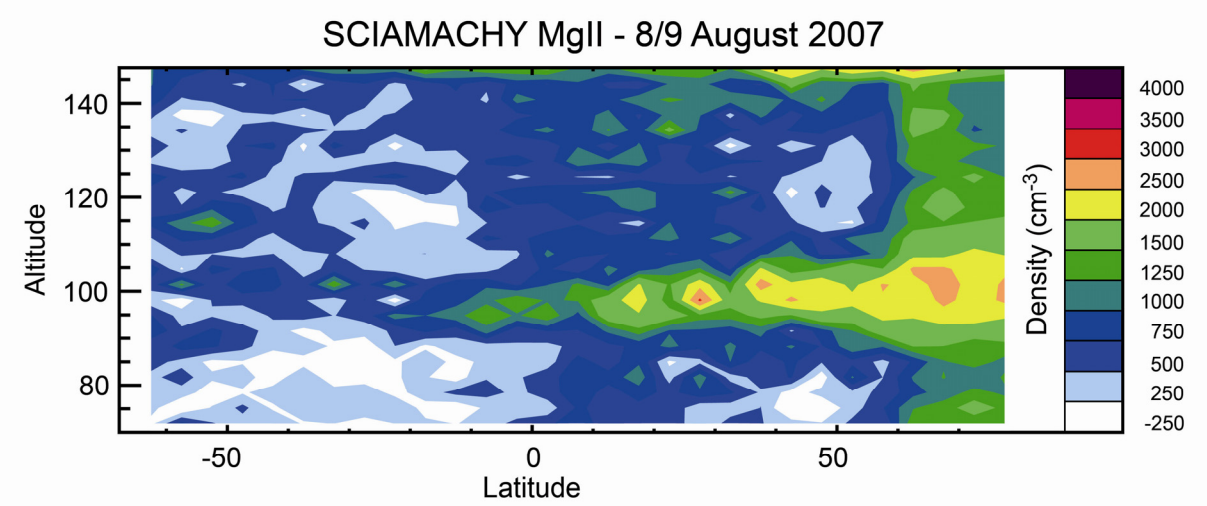

Fig. 10-37: Atmospheric abundance of MgII derived from 20 orbits scanning in the mesosphere-thermosphere limb mode from 60-160 km in August 2007. The most striking feature is the strong MgII layer around 100 km extending from high northern latitudes to the equator. (Courtesy: M. Sinnhuber, IUP-IFE, University of Bremen)

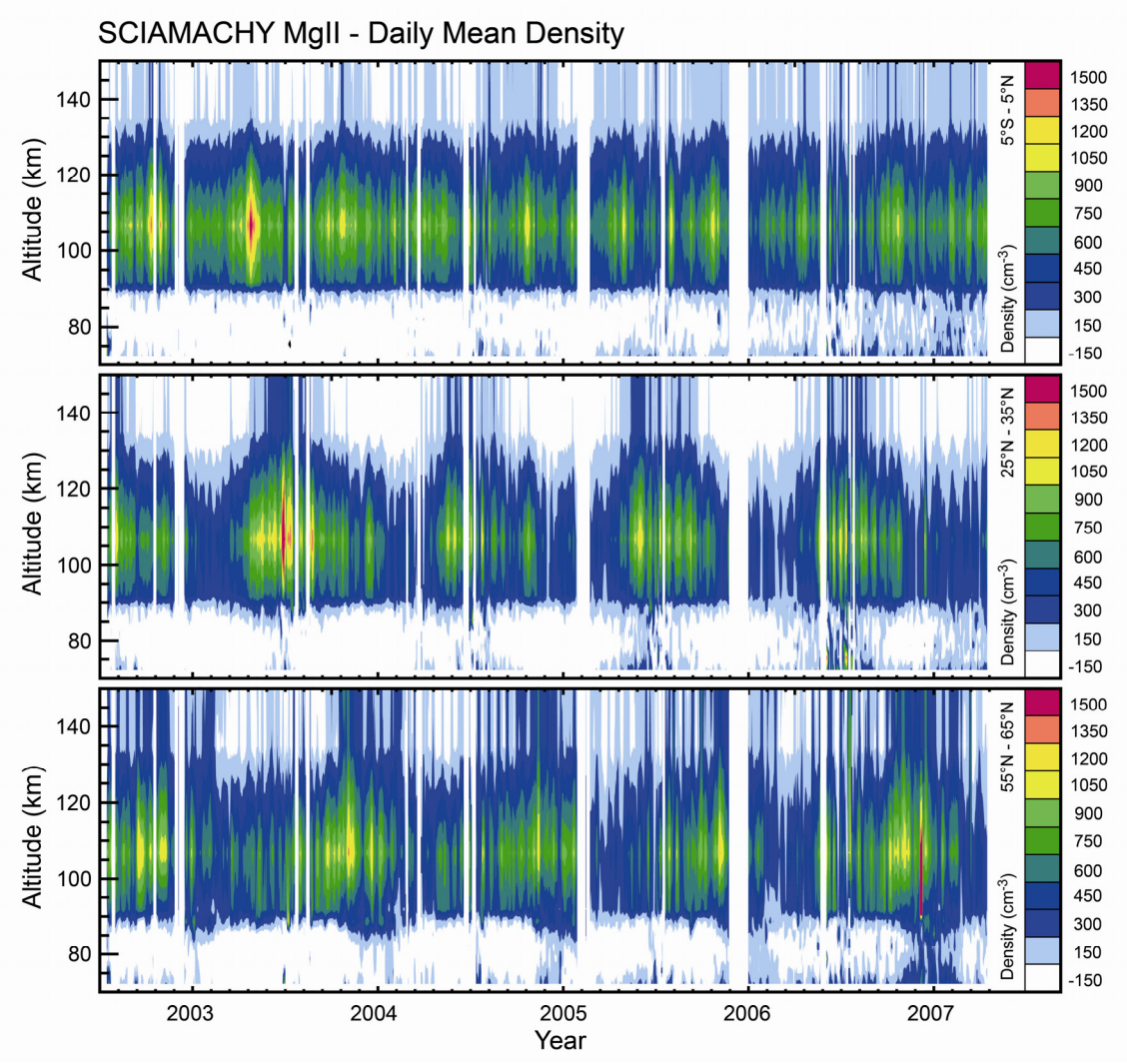

Fig. 10-38: Atmospheric abundances of MgII derived from the nominal limb scanning from the surface up to 93 km. The strong maximum around 100 km is reproduced very well, although with lower values due to the restricted vertical resolution above 93 km. The three panels show the MgII densities at different latitude bands: 5°S-5°N (top), 25°N-35°N (mid) and 55°N-65°N (bottom). (Courtesy: M. Scharringhausen/M. Sinnhuber, IUP-IFE, University of Bremen)

Observing the Active Sun - The Mg II Index

SCIAMACHY's scientific objective to explore atmospheric trace constituents is achieved by analysing solar radiation, both in terms of scattered and reflected sunlight, and also by direct viewing for calibration purposes. Due to its high sensitivity and spectral stability, SCIAMACHY is also feasible for retrieving information about those aspects of solar activity which manifest themselves in the emitted radiation. Therefore, solar observations are analysed on a regular time grid offering the possibility to monitor solar variations and their impact on the atmosphere. The solar activity shows some well known periodic variations such as the 27-day cycle caused by solar rotation. Another is the 11-year solar cycle, coupled with the 22-year magnetic cycle which correlates with changes in sunspots and Fraunhofer lines. During phases of high solar activity, an increase in the number of sunspots in the photosphere and large chromospheric plage areas are observed. The plage areas are hotter than the surrounding areas and cause the enhancement of the emission core within the absorption features of many solar Fraunhofer lines. Thus, solar proxy indicators can be given by the core-to-wing ratio of selected Fraunhofer lines. The Mg II index is defined as the core-to-wing ratio of the Mg II Fraunhofer line centered at 279.9 nm. It can be used as a proxy for spectral variations in the solar extreme UV (EUV, Viereck et al. 2001) and correlates with atmospheric ozone variations and other relevant atmospheric quantities.

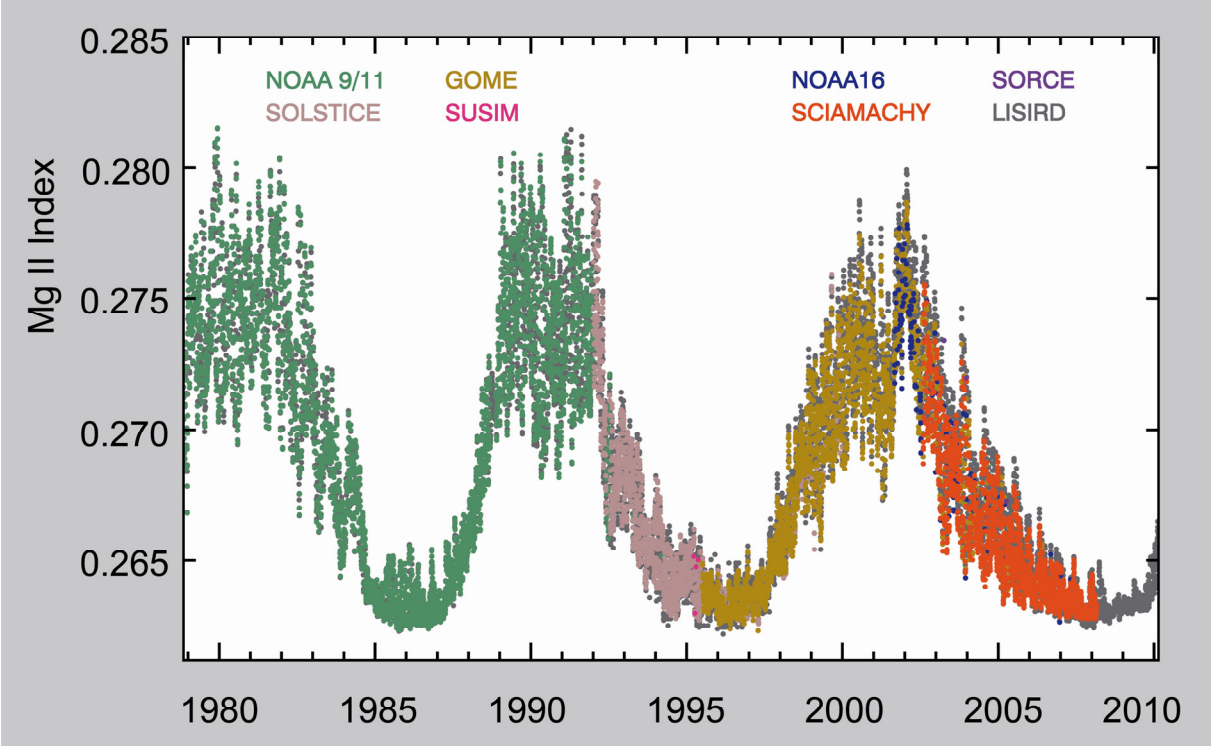

Fig. 10-39: Solar activity measured via the Mg II index by several satellite instruments, including GOME and SCIAMACHY. By combining various satellite instruments, the composite Mg II index covers more than three complete 11-year solar cycles. (Courtesy: M. Weber, IUP-IFE, University of Bremen)

For the understanding of the solar-terrestrial climate interaction, the establishment of long time series covering several solar cycles is important. Due to the limited lifetime of spaceborne missions, this has to be constructed from different satellite experiments. Figure 10-39 combines the Mg-II indices for the solar cycles 21 to 23, using data from NOAA missions (Viereck et al. 2004), GOME (Weber 1999) and SCIAMACHY (Skupin et al. 2004). Both the 27-day periodicity and the declining phase of solar cycle 23 are clearly visible. Differences between SCIAMACHY and GOME are mostly below ±0.5%, between SCIAMACHY and NOAA below ±0.25 %. The derived MgII index was used to identify a correlation of stratospheric ozone with the 27-day solar cycle (Dikty et al. 2010). SCIAMACHY is the first spaceborne instrument that observes daily solar spectral irradiance (SSI) continuously between 230 nm and 1750 nm. In order to address how much the irradiance changes in the UV-VIS-NIR and

SWIR range on 27-day and 11-year timescales, short-term SSI variations were parameterised in terms of the proxies faculae brightening, i.e. MgII index, and sunspot darkening, i.e. photometric sunspot index (Pagaran et al. (2009).

10.5 The Earth Surface and Beneath

SCIAMACHY's realm is the Earth's atmosphere. However, the measured earthshine spectra are also affected by surface reflection and absorption, i.e. by the broadband ground albedo, and by narrowband spectral structures of different origins. These features went unnoticed in trace gas retrieval algorithms for a long time. The initial approach is certainly to take them into account for improving the tropospheric trace gas information (see chapter 7). However, these features can also be used to derive various surface parameters over land or even phytoplankton properties of the oceans.

Land Vegetation Characteristics

Vegetation is a unique property of the Earth. Understanding how it changes contributes to many applications, ranging from global climate change to predicting crop yield. Usually, vegetation indices exploit spectrally broadband differences in reflectivity between the red and NIR wavelength range. Atmospheric sensors like SCIAMACHY provide a higher spectral resolution, i.e. such differences can be analysed on a much finer spectral scale. While optimising DOAS trace gas retrievals, Wagner et al. (2007) noticed that the resulting residuals displayed distinct structures, particularly over vegetated land. These structures could be reduced in amplitude when vegetation data such as spectral reflectances of conifers, deciduous trees or grass were included in the spectral fitting. Fig. 10-40 shows the fit results for deciduous vegetation for summer 2003-2004. A correspondence to deciduous vegetation is obvious, but interference with other vegetation types and coastal waters is still present. Since retrieving vegetation information from remotely sensed atmospheric data is a rather novel approach, current results are still preliminary and require further investigations. There is a clear need to collect more spectral reference data at spectral resolutions similar to SCIAMACHY.

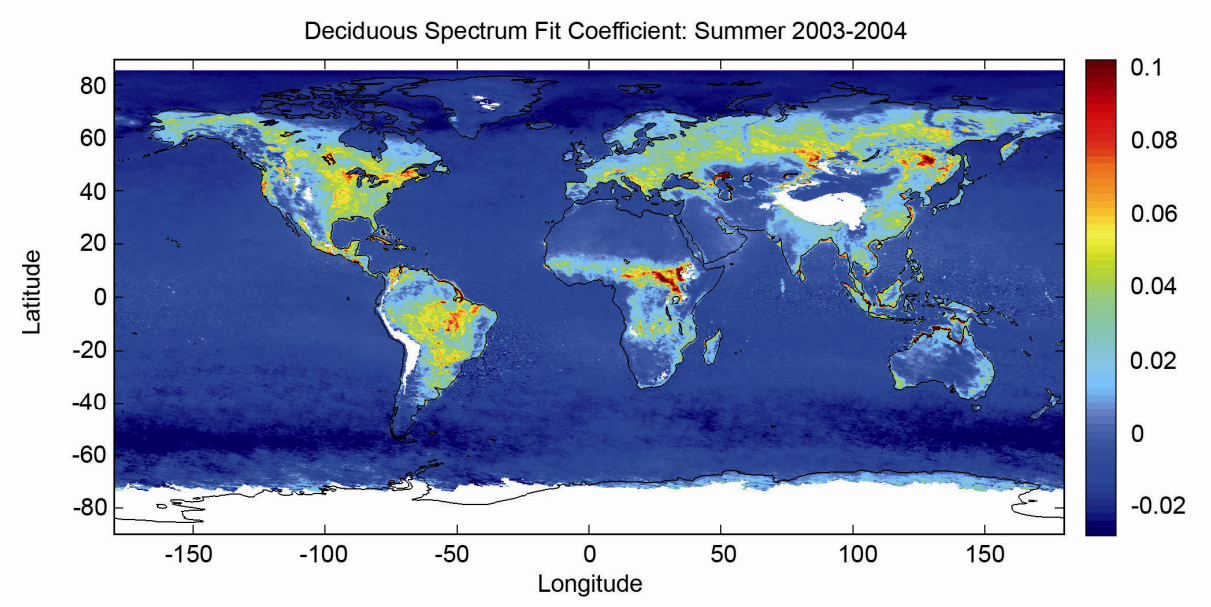

Fig. 10-40: Global mean deciduous vegetation signature – DOAS fitting coefficient of the logarithm of the deciduous vegetation spectrum – for summer 2003-2004 for cloud-free scenes. (Courtesy: T. Wagner, MPI for Chemistry, Mainz)

Oligotrophic Oceanic Regions

Certain regions of the world's oceans are oligotrophic, i.e. they contain very low levels of nutrients and are thus almost free of biogenic activity. As a consequence, solar irradiation partly penetrates into the uppermost water layers. This has two effects on the spectra of the backscattered light: first, the ocean water causes rather broadband absorptions according to its cross section. In addition, vibrational Raman scattering occurs causing high-frequent spectral structures (Vasilkov et al. 2002; Vountas et al. 2003) similar to the atmospheric *Ring* effect (see chapter 7). Global maps of fit results for vibrational Raman scattering show consistent global patterns with high values for the oligotrophic oceanic regions and have been obtained from SCIAMACHY data by applying differential optical absorption spectroscopy in the UV-A region (Vountas et al. 2007).

Oceanic Phytoplankton Characteristics

In open water, marine phytoplankton is the basis of the marine food web. They contribute 50% to the global primary production via photosynthesis. Microscopic algae also play an important role in the global carbon cycle. For photosynthesis, sunlight is absorbed by certain pigments, such as chlorophyll. The absorption spectrum is typical for particular groups of algae due to their characteristic pigment composition. The absorption signatures can be identified in SCIAMACHY data, allowing the quantitative evaluation of the global distribution of phytoplankton. By including a phytoplankton absorption spectrum in the DOAS retrieval, Vountas et al. (2007) was able to retrieve global maps of marine chlorophyll concentrations from SCIAMACHY data successfully. Furthermore, Bracher et al. (2009) could even distinguish different types of phytoplankton, namely diatoms from cyanobacteria (Fig. 10-41). The resulting global maps are in good agreement with biochemical models and with independent *in situ* measurements obtained during cruises with the German research vessels *Polarstern*, *Maria S. Merian* and *Sonne* in the Atlantic and Pacific Oceans. These comparisons again proved the validity of the phytoplankton concentrations retrieved from SCIAMACHY measurements.

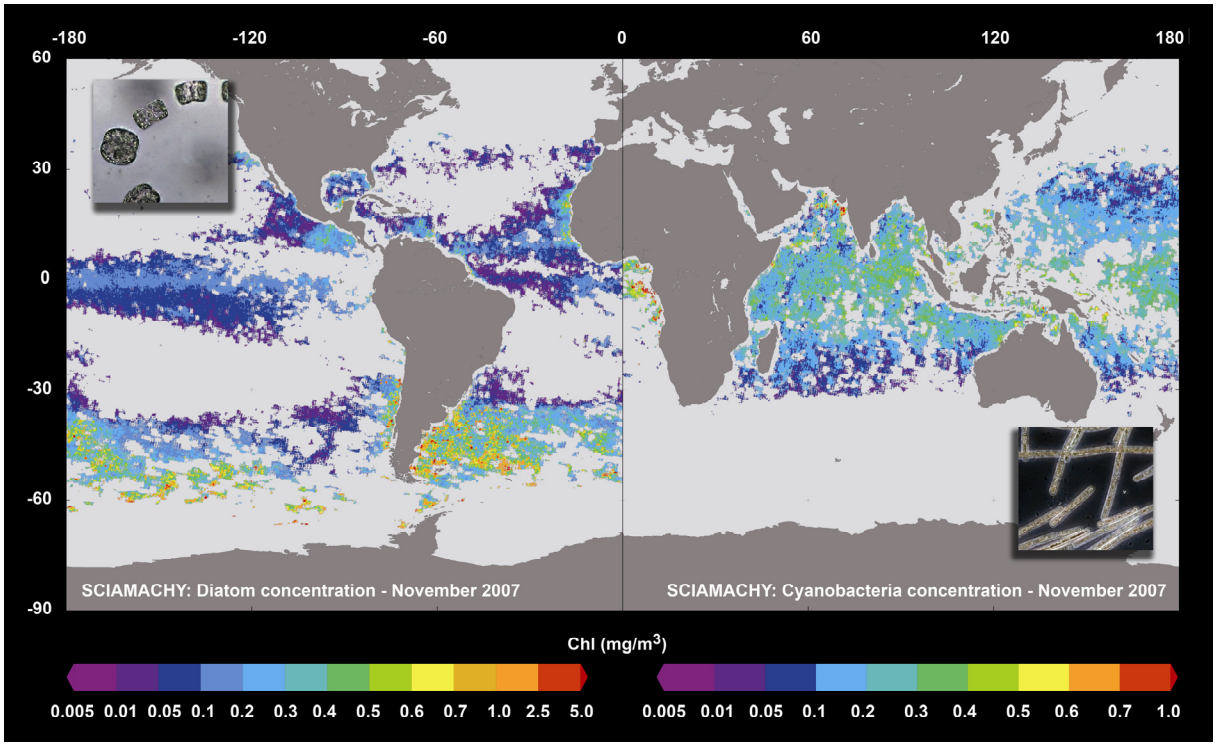

Fig. 10-41: Global biomass distributions of diatoms (left hemisphere) and cyanobacteria (right hemisphere) in November 2007 as derived from SCIAMACHY data using the PhytoDOAS method. The insets show members of the two algae groups. (Courtesy: A. Bracher IUP-IFE, University of Bremen and Alfred Wegener Institute for Polar and Marine Research, adapted from Bracher et al. 2009; photo diatoms: E. Allhusen, cyanobacteria: S. Kranz; both Alfred Wegener Institute for Polar and Marine Research)

10.6 SCIAMACHY and the Goddess of Love

Although the Earth's atmosphere is unique, most of the other planets of the solar system possess a gaseous 'envelope' as well. Interplanetary spacecraft, equipped with spectrometers to study such extraterrestrial atmospheres, sometimes steer their instruments towards our home planet. The acquired Earth spectra usually serve calibration purposes. In an opposite approach, SCIAMACHY was using Venus as a point source to better characterise the slit width of the spectrometer. During these observations, Venusian spectra were obtained which proved very valuable in terms of planetary science (Gottwald et al. 2009).

With a diameter of 12100 km and being an inner planet at distances from Earth ranging from 42 to 256 million km, Venus exhibits continuously changing viewing conditions during a full solar revolution. On 20 March 2009, when the first measurement was scheduled, Venus was close to inferior conjunction at its minimum distance with the planet passing between the Earth and the Sun. SCIAMACHY mainly looked at the night side of Venus and only a very small part of the planet was lit by sunlight. Three months later, on 25 June 2009, Venus was much farther away at 127 million km, with Sun-Venus-Earth forming a right-angled triangle. Thus, about half of Venus' sunlit side was in view. In March, the observation geometry resembled a limb configuration, while in June, it was more of nadir-type. Both occasions yielded spectra with detailed absorption features of carbon dioxide (CO_2), the gas that forms Venus' atmosphere and sustains its extreme greenhouse effect. As expected, the features are much stronger in June because the line of sight was penetrating much deeper into the atmosphere (Fig. 10-42).

SCIAMACHY's Venus observations serve two purposes. They supplement close-up measurements by the instruments SPICAV and VIRTIS onboard ESA's Venus Express (VEX) mission orbiting the Earth's neighbour since 2006. Because SCIAMACHY viewing geometries are different from those of VEX, new information about the Venusian atmosphere can be inferred. The main benefit is, however, that the SCIAMACHY measurements provide another example of how the spectral signatures of a terrestrial planet might appear when viewed from far away. Since the discovery of the first planet around a solar-type star in 1995, finding an Earth-like planet around another star – a *Second Earth* or *Exo-Earth* – has become one of the big challenges in astronomy. Most of the currently known exoplanets are giant planets, like Jupiter. In the coming years, improved and dedicated instrumentation will bring smaller, terrestrial planets within reach. Because of the exoplanets' enormous distance, they will always appear pointlike. Only by measuring and analysing their spectra can we be able to find out whether they might be suitable for harbouring life. This is why spectroscopy of solar system bodies is a greatly appreciated test case. By fully exploiting SCIAMACHY's spectral and operational capabilities, even the other bright solar system bodies – Mars, Jupiter and Saturn – come within reach.

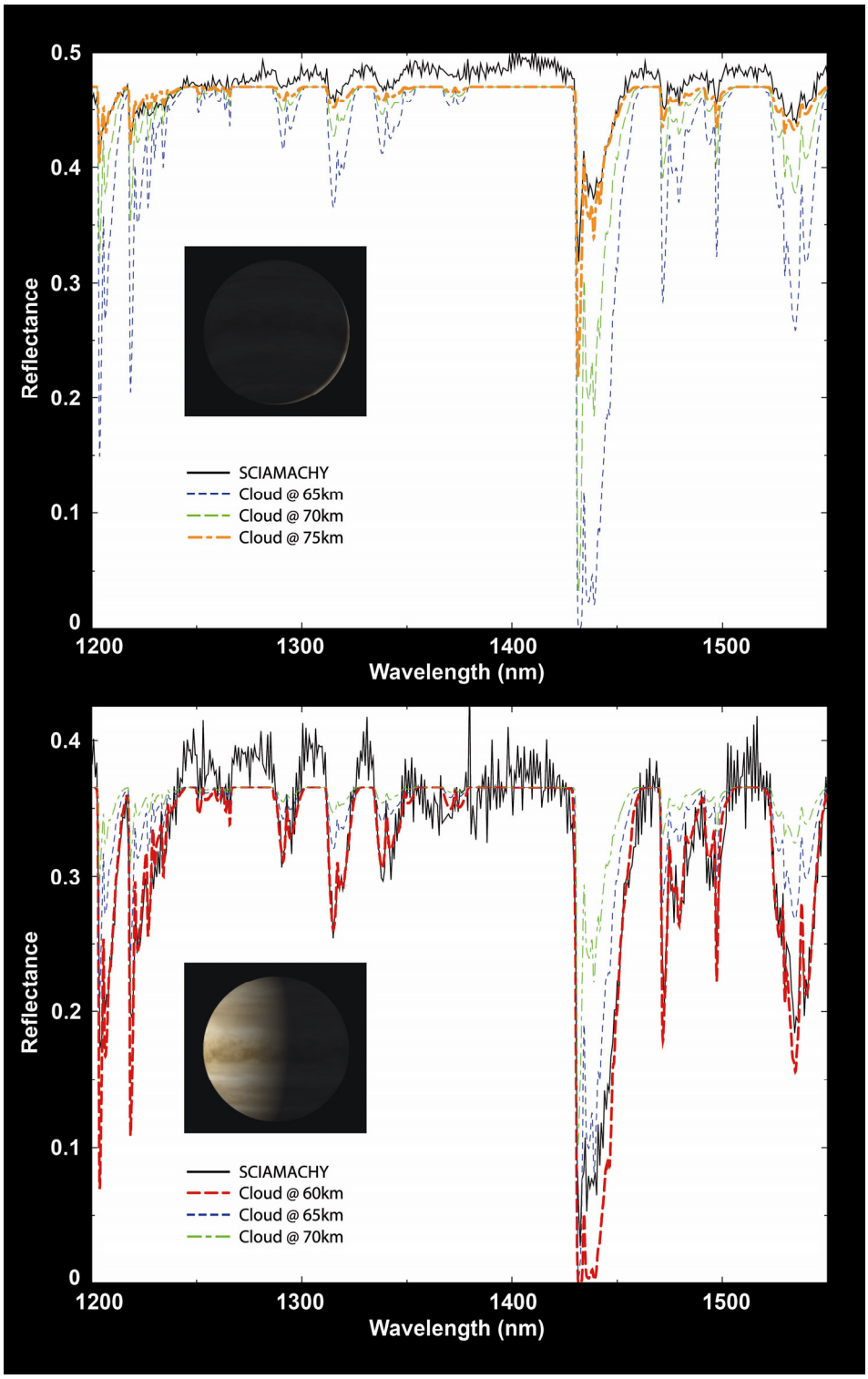

Fig. 10-42: Venus reflectance from 1200 nm to 1550 nm as measured in March (top) and June (bottom) 2009. Most absorption features are due to CO_2. The spectra are modelled by using CO_2 as absorber and H_2SO_4 clouds at different altitudes as scatterer. The illumination conditions in the insets have been derived from the NASA/JPL Solar System Simulator. (Courtesy: M. Vasquez, DLR-IMF)

References

Barkley, M.P., Monks, P.S., Hewitt, A.J., Machida, T., Desai, A., Vinnichenko, N., Nakazawa, T., Yu Arshinov, M., Fedoseev, N. and Watai, T. 2007. Assessing the near surface sensitivity of SCIAMACHY atmospheric CO_2 retrieved using (FSI) WFM-DOAS. *Atmos. Chem. Phys.*, 7, 3597-3619.

Barkley, M.P., Palmer, P.I., De Smedt, I., Karl, T., Guenther, A. and Van Roozendael, M. 2009. Regulated large-scale annual shutdown of Amazonian isoprene emissions?. *Geophys. Res. Lett.*, 36, L04803, doi:10.1029/2008GL036843.

Barrie, L.A., Bottenheim, J.W., Schnell, R.C., Crutzen, P.J. and Rasmussen, R.A. 1988. Ozone destruction and photochemical reactions at polar sunrise in the lower Arctic atmosphere. *Nature*, 334, 138-141.

Becker, E. and von Savigny, C. 2010. Dynamical heating of the polar summer mesopause induced by solar proton events. *J. Geophys. Res.* 115, doi:10.1029/2009JD012561.

Begoin, M., Richter, A., Kaleschke, L., Tian-Kunze, X., Stohl, A. and Burrows, J.P. 2010. Satellite observations of long range transport of a large BrO cloud in the Arctic. *Atmos. Chem. Phys.* , 10, 6515-6526.

Beirle, S., Platt, U. and Wagner, T. 2004. Monitoring nitrogen oxides with satellite instruments: High resolution maps from GOME narrow swath mode and SCIAMACHY. *Proc. ENVISAT & ERS Symposium 2004*, Salzburg, Austria, ESA SP-572.

Bergamaschi, P., Frankenberg, C., Meirink, J.F., Krol, M., Villani, M.G., Houweling, S., Dentener, F., Dlugokencky, E.J., Miller, K.B., Gatti, L.V., Engel, A. and Levin, I. 2009. Inverse modeling of global and regional CH_4 emissions using SCIAMACHY satellite retrievals. *J. Geophys. Res.*, 114, D22301, doi:10.1029/2009JD012287.

Bittner, M., Offermann, D., Graef, H.H., Donner, M. and Hamilton, K. 2002. An 18 year time series of OH rotational temperatures and middle atmosphere decadal variations. *J. Atmos. Sol.-Terr. Phys.*, 64, 1147-1166.

Bösch, H., Toon, G.C., Sen, B., Washenfelder, R.A., Wennberg, P.O., Buchwitz, M., de Beek, R., Burrows, J.P., Crisp, D., Christi, M., Connor, B.J., Natraj, V. and Yung, Y.L. 2006. Space-based near-infrared CO_2 measurements: Testing the Orbiting Carbon Observatory retrieval algorithm and validation concept using SCIAMACHY observations over Park Falls, Wisconsin. *J. Geophys. Res.*, 111, D23302, doi:10.1029/2006JD007080.

Boersma, K.F., Jacob, D.J., Eskes, H.J., Pinder, R.W., Wang, J. and van der A, R.J. 2008. Intercomparison of SCIAMACHY and OMI tropospheric NO_2 columns: Observing the diurnal evolution of chemistry and emissions from space. *J. Geophys. Res.,* 113, D16S26, doi:10.1029/2007JD008816.

Bracher, A., Eichmann, K.-U., von Savigny, C., Sinnhuber, B.-M., Weber, M., Bramstedt, K. and Burrows, J.P. 2005. Polar ozone distributions in the arctic winter/spring 2004/05 as measured by the Envisat instruments GOMOS and SCIAMACHY. *Geophys. Res. Abstr.*, 7, 08693.

Bracher, A., Vountas, M., Dinter, T., Burrows, J.P., Röttgers, R. and Peeken, I. 2009. Quantitative Observation of cyanobacteria and diatoms from space using PhytoDOAS on SCIAMACHY data. *Biogeosciences*, 6, 751-764.

Buchwitz, M., de Beek, R., Noël, S., Burrows, J.P., Bovensmann, H., Bremer, H., Bergamaschi, P., Körner, S. and Heimann, M. 2005a. Carbon monoxide, methane and carbon dioxide columns retrieved from SCIAMACHY by WFM-DOAS: Year 2003 initial data set. *Atmos. Chem. Phys.*, 5, 3313-3329.

Buchwitz, M., de Beek, R., Burrows, J.P., Bovensmann, H., Warneke, T., Notholt, J., Meirink, J.F., Goede, A.P.H., Bergamaschi, P., Körner, S., Heimann, M. and Schulz, A. 2005b. Atmospheric methane and carbon dioxide from SCIAMACHY satellite data: Initial comparison with chemistry and transport models. *Atmos. Chem. Phys.*, 5, 941-962.

Buchwitz, M., Schneising, O., Burrows, J.P., Bovensmann, H., Reuter, M. and Notholt, J. 2007a. Corrigendum to 'First direct observation of the atmospheric CO_2 year-to-year increase from space' published in Atmos. Chem. Phys., 7, 4249-4256, 2007. *Atmos. Chem. Phys.*, 7, 5341-5342.

Buchwitz, M., Khlystova, I., Bovensmann, H. and Burrows, J.P. 2007b. Three years of global carbon monoxide from SCIAMACHY: Comparison with MOPITT and first results related to the detection of enhanced CO over cities. *Atmos. Chem. Phys.*, 7, 2399-2411.

Correira, J., Aikin, A.C., Grebowsky, J.M., Pesnell, W.D. and Burrows, J.P. 2008. Seasonal variation of magnesium atoms in the mesosphere-thermosphere. *Geophys. Res. Lett.*, 35, doi:10.1029/2007GL033047.

de Graaf, M., Tilstra, L.G., Aben, I., Stammes, P. 2010. Satellite observations of the seasonal cycle of absorbing aerosols in Africa related to the monsoon rainfall. *Atmos. Env.*, 44, 1274-1283, doi:10.1016/j.atmosenv.2009.12.038.

de Laat, A.T.J., Gloudemans, A.M.S., Schrijver, H., van den Broek, M.M.P., Meirink, J.F., Aben, I. and Krol,, M. 2006. Quantitative analysis of SCIAMACHY total carbon monoxide column measurements. *Geophys. Res. Lett.*, 33, L07807, doi:10.1029/2005GL025530.

De Smedt, I., Müller, J.-F., Stavrakou, T., van der A, R., Eskes, H. and Van Roozendael, M. 2008. Twelve years of global observations of formaldehyde in the troposphere using GOME and SCIAMACHY sensors. *Atmos. Chem. Phys.*, 8, 4947-4963.

De Smedt, I., Stavrakou, T., Müller, J.F., van der A, R.J., and Van Roozendael, M. 2010. Trend detection in satellite observations of formaldehyde tropospheric columns. *Geophys. Res. Lett.*, 37, L18808, doi:10.1029/2010GL044245.

Dikty, S., Weber, M., von Savigny, C., Sonkaew, T., Rozanov, A. and Burrows, J.P. 2010. Modulations of the 27-day solar cycle signal in stratospheric ozone from SCIAMACHY. *J. Geophys. Res.*, 115, D00I15, doi:10.1029/2009JD012379.

Dufour, G., Wittrock, F., Camredon, M., Beekmann, M., Richter, A., Burrows, J.P. 2009. SCIAMACHY formaldehyde observations: Constraint for isoprene emissions over Europe?. *Atmos. Chem. Phys.*, 9, 1647-1664.

Ern, M., Lehmann, C., Kaufmann, M. and Riese, M. 2009. Spectral wave analysis at the mesopause from SCIAMACHY airglow data compared to SABER temperature spectra. *Annales Geophysicale*, 27, 1, 407-416.

Eskes, H., Segers, A. and van Velthoven, P.F.J. 2005. Ozone Forecasts of the Stratospheric Polar Vortex-Splitting Event in September 2002. *J. Atmos. Sci.*, 62, 812-821.

Franke, K., Richter, A., Bovensmann, H., Eyring, V., Jöckel, P. and Burrows, J.P. 2009. Ship emitted NO_2 in the Indian Ocean: Comparison of model results with satellite data. *Atmos. Chem. Phys.*, 9, 7289-7301.

Frankenberg, C., Meirink, J.F., van Weele, M., Platt, U. and Wagner, T. 2005. Assessing methane emissions from global space-borne observations. *Science*, 308, 1010-1014.

Frankenberg, C., Bergamaschi, P., Butz, A., Houweling, S., Meirink, J.F., Notholt, J., Petersen, A.K., Schrijver, H., Warneke, T. and Aben, I. 2008. Tropical methane emissions: A revised view from SCIAMACHY onboard ENVISAT. *Geophys. Res. Lett.*, 35, L15811, doi:10.1029/ 2008GL034300.

Frankenberg, C., Yoshimura, K., Warneke, T., Aben, I., Butz, A., Deutscher, N., Griffith, D., Hase, F., Notholt, J., Schneider, M., Schrijver, H. and Röckmann, T. 2009. Dynamic Processes Governing Lower-Tropospheric HDO/H2O Ratios as Observed from Space and Ground. *Science*, 325, 1374, DOI: 10.1126/science.1173791.

Fu, T.-M., Jacob, D.J., Wittrock, F., Burrows, J.P., Vrekoussis, M. and Henze, D.K. 2008. Global budgets of atmospheric glyoxal and methylglyoxal, and implications for formation of secondary organic aerosols. *J. Geophys. Res.*, 113, D15303, doi:10.1029/2007JD009505.

Gloudemans, A.M.S., Schrijver, H., Kleipool, Q., van den Broek, M.M.P., Straume, A.G., Lichtenberg, G., van Hees, R.M., Aben, I. and Meirink, J.F. 2005. The impact of SCIAMACHY instrument calibration on CH_4 and CO total columns. *Atmos. Chem. Phys.*, 5, 2369-2383.

Gloudemans, A.M.S., de Laat, A.T.J., Schrijver, H., Aben, I., Meirink, J.F., and van der Werf, G.R. 2009. SCIAMACHY CO over land and oceans: 2003-2007 inter-annual variability. *Atmos. Chem. Phys.*, 9, 3799-3813.

Gottwald, M., Slijkhuis, S., Krieg, E., Schreier, F., Lichtenberg, G., Vasquez, M., Snel, R., Stam, D. and de Kok, R. 2009. Venus Observations with SCIAMACHY. *Proc Atmospheric Science Conference*, Barcelona, Spain, ESA SP-676.

Hendrick, F., Rozanov, A., Johnston, P.V., Bovensmann, H., De Maziere, M., Fayt, C., Hermans, C., Kreher, K., Lotz, W., Sinnhuber, B.-M., Theys, N., Thomas, A., Burrows, J.P. and Van Roozendael, M. 2009. Multi-year comparison of stratospheric BrO vertical profiles retrieved from SCIAMACHY limb and ground-based UV-visible measurements. *Atmos. Meas. Tech.*, 2, 273-285.

Kaleschke, L., Richter, A., Burrows, J.P., Afe, O., Heygster, G., Notholt, J., Rankin, A.M., Roscoe, H.K., Hollwedel, J., Wagner, T. and Jacobi, H.-W. 2004. Frost flowers on sea ice as a source of sea salt and their influence on tropospheric halogen chemistry. *Geophys. Res. Lett.*, 31, doi:10.1029/2004GL020655.

Kaufmann, M., Lehmann, C., Hoffmann, L., Riese, M., Lopez-Puertas, M., Funke, B. and von Savigny, C. 2007. Chemical heating rates derived from SCIAMACHY vibrationally excited OH limb emission spectra. *Adv. Space Res.*, 41(11), 1914-1920.

Kim, S.-W., Heckel, A., McKeen, S.A., Frost, G.J., Hsie, E.-Y., Trainer, M.K., Richter, A., Burrows, J.P., Peckham, S.E. and Grell, G.A. 2006. Satellite observed U.S. power plant NOx emission reductions and their impact on air quality. *Geophys. Res. Lett.*, 33, L22812, doi:10.1029/2006GL027749.

Kim, S.-W., Heckel, A., Frost, G.J., Richter, A., Gleason, J., Burrows, J.P., McKeen, S., Hsie, E.-Y., Granier, C. and Trainer, M. 2009. NO_2 columns in the western United States observed from space and simulated by a regional chemistry model and their implications for NOx emissions. *J. Geophys. Res.*, 114, D11301, doi:10.1029/2008JD011343.

Konovalov, I., Beekmann, M., Burrows, J.P. and Richter, A. 2008. Satellite measurement based estimates of decadal changes in European nitrogen oxides emissions. *Atmos. Chem. Phys.*, 8, 2623-2641.

Konovalov, I.B., Beekmann, M., Richter, A., Burrows, J.P., Hilboll, A. 2010. Multi-annual changes of NOx emissions in megacity regions: Nonlinear trend analysis of satellite measurement based estimates. *Atmos. Chem. Phys.*, 10, 8481-8498.

Kühl, S., Dörnbrack, A., Wilms-Grabe, W., Sinnhuber, B.-M., Platt, U. and Wagner, T. 2004. Observational evidence of rapid chlorine activation by mountain waves above northern Scandinavia. *J. Geophys. Res.*, 109, D22309, doi:10.1029/2004JD004797.

Kühl, S., Wilms-Grabe, W., Frankenberg, C., Grzegorski, M., Platt, U. and Wagner, T. 2006. Comparison of OClO Nadir Measurements from SCIAMACHY and GOME. *Adv. Space Res.*, 37, 2247-2253.

Kühl, S., Puķīte, J., Deutschmann, T., Platt, U. and Wagner, T. 2008. SCIAMACHY limb measurements of NO_2, BrO and OClO. Retrieval of vertical profiles: Algorithm, first results, sensitivity and comparison studies. *Advances in Space Research*, 42, 1747-1764.

Loyola, D., Coldewey-Egbers, M., Dameris, M., Garny, H., Stenke, A., Van Roozendael, M., Lerot, C., Balis, D. and Koukouli, M. 2009. Global long-term monitoring of the ozone layer - a prerequisite for predictions. *Int. J. Rem. Sens.*, 30(15), 4295-4318.

Marbach, T., Beirle, S., Platt, U., Hoor, P., Wittrock, F., Richter, A., Vrekoussis, M., Grzegorski, M., Burrows, J.P. and Wagner, T. 2009. Satellite measurements of formaldehyde from shipping emissions. *Atmos. Chem. Phys.*, 9, 8223-8234.

Meirink, J.F., Bergamaschi, P., Frankenberg, C., d'Amelio, M T.S., Dlugokencky, E.J., Gatti, L.V., Houweling, S., Miller, J.B., Röckmann, T., Villani, M.G. and Krol, M. 2008. Four-dimensional variational data assimilation for inverse modelling of atmospheric methane emissions: Analysis of SCIAMACHY observations. *J. Geophys. Res.*, 113, D17301, doi:10.1029/2007JD009740.

Mieruch, S., Noël, S., Bovensmann, H. and Burrows, J.P. 2008. Analysis of global water vapour trends from satellite measurements in the visible spectral range. *Atmos. Chem. Phys.*, 8, 491-504.

Myriokefalitakis, S., Vrekoussis, M., Tsigaridis, K., Wittrock, F., Richter, A., Brühl, C., Volkamer, R., Burrows, J.P. and Kanakidou, M. 2008. The influence of natural and anthropogenic secondary sources on the glyoxal global distribution. *Atmos. Chem. Phys.*, 8, 4965-4981.

Newman, P.A., Daniel, J.S., Waugh, D.W. and Nash, E.R. 2007. A new formulation of equivalent effective stratospheric chlorine (EESC). *Atmos. Chem. Phys.*, *7*, 4537-4552.

Noël, S., Buchwitz, M., Bovensmann, H. and Burrows, J.P. 2004. First retrieval of global water vapour column amounts from SCIAMACHY measurements. *Atmos. Chem. Phys.*, 4, 111-125.

O'Dowd, C.D., Jimenez, J.L., Bahreini, R., Flagan, R.C., Seinfeld, J.H., Hameri, K., Pirjola, L., Kulmala, M., Jennings, S.G. and Hoffmann, T. 2002. Marine aerosol formation from biogenic iodine emissions. *Nature*, 417, 632-636.

Pagaran, J.,Weber, M., Burrows, J.P. 2009. Solar variability from 240 to 1750 nm in terms of faculae brightening and sunspot darkening from SCIAMACHY. *Astrophys. J.,* 700, 1884-1895.

Piot, M. and von Glasow, R. 2008. The potential importance of frost flowers, recycling on snow, and open leads for ozone depletion events. *Atmos. Chem. Phys.*, 8, 2437-2467.

Puķīte, J., Kühl, S., Deutschmann, T., Platt, U. and Wagner, T. 2008. Accounting for the effect of horizontal gradients in limb measurements of scattered sunlight. *Atmos. Chem. Phys.*, 8, 3045-3060.

Rahpoe, N., von Savigny, C., Robert, C.E., DeLand, M.T. and Burrows, J.P. 2010. Impact of Solar Proton Events on Noctilucent Clouds. *J. Atmosph. Sol.-Terr. Phys.*, doi:10.1016/j.jastp.201007017 (in press)

Reuter, M., Buchwitz, M., Schneising, O., Heymann, J., Bovensmann, H. and Burrows, J.P. 2010. A method for improved SCIAMACHY CO_2 retrieval in the presence of optically thin clouds. *Atmos. Meas. Tech.*, 3, 209-232.

Rex, M., Salawitch, R.J., Deckelmann, H., von der Gathen, P., Harris, N.R.P., Chipperfield, M.P., Naujokat, B., Reimer, E., Allaart, M., Andersen, S.B., Bevilacqua, R., Braathen, G.O., Claude, H., Davies, J., De Backer, H., Dier, H., Dorokhov, V., Fast, H., Gerding, M., Godin-Beekmann, S., Hoppel, K., Johnson, B., Kyrö, E., Litynska, Z., Moore, D., Nakane, H., Parrondo, M.C., Risley, A.D., Skrivankova, P., Stübi, R., Viatte, P., Yushkov, V., Zerefos, C. 2006. Arctic winter 2005: Implications for stratospheric ozone loss and climate change. *Geophys. Res. Lett.*, 33, L23808, doi:10.1029/2006GL026731.

Richter, A., Eyring, V., Burrows, J.P., Bovensmann, H., Lauer, A., Sierk, B. and Crutzen, P.J. 2004. Satellite Measurements of NO_2 from International Shipping Emissions. *Geophys. Res. Lett.*, 31, L23110, doi:10.1029/2004GL020822.

Richter, A., Burrows, J.P., Nüß, H., Granier, C. and Niemeier, U. 2005a. Increase in nitrogen dioxide over China observed from space. *Nature*, 437, 129-132.

Richter, A., Wittrock, F., Weber, M., Beirle, S., Kühl, S., Platt, U., Wagner, T., Wilms-Grabe, W. and Burrows, J.P. 2005b. GOME observations of stratospheric trace gas distributions during the splitting vortex event in the Antarctic winter 2002 Part I: Measurements. *J. Atm. Sci.*, 62, 778-785.

Robert, C.E., von Savigny, C., Rahpoe, N., Burrows, J.P., DeLand, M.T. and Schwartz, M.J. 2010. First evidence of a 27-day signature in noctilucent cloud occurrence frequency. *J. Geophys. Res.*, 115, D00I12, doi:10.1029/2009JD012359.

Rohen, G.J., von Savigny, C., Sinnhuber, M., Eichmann, K.-U., Kaiser, J.W., Llewellyn, E.J., Rozanov, A., Bovensmann, H. and Burrows, J.P. 2005. Impact of the October/November 2003 Solar Proton Events on Mesospheric Ozone: SCIAMACHY Measurement and Model Results. *J. Geophys. Res.*, 110, A09S39, doi:10.1029/2004JA010984.

Rozanov, A., Bovensmann, H., Bracher, A., Hrechanyy, S., Rozanov, V., Sinnhuber, M., Stroh, F., and Burrows, J.P. 2005. NO_2 and BrO vertical profiles retrieval from SCIAMACHY limb measurements: Sensitivity studies. *Adv. Space Res.*, 36, 846-854, doi:10.1016/j.asr.2005.03.013.

Saiz-Lopez, A., Chance, K., Liu, X., Kurosu, T.P. and Sander, S.P. 2007. First observations of iodine oxide from space. *Geophys. Res. Letters*, 34, L12812, doi:10.1029/2007GL030111.

von Savigny, C., Kokhanovsky, A., Bovensmann, H., Eichmann, K.-U., Kaiser, J.W., Noël, S., Rozanov, A.V., Skupin, J. and Burrows, J.P. 2004a. NLC Detection and Particle Size Determination: First Results from SCIAMACHY on ENVISAT. *Adv. Space Res.*, 34, 851-856.

von Savigny, C., Eichmann, K.-U., Llewellyn, E.J., Bovensmann, H., Burrows, J.P., Bittner, M., Höppner, K., Offermann, D., Steinbrecht, W., Winkler, P., Taylor, M.J. and Cheng, Y. 2004b. First near-global retrieval of OH rotational temperatures from satellite-based Meinel band emission measurements. *Geophys. Res. Lett*., 31, L15111, doi:10.1029/2004GL020410.

von Savigny, C., Rozanov, A., Bovensmann, H., Eichmann, K.-U., Noël, S., Rozanov, V.V., Sinnhuber, B.-M., Weber, M. and Burrows, J.P. 2005a. The ozone hole break-up in September 2002 as seen by SCIAMACHY on ENVISAT. *J. Atmosph. Sci.*, 62, 721-734.

von Savigny, C., Ulasi, E.P., Eichmann, K.-U., Bovensmann, H. and Burrows, J.P. 2005b. Detection and Mapping of Polar Stratospheric Clouds using Limb Scattering Observations. *Atmos. Chem. Phys.*, 5, 3071-3079.

von Savigny, C., Sinnhuber, M., Bovensmann, H., Burrows, J.P., Kallenrode, M.-B. and Schwartz, M.J. 2007a. On the Disappearance of Noctilucent Clouds during the January 2005 Solar Proton Events. *Geophys. Res. Lett.*, 34, L02805, doi:10.1029/2006GL128106.

von Savigny, C., Robert, C., Bovensmann, H., Burrows, J.P. and Schwartz, M. 2007b. Satellite observations of the quasi 5-day wave in noctilucent clouds and mesopause temperatures. *Geophys. Res. Lett.*, 34, L24808, doi:10.1029/2007GL030987.

von Savigny, C. and Burrows, J.P. 2007. Latitudinal variation of NLC particle radii derived from northern hemisphere SCIAMACHY/Envisat limb measurements. *Adv. Space Res.,* 40(6), 765-771, doi:10.1016/j.asr.2007.12.032.

von Savigny, C., Robert, C.E., Baumgarten, G., Bovensmann, H. and Burrows, J.P. 2009. Comparison of NLC particle sizes derived from SCIAMACHY/Envisat observations with ground-based LIDAR measurements at ALOMAR (69°N). *Atmos. Meas. Tech.*, 2, 523-531.

Scharringhausen, M. 2007. Investigation of mesospheric and thermospheric magnesium species from space. *PhD thesis*, University of Bremen.

Scharringhausen, M., Aikin, A.C., Burrows, J.P. and Sinnhuber, M. 2008. Space-borne measurements of mesospheric magnesium species - a retrieval algorithm and preliminary profiles. *Atmos. Chem. Phys.*, 8, 1963-1983.

Schneising, O., Buchwitz, M., Burrows, J.P., Bovensmann, H., Reuter, M., Notholt, J., Macatangay, R. and Warneke, T. 2008. Three years of greenhouse gas column-averaged dry air mole fractions retrieved from satellite - Part 1: Carbon dioxide. *Atmos. Chem. Phys.*, 8, 3827-3853.

Schneising, O., Buchwitz, M., Burrows, J.P., Bovensmann, H., Bergamaschi, P. and Peters, W. 2009. Three years of greenhouse gas column-averaged dry air mole fractions retrieved from satellite - Part 2: Methane. *Atmos. Chem. Phys.*, 9, 443-465.

Schönhardt, A., Richter, A., Wittrock, F., Kirk, H., Oetjen, H., Roscoe, H.K. and Burrows, J.P. 2008. Observations of iodine monoxide columns from satellite. *Atmos. Chem. Phys.*, 8, 637-653.

Schrijver, H., Gloudemans, A.M.S., Frankenberg, C. and Aben, I. 2009. Water vapour total columns from SCIAMACHY spectra in the 2.36μm window. *Atmos. Meas. Tech.*, 2, 561-571.

Simpson, W.R., von Glasow, R., Riedel, K., Anderson, P., Ariya, P., Bottenheim, J., Burrows, J., Carpenter, L.J., Frieß, U., Goodsite, M.E., Heard, D., Hutterli, M., Jacobi, H.-W., Kaleschke, L., Neff, B., Plane, J., Platt, U., Richter, A., Roscoe, H., Sander, R., Shepson, P., Sodeau, J., Steffen, A., Wagner, T. and Wolff, E. 2007. Halogens and their role in polar boundary-layer ozone depletion. *Atmos. Chem. Phys.*, 7, 4375-4418.

Sinnhuber, B.-M., Rozanov, A., Sheode, N., Afe, O.T., Richter, A., Sinnhuber, M., Wittrock, F., Burrows, J.P., Stiller, G.P., von Clarmann, T. and Linden, A. 2005. Global observations of stratospheric bromine monoxide from SCIAMACHY. *Geophys. Res. Lett.*, 32, L20810, doi: 10.1029/2005GL023839.

Sioris, C.E., Kovalenko, L.K., McLinden, C.A., Salawitch, R.J., Van Roozendael, M., Goutail, F., Dorf, M., Pfeilsticker, K., Chance, K., von Savigny, C., Liu, X., Kurosu, T.P., Pommereau, J.P., Bösch, H. and Frerick J. 2006. Latitudinal and vertical distribution of bromine monoxide in the lower

stratosphere from Scanning Imaging Absorption Spectrometer for Atmospheric Chartography limb scattering measurements. *J. Geophys. Res.*, 111, D14301, doi:10.1029/2005JD006479.

Skupin, J., Weber, M., Bovensmann, H. and Burrows, J.P. 2004. The Mg II solar activity proxy indicator derived from GOME and SCIAMACHY. *Proc. ENVISAT and ERS Symposium*, Salzburg, Austria, ESA SP-572.

Sonkaew, T., von Savigny, C., Eichmann, K.-U., Rozanov, A., Weber, M., Bovensmann, H. and Burrows, J.P. 2010. Chemical ozone loss in Arctic and Antarctic polar winter/spring derived from SCIAMACHY limb measurements 2002-2009. *in preparation.*

Stavrakou, T., Müller, J.-F., Boersma, K.F., De Smedt, I. and van der A, R.J. 2008. Assessing the distribution and growth rates of NOx emission sources by inverting a 10-year record of NO_2 satellite columns. *Geophys. Res. Lett.*, 35, L10801, doi:10.1029/ 2008GL033521.

Stavrakou, T., Müller, J.-F., De Smedt, I., Van Roozendael, M., van der Werf, G.R., Giglio, L. and Guenther, A. 2009. Evaluating the performance of pyrogenic and biogenic emission inventories against one decade of space-based formaldehyde columns. *Atmos. Chem. Phys.*, 9, 1037-1060.

Steinbrecht, W., Claude, H., Schönenborn, F., McDermid, I.S., Leblanc, T., Godin, S., Keckhut, P., van Gijsel, A., Swart, D.P.J., Bodeker, G., Parrish, A., Boyd, I., Kämpfer, N., Hocke, C., Stolarski, R.S. Frith, S.M., Thomason, L.W., Remsberg, E.E., von Savigny, C., Rozanov, A. and Burrows, J.P. 2009. Ozone and temperature trends in the upper stratosphere at five stations of the Network for the Detection of Atmospheric Composition Change. *Int. J. Rem. Sens.*, 30(15-16), 3875-3886.

Tangborn, A., Stajner, I., Buchwitz, M., Khlystova, I., Pawson, S., Burrows, .J, Hudman, R., Nedelec, P. 2009. Assimilation of SCIAMACHY total column CO observations: Global and regional analysis of data impact. *J. Geophys. Res.*, 114, D07307. doi10.1029/2008JD010781

Theys, N., Van Roozendael, M., Errera, Q., Hendrick, F., Daerden, F., Chabrillat, S., Dorf, M., Pfeilsticker, K., Rozanov, A., Lotz, W., Burrows, J.P., Lambert, J.-C., Goutail, F., Roscoe, H.K. and De Mazière, M. 2009. A global stratospheric bromine monoxide climatology based on the BASCOE chemical transport model. *Atmos. Chem. Phys.*, 9, 831-848.

van der A, R.J., Eskes, H.J., Boersma, K.F., van Noije, T.P.C., Van Roozendael, M., De Smedt, I., Peters, D.H.M.U. and Meijer, E.W. 2008. Trends, seasonal variability and dominant NO_x source derived from a ten year record of NO_2 measured from space. *J. Geophys. Res.*, 113, D04302, doi:10.1029/2007JD009021.

Vasilkov, A.P., Joiner, J., Gleason, J. and Bhartia, P.K. 2002. Ocean Raman scattering in satellite backscatter UV measurements. *Geophys. Res. Lett.*, 29(17), 1837, doi:10.1029/2002GL014955

Viereck, R.A., Puga, L.C., McMullin, D., Judge, D., Weber, M. and Tobiska, W.K. 2001. The Mg II Index: A Proxy for Solar EUV. *Geophys. Res. Lett.*, 28, 1343-1346.

Viereck, R.A., Floyd, L.E., Crane, P.C., Woods, T.N., Knapp, B.G., Rottman, G., Weber, M., Puga, L.C. and DeLand, M.T. 2004. A composite Mg II index spanning from 1978 to 2003. *Space Weather*, 2, S10005, doi:10.1029/2004SW000084.

Vountas, M., Richter, A., Wittrock, F. and Burrows, J.P. 2003. Inelastic scattering in ocean water and its impact on trace gas retrievals from satellite data. *Atmos. Chem. Phys.*, 3, 1365-1375.

Vountas, M., Dinter, T., Bracher, A., Sierk, B. and Burrows, J.P. 2007. Spectral studies of ocean water with space-borne sensor SCIAMACHY using Differential Optical Absorption Spectroscopy (DOAS). *Ocean Sciences*, 3, 429-440.

Vrekoussis, M., Wittrock, F., Richter, A. and Burrows, J.P. 2009. Temporal and spatial variability of glyoxal as observed from space. *Atmos. Chem. Phys.*, 9, 4485-4504.

Wagner, T., Leue, C., Pfeilsticker, K. and Platt, U. 2001. Monitoring of the stratospheric chlorine activation by Global Ozone Monitoring Experiment (GOME) OClO measurements in the austral and boreal winters 1995 through 1999. *J. Geophys. Res.*, 106, 4971-4986.

Wagner, T., Beirle, S., Deutschmann, T., Grzegorski, M. and Platt, U. 2007. Satellite monitoring of different vegetation types by differential optical absorption spectroscopy (DOAS) in the red spectral range. *Atmos. Chem. Phys.*, 7, 69-79.

Weber, M. 1999. Solar activity during solar cycle 23 monitored by GOME. *Proc. European Symposium Atmospheric Measurements from Space (ESAMS'99)*.

Wittrock, F., Richter, A., Oetjen, H., Burrows, J.P., Kanakidou, M., Myriokefalitakis, S., Volkamer, R., Beirle, S., Platt, U. and Wagner, T. 2006. Simultaneous global observations of glyoxal and formaldehyde from space. *Geophys. Res. Lett.*, 33, L16804, doi:10.1029/2006GL026310.

WMO (World Meteorological Organization). 2007. Scientific Assessment of Ozone Depletion: 2006, Global Ozone Research and Monitoring Project – Report No. 50, 572pp., Geneva, Switzerland.